ISAS - INTERNATIONAL SCHOOL
FOR ADVANCED STUDIES

ELECTROPHYSIOLOGICAL STUDY OF VOLTAGE ACTIVATED MEMBRANE CURRENTS AND THEIR MODULATION IN RAT HYPOGLOSSAL MOTONEURONS IN VITRO

Thesis submitted for the degree of *Doctor Philosophiae*

Candidate:
Remigijus Lape

Supervisor:
Andrea Nistri

Trieste, October 2000
International School for Advanced Studies

SISSA - SCUOLA
INTERNAZIONALE
SUPERIORE
DI STUDI AVANZATI
TRIESTE
Via Beirut 2-4

TRIESTE

CONTENTS

NOTE

All work reported arises solely from my own experiments and data analysis. Part of the data reported in the present thesis have been published in the articles listed below.

LAPE, R. AND NISTRI, A. Voltage-activated K^+ currents of hypoglossal motoneurons in a brain stem slice preparation from the neonatal rat. *J. Neurophysiol.* 81: 140-148, 1999.

LAPE, R. AND NISTRI, A. Current and voltage clamp studies of the spike medium afterhyperpolarization of hypoglossal motoneurons in a brain stem slice preparation from the neonatal rat. *J. Neurophysiol.* 83: 2987-2995, 2000.

ACKNOWLEDGEMENTS

I wish to express my gratitude to Prof. Andrea Nistri for his careful supervising, invaluable help and support during my PhD programe.

I wish to thank the people of the Biophysics Sector for such a pleasant scientific environment and friendly atmosphere.

I also wish to thank three Gytis: Gintautas (Gytis) Saulis, Gytis Baranauskas, and Gytis Svirskis for stimulating scientific discussions and technical and moral support.

Finally, many thanks to my wife Roberta for patience and support during these years spent together.

This thesis is dedicated to my parents and my sisters Rima and Dalia.

ABSTRACT

Whole-cell patch clamp recordings were performed on hypoglossal motoneurons (HMs) in a brainstem slice preparation from the neonatal rat brain. The aim was to study membrane currents activated by membrane depolarization and/or Ca^{2+} under voltage clamp conditions. In addition, the function of membrane currents was investigated under current clamp experiments or by computer simulations.

Fast transient Na^+ current (I_{Na}) was investigated under voltage clamp in low extracellular Na^+ solution. I_{Na} activated at membrane potentials positive to –45 mV and was halfmaximally activated at –30 mV. I_{Na} quickly activated (1- 4 ms τ) and inactivated (1.6 ms τ at 0 mV) during depolarization. Inactivation was strongly voltage dependent (half inactivation was –44 mV) and recovery from inactivation was biexponential with fast and slow τ values of 14 and 160 ms, respectively, at -58 mV.

In a Ca^{2+} free medium containing TTX and Cs^+, depolarizing voltage commands from a holding potential of -50 mV induced slow K^+ currents (I_{Kslow}) with τ= 34 ms onset at 0 mV and minimal decline during a 1 s pulse depolarization. When the depolarizing command was preceded by a prepulse to -110 mV, the outward current became biphasic as it comprised a faster component (I_{Kfast}), which could be investigated in isolation by subtracting the two sets of records. I_{Kfast} showed rapid kinetics (2.3 ms activation and 70 ms inactivation τ at 0 mV) and strong voltage-dependent inactivation (half inactivation was at -93 mV) from which it readily recovered with a biexponential timecourse (4.4 and 17 ms τ at -110 mV membrane potential). I_{Kslow} was selectively blocked by TEA (10-30 mM) while I_{Kfast} was preferentially depressed by 2-3 mM 4-aminopyridine. The medium afterhyperpolarization (mAHP) was always present after single or multiple spikes, making it suitable for studying its role in firing behavior. At resting membrane potential (–69 mV) mAHP (23 ms rise and 150 ms decay τ) had 9.5 mV amplitude, was suppressed in Ca^{2+}-free medium or by 100 nM apamin, and reversed at –94 mV membrane potential. These observations suggest that mAHP was due to activation of Ca^{2+}-dependent, SK-type K^+ channels. Carbachol (10-100 μM) reversibly and dose dependently blocked the mAHP and depolarized HMs. Similar mAHP block was produced by muscarine (50 μM). In control solution a constant current pulse induced HM repetitive firing with small spike frequency adaptation, while the same current pulse evoked much higher frequency

firing with strong spike frequency adaptation in apamin. Voltage clamp experiments demonstrated a slowly deactivating, apamin-sensitive K^+ current (I_{AHP}) which could account for the mAHP. I_{AHP} was activated by depolarization as short as 1 ms, decayed with a τ of 154 ms at -50mV, and was also blocked by 50 μM carbachol.

HMs possess metabotropic glutamate receptors, activation of which depolarized HMs, but apparently did not influence discharge pattern. In addition, activation of these receptors depressed evoked glutamatergic synaptic currents, especially their paired pulse facilitation perhaps via presynaptic metabotropic glutamate receptors.

In summary, these data suggest that I_{Na} current was responsible for the fast upstroke of action potential, while slow inactivation of I_{Na} might contribute to spike frequency adaptation. mAHP had an important role for controlling firing behavior as clearly demonstrated after its pharmacological block, and was potently modulated by muscarinic receptor activity. In addition, membrane depolarization activated distinct K^+ conductances which, in view of their largely dissimilar kinetics, are likely to play a differential role in regulating the firing behavior of HMs. Muscarinic or metabotropic glutamate receptors activation during various behavioral states is supposed to contribute to HM excitability changes in vivo.

INTRODUCTION

1. HYPOGLOSSAL MOTONEURONS CONTROL TONGUE MUSCLES

1.1. Hypoglossal motoneurons (HMs) innervate tongue muscles

In mammals motoneurons of the hypoglossal motor nucleus (nXII) are responsible for movements of the tongue and, thus, play a role in vital physiological functions like swallowing, suckling, or mastication (Lowe 1981). Due to the critical position of tongue in the upper airways, HMs are also important for the respiration function. The upper airways not only convey air to and from the lungs, but they also warm up, humidify and filter air and are involved in cough, swallowing and speech (Lowe 1981).

To perform all these functions, the tongue must be able to assume a variety of shapes and positions within the oral cavity. Its complex muscular structure enables it to do so. The tongue is composed of both extrinsic and intrinsic muscles, which are mainly innervated by motoneurons of nXII (Lowe 1981). A small number of axons arriving from the facial and ambiguus brain stem nuclei also contribute to the hypoglossal nerve, but, their muscular target is not known (O'Reilly and Fitzgerald 1990; Sokoloff and Deacon 1992). Extrinsic muscles originate from bony attachments to insert themselves to the body of the tongue, and their primary function is to position the base of the tongue. Extrinsic muscles include styloglossus and hyoglossus, both tongue retractors, and genioglossus, the primary tongue protrusor. Intrinsic muscles have no bony attachments as they are fully contained within the body of the tongue. These muscles are oriented along the tongue's transverse, vertical, and longitudinal axes. The intrinsic muscles shape the body and tip of the tongue. Co-ordination of extrinsic and intrinsic muscle activity is required for the execution of precise tongue movements.

A defined pattern of rhythmic HM activity is correlated with the respiratory rhythm generated in close proximity to the nucleus ambiguus in the pre-Bötzinger complex of the lower brainstem (Johnson et al. 1994; Smith et al. 1991, 1992). Rhythmic inspiratory-related activity of HM has been monitored in different experimental systems, including *in vivo* recordings in various mammals (Kubin et al. 1996; Okabe et al. 1994; Pierrefiche et al. 1997; Richmonds and Hudgel 1996), *in vitro* recordings of en bloc preparations containing the brainstem and spinal cord (Suzue 1984), and

patch-clamp recordings from brain stem slice preparations (Elsen and Ramirez 1998; Frermann et al. 1999; Lips and Keller 1998; Smith et al. 1991).

Considerable interest is centered on HMs because their dysfunction may result in diseases like obstructive sleep apnoea or sudden infant death syndrome (Gauda et al. 1987; Wiegand et al. 1991; Willinger 1989). Developmental abnormalities in the control of tongue musculature have been implicated in upper airway obstruction pathophysiology, including apnoea of prematurity (Gauda et al. 1987), a significant risk factor for the occurrence of sudden infant death syndrome. Even in normal individuals there is some collapse of upper airways with increased airway resistance during sleep: this may be exaggerated in obstructive sleep apnoea, in which collapse is so greet that arousal from sleep is required to restore adequate ventilation. The resulting disturbed sleep and hypoxia produce daytime sleepiness plus neurophysiological and cardiorespiratory morbidity (Pierce and Worsnop 1999; Wiegand and Zwillich 1994).

Moreover, HMs have a very special vulnerability to calcium-related excitotoxic stress (Doble 1995; Krieger et al. 1994; Reiner et al. 1995). In this context cell-specific homeostasis of intracellular calcium has been implicated as one important cause for such a neuronal vulnerability (Ho et al. 1996; Kiernan and Hudson 1991; Krieger et al. 1996). Interestingly, the degenerative motoneuron disease amyotrophic lateral sclerosis (ALS) has been shown to affect preferentially some brainstem motoneuron groups (for example hypoglossal, trigeminal, facial, and ambiguous; DePaul et al. 1988), which do not contain the Ca^{2+}-chelating protein parvalbumin, while motoneurons containing this protein are more resistant to ALS (Reiner et al. 1995). Recent studies have demonstrated low Ca^{2+} buffering capacity in HMs (Lips and Keller 1998). This finding raises the possibility that motoneuron death in ALS is related to some factor that promotes cytosolic Ca^{2+} accumulation in motoneurons (Krieger et al. 1996; Medina et al. 1996).

1.2. Functional implications of motoneuron firing

Each mammalian muscle is controlled by a certain group of motoneurons. Smooth, co-ordinated movement is activated by two mechanisms often used in parallel. One is to vary the number of activated motor units (recruitment) and the other one is to modulate the discharge rate of already recruited units (rate gradation) (Gustafsson and Pinter 1985). Both mechanisms relay on the discharge properties of motoneurons.

Since most muscles are highly heterogeneous in terms of muscle fibre properties, there is a broad range of activity ranging from the slower motor units which often are weak in terms of strength but are fatigue resistant to the faster units which are strong, yet prone to fatigue (Bakels and Kernell 1993; Burke 1981; Gardiner 1993). During normal motor behaviour the weakest and slowest units are those most easily recruited and the strongest ones are mainly employed for short lasting periods of forceful contractions (Henneman and Mendell 1981). Both recruitment and rate gradation are strictly linked to the excitability of motoneurons.

'The size principle' has been the first attempt to relate variations in motoneuron excitability to the variation in muscle unit tension (Henneman and Mendell 1981). The rationale is that, since smaller motoneurons possess less surface area, their higher input resistance requires less synaptic input to initiate action potentials. According to the 'size principle', the motoneuron pool should consist of a relatively large number of small neurons that innervate many low-tension units and a successively decreasing number of larger motoneurons that innervate fewer high-tension fibres (Henneman and Mendell 1981). Available evidence is, however, not consistent with the wide and skewed distribution of motoneuron size implied by this description. The soma diameter appears to be normally distributed (Curtis and Appenteng 1993; Ulfhake and Kellerth 1983), even if a study has demonstrated that the dendritic trees of motoneurons projecting to fast- twitch muscle units are relatively more extensive than those of motoneurons projecting to slow-twitch units (Gustafsson and Pinter 1984).

As an alternative, variation in motoneuron excitability required for recruitment may be due to differences in intrinsic membrane properties unrelated to motoneuron size. Moreover, the rate gradation would be fully dependent on multiple conductances participating in the control of the resting and active state of motoneurons. Specific inputs, connections with the neighbouring neurons, and characteristic morphology introduce further complexity into the control of neurone behaviour. The difference in spike generating apparatus between motoneurones innervating fast and slow muscle units has been demonstrated (Burke and Nelson 1971; Fleshman et al. 1981; Kernell and Zwaagstra 1980). Also has been established that the twitch contraction time is well correlated with the duration of the motoneuron post-spike afterhyperpolarization (AHP) (Pinter et al. 1983; Zwaagstra and Kernell 1980).

High initial firing rates (with instantaneous frequencies of 50-300 Hz) have been seen in spinal motoneurons during motor behaviour (Hoffer et al. 1987; Kirkwood and

Munson 1996; Kudina and Alexeeva 1992; Zajac and Young 1980). Initial firing at high frequency may permit motoneurons to generate extra force at the onset of a contraction (Hennig and Lomo 1987), which overcomes inertia. When near maximal force is reached in some motor units, the fast decrease in frequency (initial phase of adaptation) may prevent excessive discharge (Burke and Nelson 1971; Zajac and Young 1980). On the other hand, the late phase of adaptation can be matched to the progressive increase in twitch contraction time that occurs during prolonged contractions and allows motor units to maintain a given force level with a progressively decreasing activation rate (Bigland-Ritchie and Woods 1984; Bigland-Ritchie et al. 1983). Matching the progressive decrease in motoneuron discharge rates with the increase in motor unit contraction time has been suggested to be a strategy to optimise force production in the presence of fatiguing conditions (Enoka and Stuart 1992; Kernell and Monster 1982; Spielmann et al. 1993).

In some motoneurons plateau-like firing appears during fictive locomotion (Hochman et al. 1994; Schomburg and Steffens 1996) or tonic contractions associated with postural control (Kiehn and Eken 1997). Long-lasting plateau potentials are preferentially found in motoneurons with low thresholds for spike initiation and slow axonal conduction velocity, which underlie most postural tasks (Lee and Heckman 1998a,b). The threshold for somatic activation of plateau potentials in cat spinal motoneurons is lowered by tonic excitatory afferent input, thus, plateau potentials under normal circumstances could play a role in amplifying the recruitment step rather than generating bistable behaviour (Bennett et al. 1998a). Another possible role of plateau potentials is to reduce the need for a steady synaptic drive during maintained postural muscle contraction (Kiehn and Eken 1998). Plateau generation in cat spinal motoneurons exhibits the phenomenon of "warm up", a progressive lowering of threshold for plateau activation with repeated activation (3- to 6-s intervals) (Bennett et al. 1998b). Plateau warm up may represent a form of short-term plasticity in motoneurons that ensures an increased motoneuronal output during repetitive movements, for example, locomotion.

Both in vivo and in vitro investigations of HMs have provided a wealth of information about the underlying electrophysiological parameters, including passive membrane properties at different postnatal stages of development (Berger et al. 1996; Viana et al. 1994), functional characteristics of synapses and their modulation by second messenger systems (O'Brien et al. 1997; Umemiya and Berger 1995b), and various

voltage-dependent conductances (Bayliss et al. 1995; Umemiya and Berger 1994b; Viana et al. 1993a,b).

The activity of HMs is controlled by many inputs including those from related centers in the medulla such as the respiratory and swallowing centers (Lowe 1981; Smith et al. 1991). However, how these inputs are integrated within the nXII is still unanswered. Although the tongue is capable of highly organized and delicate movements, the present neurophysiological knowledge of this system does not yet allow a mechanism-based reconstruction of these precisely coordinated events.

2. Basic intrinsic properties of HMs

The combination of specific types of voltage and ligand activated membrane conductances, their density and localization in certain CNS neurons creates characteristic firing behaviour (Hille 1992; Llinas 1988; Storm 1990). Neuronal membrane properties may be altered during normal development by the removal or addition of channel types (Desarmenien et al. 1993; Spitzer 1991) or as a result of modulation of existing ion channels by neurotransmitters (Nicoll 1988).

To understand the basic properties controlling the firing behaviour of HMs thus requires detailed description of the various voltage-dependent currents of these cells. As shown below, data are available for certain motoneurons but a quantitative analysis of HM currents is still incomplete.

2.1. Action potential and Na^+ currents

Like all motoneurons, HMs fire AP sensitive to TTX (Haddad et al. 1990; Mosfeldt-Laursen and Rekling 1989; Schwindt and Crill 1982; Viana et al. 1993a; Walton and Fulton 1986; Yarom et al. 1985). Studies using sharp electrode recording have demonstrated that adult HMs have an AP lasting 0.6 ms, which is significantly shorter than the AP duration (1 ms) in newborn HMs (measured at midhei; Haddad et al. 1990; Mosfeldt-Laursen and Rekling 1989; Viana et al. 1994, 1995), while spike height (60 to 90 mV) does not vary significantly between neonatal and adult HMs . These values are in the range of those estimated for vagal, facial, trigeminal, and spinal motoneurons (Chandler et al. 1994; Schwindt and Crill 1982; Walton and Fulton 1986; Yarom et al. 1985).

The fast rising AP in motoneurons is mediated by a fast inactivating, TTX-sensitive Na^+ current (I_{Na}) (Barrett and Crill 1980; Sah and McLachlan 1992; Takahashi 1990).

However, the voltage dependence and kinetics of activation of Na^+ current in motoneurons is difficult to study with conventional microelectrodes or with patch-clamp pipettes in whole-cell configuration, because of the complicated structure and long processes of such cells. Their membrane charging is slow so as obtaining good "space and voltage clamp" is difficult. If I_{Na} appears to activate abruptly at potentials around –50 mV (Takahashi 1990), this observation demonstrates its escape from voltage and space clamp. Until now few data about the kinetics of macroscopic I_{Na} in motoneurons of a slice preparation have been available.

Two-electrode voltage-clamp recordings from spinal motoneurons have revealed that somatic I_{Na} activates and inactivates rapidly (inactivation time constant, τ_h= 0.1-1.3 ms) and exhibits steady-state inactivation which varies with membrane potential (Barrett and Crill 1980).

Single channel recordings have demonstrated that the somatic membrane of neonatal rat spinal motoneurons has TTX sensitive, 14 pS conductance channels (Safronov and Vogel 1995). Activation of ensemble averaged I_{Na} occurs between -60 and -20 mV (half-activation at –39 mV with slope factor of 6 mV). Inactivation kinetics have been fitted by a single exponential function (~1-4 ms) with a half-inactivation potential of -82 mV (slope factor –10 mV). The time course of recovery from inactivation at –80 mV potential has been fitted with two exponentials with time constants of 16 ms and 154 ms, suggesting that control of firing frequency in motoneurons may be affected by recovery time from Na^+ channel inactivation.

Another type of Na^+ current, a persistent noninactivating Na^+ current (I_{NaP}), has been found in CNS neurons (Crill 1996) and has been confirmed to be present also in adult ocular, facial and trigeminal motoneurons (Chandler et al. 1994; Nishimura et al. 1989; Rekling and Mosfeldt Laursen 1989). As I_{NaP} activates below spike threshold, it would accelerate subthreshold membrane depolarization up to spike threshold and/or would sustain spontaneous firing.

2.2. Spike after-potentials, K^+, and Ca^{2+} currents

2.2.1. After-potentials and their characteristics. Repolarization of AP is mediated by inactivation of Na^+ channels and activation of several K^+ channel types (McLarnon 1995; Rudy 1988; Storm 1990). Since these K^+ channels have different voltage dependences and kinetic properties, they generate the spike afterpotentials usually

seen in motoneurons (Chandler et al. 1994; Gueritaud 1988; Haddad et al. 1990; Nishimura et al. 1989; Sah and McLachlan 1992; Viana et al. 1993a,b; Walton and Fulton 1986; Zhang and Krnjevic 1987; Yarom et al. 1985).

An intracellularly evoked AP of neonatal HMs is usually followed by an afterhyperpolarization (AHP) consisting of two phases (Viana et al. 1993a,b). The first phase is short lasting (<5 ms) and is a continuation of the repolarization of AP (fast AHP or fAHP). The second phase peaks ~20 ms after the AP and lasts ~100- 200 ms (medium AHP or mAHP). A slow AHP appears after a train of APs (Haddad et al. 1990; Viana et al. 1993b). fAHP and mAHP are separated by a short lasting afterdepolarization (ADP). Analogous afterpotentials have been seen in facial, ocular, and trigeminal motoneurons (Chandler et al. 1994; Gueritaud 1988; Nishimura et al. 1989), while vagal motoneurons exhibit a slow AHP (lasting ~1s) after a single AP (Sah and McLachlan 1992; Yarom et al. 1985).

Both fAHP and mAHP of HMs strongly depend on extracellular K^+ concentration even if fAHP reverses at more positive membrane potential (-63 mV) compared to the reversal potential of mAHP (-89 mV; Viana et al. 1993b). Bath application of a low dose of TEA (1 mM) to neonatal HMs produces a clear prolongation of the AP (by ~90%) and block of the fAHP (Viana et al. 1993b). Increase in TEA concentration to 10 mM further prolonges the AP (by ~300%; Haddad et al. 1990; Mosfeldt-Laursen and Rekling 1989; Viana et al. 1993b). In contrast, the mAHP remains unchanged or even enhanced (Viana et al. 1993b). Another widely used blocker of K^+ channels, 4-AP (0.1-0.5 mM), also causes prolongation of the AP (Viana et al. 1993b). Replacing extracellular Ca^{2+} with Mn^{2+} significantly, albeit weakly, increases spike duration (by ~15%) and almost completely blocks the mAHP (Mosfeldt-Laursen and Rekling 1989; Viana et al. 1993b; Umemiya and Berger 1994a). The bee venom apamin also completely blocks mAHP (Viana et al. 1993b). This result is in contrast with the finding of Haddad et al. (1990) that mAHP was not affected by Co^{2+} or apamin.

Similar pharmacological effects (prolongation by TEA and 4-AP of AP, moderate effect of Ca^{2+} influx block on AP duration, and effective blocking of mAHP by apamin and Ca^{2+} channel blockers) have been found in other cranial and spinal motoneurons (Chandler et al. 1994; Hounsgaard et al. 1988b; Nishimura et al. 1989; Shwindt and Crill 1981; Takahashi 1990; Zhang and Krnjevic 1987). The AP of vagal motoneurons is prolonged by charybdotoxin (Sah and McLachlan 1992).

This pharmacological profile suggests that several K^+ currents like delayed rectifier (I_{KDR}), transient outward (I_A), and Ca^{2+}-activated K^+ currents (I_C, I_{AHP}) participate in the shaping of AP and its afterpotentials in motoneurons like in other central neurons (Llinas 1988; McLarnon 1995; Rudy 1988; Storm 1990).

2.2.2. I_{KDR}. A delayed rectifier type outward K^+ current sensitive to TEA and activated by depolarization, with activation kinetics slower than that of I_{Na}, has been identified in spinal motoneurons (Barrett et al. 1980). Ninety % activation occurs within 5 ms while deactivation has a time constant of 2-4 ms.

Single K^+ channels of the delayed rectifier type (DR-channels) have been observed in patches from the soma of neonatal spinal motoneurons (Safronov and Vogel 1995). They have a ~10-pS channel conductance (in normal Ringer solution), activate between -70 and 0 mV (with half activation of -44 mV and slope factor of 8.5 mV), and deactivate slowly (60 ms τ at 60 mV). However, no selective blocker of these channels has been demonstrated, since TEA, 4-AP, and dendrotoxin all reduce unitary currents in outside out patches (Safronov and Vogel 1995).

2.2.3. I_A. A I_A-like outward K^+ current has been observed in spinal cord, trigeminal, and vagal motoneurons (Hsiao and Chandler 1995; Safronov and Vogel 1995; Sah and McLachlan 1992; Takahashi 1990). This current activates by depolarization, inactivates during depolarization and recovers from inactivation by hyperpolarization (Rogawski 1985; Rudy 1988; Storm 1990). 4-AP has been frequently used as a selective blocker of this current (Rudy 1988). In trigeminal motoneurons (Hsiao and Chandler 1995) bathed with low Ca^{2+} and 20 mM TEA solutions I_A activates at -55 to -60 mV, peaks within 5 ms and decays monoexponentially (6-8 ms τ). Half maximal values for inactivation and activation are -72 mV (slope factor –6 mV) and –37 mV (slope factor 7 mV), respectively. Bath application of 5 mM 4-AP suppresses this current by approximately 90%.

In spinal motoneurons of neonatal rat, I_A activates between -60 and -20 mV (half activation at –36mV with slope factor of 9 mV) and quickly inactivates (half maximal at –87 with slope factor of –13 mV) with a time constant ~15-60 ms (Safronov and Vogel 1995). Single channels have a conductance of ~19 pS in normal Ringer solution and are blocked by both 4-AP and TEA (Safronov and Vogel 1995).

A slower transient K^+ current similar to I_D (Rudy 1988; Storm 1990) has been observed in vagal motoneurons (Sah and McLachlan 1992), and it inactivates with τ of ~400 ms.

2.2.4. I_C and I_{AHP}. Ca^{2+}-activated K^+ currents found in central neurons are the result of activation of large (BK) and small conductance (SK) K^+ channels gated by a rise in intracellular Ca^{2+}, and, in the case of BK channels, also by voltage (Rudy 1988). Both I_C and I_{AHP} are present in motoneurons (Chandler et al. 1994; Hounsgaard et al. 1988b; Kobayashi et al. 1997; Krnjevic et al. 1975, 1979; McLarnon et al. 1995; Mosfeldt-Laursen and Rekling 1989; Nishimura et al. 1989; Safronov and Vogel 1998; Takahashi 1990; Umemiya and Berger 1994a; Viana et al. 1993b).

In patches from cultured mouse motoneurons (McLarnon et al. 1995), BK channels have large conductance (240 pS in symmetrical K^+). Their activation has a sigmoidal dependence on potential and their open probability is enhanced with increasing Ca^{2+} concentrations. BK channels inactivate with time constant of 40 ms at low Ca^{2+} concentration (0.5 μM) and are blocked by external TEA.

Unitary Ca^{2+}-activated K^+ currents of the BK type in somatic membrane patches of rat spinal motoneurons (Safronov and Vogel 1998) have a conductance of 82 pS in normal Ringer solution and are activated by intracellular Ca^{2+} and depolarization. They activate rapidly (within 2-3 ms at +50 mV), do not inactivate with 100 μM internal Ca^{2+}, and are blocked by external TEA and charybdotoxin.

I_{AHP} is a Ca^{2+}-activated, voltage-independent K^+ current blocked by apamin and is the dominant conductance underlying medium and slow afterhyperpolarizations in motoneurons (Chandler et al. 1994; Sah and McLachlan 1992; Viana et al. 1993b; Zhang and Krnjevic 1987).

Unitary single channel currents from SK channels have been detected in the membrane of mouse motoneurons in culture (McLarnon et al. 1995). These unitary currents have a ~18-pS conductance and a 3.5-ms mean open time. The mean open time does not change when the patch is depolarized, thus indicating little or no voltage dependence of kinetic behaviour.

2.2.5. Ca^{2+} currents. At least six types of voltage-gated Ca^{2+} channels (L, N, P, Q, R, and T types) are expressed in CNS neurons generating two types of macroscopic Ca^{2+} currents (Randal and Tsien 1997; Tsien et al. 1991). One referred to as HVA Ca^{2+} current activates at high voltages and is apparently non inactivating. The second one

is transient and activates at low voltage (LVA Ca^{2+} current; Randal and Tsien 1997; Tsien et al. 1991).

Ca^{2+} currents participate in the shaping of the AP and its afterpotentials directly and indirectly. Influx of Ca^{2+} activates BK and SK channels (McLarnon 1995). The ADP seems to be the direct expression of Ca^{2+} conductances in HMs, since this hump depolarization during spike repolarization is more prominent in high extracellular Ca^{2+} solutions (4-8 mM) and is abolished when Ca^{2+} is replaced with Mn^{2+} (Viana et al. 1993a). Moreover, HMs are able to generate Ca^{2+} dependent spikes in the presence of TEA and/or TTX (Mosfeldt Laursen and Rekling 1989; Viana et al. 1993a). Pharmacological dissection has demonstrated that ADP results from activation of both LVA and HVA currents, while mAHP is dependent on HVA Ca^{2+} channels (Kobayashi et al. 1997; Umemiya and Berger 1994a; Viana et al. 1993b).

The pharmacological and single-channel properties of motoneuronal Ca^{2+} channel subtypes have been investigated in detail in neonatal HMs (Umemiya and Berger 1994a, 1995a). Three types of high-voltage-activated (HVA; L, N, and P type) and one type of low-voltage-activated (LVA; T type) Ca^{2+} channel types are present in the membrane of HMs (Umemiya and Berger 1994a), with single-channel conductances (with 110 mM Ba^{2+} as charge carrier) of 28 pS (L type), 14 pS (N type), 20 pS (P type), and 7 pS (T type). L- and P-type channels do not inactivate, whereas T- and N-type channels do (τ= 20 and 58 ms, respectively).

Voltage clamp recordings of macroscopic Ca^{2+} currents in HMs have revealed the transient (LVA) and persistant (HVA) components (Bayliss et al. 1995; Umemiya and Berger 1994a). The total Ca^{2+} current reaches its peak relatively slowly in 19 ms and inactivates during depolarization with a time constant of 30 ms at –40 mV, while at 0 mV these values are 7 and 730 ms, respectively (Umemiya and Berger 1994a). Pharmacologically isolated LVA current peaks at 14 ms (at –40 mV) and at 8 ms (at 0 mV), while inactivation time constant is 36 ms at 0 mV. Half activation voltage is –29 mV, while half inactivation potential is –62 mV for the currents activated at –40 mV (Umemiya and Berger 1994a).

Spinal and facial motoneurons also have HVA and LVA Ca^{2+} channel types in their somatic membrane (Hounsgaard and Mintz 1988; Mynlieff and Beam 1992; Plant et al. 1998). However, the HVA P-type channel is absent in the somatodendritic

membrane of facial motoneuron, and a novel type (R_{slow}) carries a major component of the total HVA Ca^{2+} current (Plant et al. 1998).

2.3. Repetitive firing

2.3.1. Frequency-current relation. When a HM is stimulated by a just suprathreshold current, it discharges at a minimum rate of steady firing (Mosfeldt-Laursen and Rekling 1989; Viana et al. 1995). A further increase in current intensity causes an increase in steady discharge rate with a linear frequency-current relation (f-I). The f-I has been shown to be composed by two linear ranges in spinal motoneurons (Baldissera and Gustafsson 1974b; Kernell 1965b; Schwindt 1973). The first one (from minimal firing frequency upwards) is referred to as 'primary range'. At high firing rates the f-I curve deviates in an upward direction, indicating that the cell becomes more sensitive to changes in excitatory input. Firing at these higher rates has been referred to as 'secondary range' (Baldissera and Gustafsson 1974b; Kernell 1965b; Schwindt 1973). In cat lumbosacral motoneurons, the secondary range starts when steady-state firing reaches ~50 spikes/s, with a slope 2-6 times that of the primary range (Kernell 1965b). HMs and many other cranial motoneurons (for example facial, trigeminal, and phrenic) lack the secondary range at steady state, with a linear f-I relationship over the entire firing range (Jodkowski et al. 1988; Moore and Appenteng 1990; Mosfeldt-Laursen and Rekling 1989; Nishimura et al. 1989). HMs exhibit minimal firing rate in the range 10- 20 spikes per second with a firing slope of ~30 Hz/nA and ~15 Hz/nA for neonatal and adult HMs, respectively, as calculated from f-I relations of steady-state firing (Haddad et al. 1990; Mosfeldt-Laursen and Rekling 1989; Nunez-Abades et al. 1993; Sawczuk et al. 1995; Viana et al. 1993b, 1995). Similar values have been found for facial and trigeminal motoneurons (Chandler et al. 1994; Nishimura et al. 1989).

2.3.2. Spike frequency adaptation. In general, motoneurons fire with high frequency only for a brief initial period just after the abrupt onset of stimulation. After that there is a rapid decline in firing rate (initial adaptation; Granit et al. 1963; Kernell 1965a,b). Often an initial doublet (two spikes at short interval (<20 ms)) at the onset of a long current pulse occurs, which is part of the initial adaptation phase (0.5-1 s) during which the firing frequency drops sharply, and is followed by a phase of slow frequency decline referred to as 'late adaptation' (0.5-1 min; Kernell 1965a; Kernell and Monster 1982).

Adult HMs exhibit three adaptation phases (Sawczuk et al. 1995, 1997). The initial phase is linear in time, lasts tens of milliseconds, and is complete after the first few spikes. The early and late phases of adaptation can be described by two exponentials with mean time constants of 250 ms and 20 s, respectively (Sawczuk et al. 1995, 1997).

In contrast to adults, neonatal HMs do not show strong spike frequency adaptation (Viana et al. 1993b). An extensive study of repetitive firing in neonatal HMs has revealed three groups of cells which differ in their type of firing pattern (Viana et al. 1995). In about 40% of neonatal HMs, the discharge rate is maximal at the beginning of a constant current step, after which it declines to steady-state. Most of the decline occurs during the first 200 ms, but, after this early adaptation, firing frequency continues to drop albeit at a slower rate. In 20% of neonatal HMs a completely different discharge pattern is observed in response to a constant current step (Viana et al. 1995). In these HMs the first interspike interval is the longest one as neurons show progressive acceleration to steady-state firing rate. In 25% of recorded neurons the accelerating phase is followed by adaptation. Among the remaining cells 8% show no firing frequency modulation at all and 8% have complex firing patterns (Viana et al. 1995). mAHP decreases in amplitude during the trains of APs in accelerating HMs, while the same trains cause mAHP amplitude to increase in HMs with spike frequency adaptation. Progressive AP prolongation during repetitive firing is observed in adapting HMs (Viana et al. 1995).

The mechanisms involved in the spike frequency adaptation are still not clear. It has been proposed that an increase in the magnitude and duration of spike AHP contributes to the initial adaptation (Baldissera et al. 1978; Barrett et al. 1980; Viana et al. 1995), which is dependent on Ca^{2+} entry (activating I_{AHP}) during the first few spikes (Sawczuk et al. 1997). However, block of Ca^{2+} influx does not entirely abolish initial adaptation. Late adaptation is also not abolished by Ca^{2+} channel blockers; it actually increases with these treatments (Sawczuk et al. 1997; Viana et al. 1993b), indicating that a number of Ca^{2+}-independent mechanisms contribute to late adaptation. Spike duration lengthening and spike amplitude decrease during repetitive firing (Viana et al. 1995) indicate some AP conductance changes during maintained firing. These changes may be achieved by progressive increase/decrease in an outward/inward current, an issue not yet resolved in HMs.

2.3.3. Bistable firing. Some motoneurons show an ability to generate repetitive firing that outlasts the current injection (Conway et al. 1988; Crone et al. 1988; Eken et al. 1989; Hounsgaard et al. 1986, 1988a; Hsiao et al. 1998; Lindsay and Feldman 1993; Schwindt and Crill 1980a). Plateau potentials underlie this behavior, which can be elicited in motoneurons by either short trains of excitatory synaptic input or current injection. In most motoneurons, plateau potential is a property unmasked by neuromodulators, such like glutamate (acting through metabotropic glutamate receptors), 5-HT, norepinephrine, and dopamine (Conway et al. 1988; Crone et al. 1988; Delgado-Lezama et al. 1997; Hounsgaard et al. 1988a; Hsiao et al. 1998; Svirskis and Hounsgaard 1998). An HVA Ca^{2+} current, possibly located in the dendrites, is the proposed ionic mechanism for generation of these plateau potentials in motoneurons (Hounsgaard and Kiehn 1989, 1993; Hsiao et al. 1998; Lee and Heckman 1996). Perturbations of the balance between inward and outward currents by neurotransmitters, which may decrease outward K^+ currents, can lead to plateau potentials and bistable membrane behavior by uncovering inward HVA Ca^{2+} currents (Delgado-Lezama et al. 1997; Hounsgaard et al. 1988a; Svirskis and Hounsgaard 1998).

Other mechanisms may also produce plateau potentials. Motoneurons in the nucleus ambiguus have a Ca^{2+}-activated Na^+ current that produces prolonged firing in response to brief afferent input or current injection (Partridge et al. 1994).

Plateau potentials have been observed in adult HMs in artificial conditions (Mosfeldt-Laursen and Rekling 1989). Addition of Ba^{2+} and Cs^+, known to block K^+ currents, unmask a plateau potential outlasting the current step. This plateau persists in TTX solution, thus suggesting that a slow inward current probably produced by Ba^{2+} flow through Ca^{2+} channels is responsible (Mosfeldt- Laursen and Rekling 1989). Interestingly, in motoneurons of prepositus hypoglossus (ocular motor nucleus) the TTX-sensitive plateau potential is evoked in the presence of Cs^+ and Co^{2+} (Rekling and Mosfeldt Laursen 1989).

2.4. Active and passive membrane properties below AP threshold

2.4.1. V_{rest} and R_{in}. The resting membrane potential (V_{rest}) and input resistance (R_{in}) of HMs have been estimated to be in range –63 to –73 mV and 13-85 MΩ, respectively (Haddad et al. 1990; Mosfeldt-Laursen and Rekling 1989; Nunez-Abades

et al. 1993; Sawzcuk et al. 1995; Viana et al. 1994, 1995). These measurments have been done using sharp intracellular electrodes. It has been demonstrated that using patch pipettes leads to higher values of V_{rest} and R_{in} (Spruston and Johnston 1992; Staley et al. 1992). This difference has been proposed to be due to electrode induced leak, which is larger with sharp electrodes. Average V_{rest} and R_{in} of HMs measured with a patch pipette are -64 mV and 129 MΩ, respectively (Robinson and Cameron 2000). R_{in} tends to increase during the recording time, perhaps because of a significant washout of intracellular mediators controlling ion permeability.

These V_{rest} values suggest that main factor controlling the resting state of the membrane is K^+ permeability. The relative contribution by Na^+, K^+, and Cl^- leak conductances to spinal motoneurons has been estimated as $g_{Na}/g_K = 0.13$ and $g_{Cl}/g_K = 0.25$ (Forsythe and Redman 1988). Active ionic currents, such as the hyperpolarization-activated inward current (I_h), inward rectifier K^+ current (I_{KIR}), I_A, I_C, and I_{AHP} may also contribute to V_{rest} (Bayliss et al. 1994b; Hsiao and Chandler 1995; Krnjevic et al. 1975; Talley et al. 2000; Topert et al. 1998).

2.4.2. I_h. A common membrane property of many central neurons is inward rectification, namely a conductance increase upon hyperpolarization from V_{rest} (Hille 1992). Two general types of inwardly rectifying currents have been described. One type referred to as I_h is a slowly activating, non-inactivating, nonspecific cationic current with reversal potential more depolarized than resting membrane potential (Pape 1996). I_h has been found in HMs as well as in some other motoneurons (Aghajanian and Rasmussen 1989; Barrett et al. 1980; Bayliss et al. 1994a; Chandler et al. 1994; Mosfeldt-Laursen and Rekling al. 1989; Nishimura et al. 1989; Takahashi 1990). In HMs I_h has relatively slow activation kinetics (~100-400 ms), a reversal potential positive (~40 mV) to resting membrane potential, and is blocked by Cs^+ (Bayliss et al. 1994a). This current underlies the time dependent depolarizing "sag" or rebound evident in voltage responses to hyperpolarizing current pulses, which (in combination with Ca^{2+} currents) may even generate APs (Bayliss et al. 1994a; Mosfeldt-Laursen and Rekling 1989; Nunez-Abades et al. 1993; Viana et al. 1993a, 1994). I_h may be partially active at rest, thereby contributing to resting membrane potential (Bayliss et al. 1994a). The AHP or a hyperpolarizing inhibitory synaptic input can activate I_h, which in turn can shorten these hyperpolarizations, thus stabilizing the membrane potential.

2.4.3. I_{KIR}. Another class of inwardly rectifying current, I_{KIR}, has a more hyperpolarized range of activation, faster kinetics, much greater sensitivity to Ba^{2+} and is selectively mediated by K^+ (Hille 1992; Rudy 1988). In some neurons I_{KIR} is active at resting membrane potential, giving rise to a steady outward current, which is in balance with the leak inward current. When the membrane is relatively unperturbed, this equilibrium ensures that the membrane potential is stable near E_K. However, if the membrane is depolarized, I_{KIR} deactivates, thus releasing the membrane to depolarize further.

Recently, several novel inwardly rectifying K^+ channels ($Kir_{2.1}$, $Kir_{2.2}$, $Kir_{2.4}$, GIRK1-3) have been identified in HMs (Topert et al. 1998). In neonatal HMs, block of $I_{Kir2.2}$ and $I_{Kir2.4}$ by extracellular Ba^{2+} leads to depolarization and firing, suggesting that these and related conductances contribute to motoneuronal resting membrane potential.

2.5. Modulation of HMs

2.5.1. Inputs to hypoglossal nucleus (nXII). Sensory information from several muscles is relayed to the nXII through other nuclei. Information from mastication muscles reaches the nXII via the trigeminal mesencephalic nucleus (Raappana and Arvidsson 1993). Afferent information from other peripheral sensors enters the brain stem through vagal, glossopharyngeal, and accessory nerves and is conveyed to the nXII via premotor neurons in the nucleus of the solitary tract (Beckman and Whitehead 1991; Borke et al. 1983; Lowe 1981; Travers and Norgren 1983). A third major sensory afferent input to the nXII is from the spinal trigeminal complex (Borke et al. 1983; Travers and Norgren 1983). The largest concentration of hypoglossal premotor neurons is ventrolateral and dorsolateral within the medullary reticular formation (Borke et al. 1983; Dobbins and Feldman 1995; Travers and Norgren 1983). A smaller number of premotor neurons upstream to the nXII are located in pontine nuclei, periaqueductal gray of the midbrain, periambigual region, and gigantocellular reticular nucleus (Dobbins and Feldman 1995; Li et al. 1997; Ono et al. 1994; Takada et al.1984; Travers and Norgren 1983; Yang et al. 1995).

Some premotor neuron groups projecting to the nXII are involved in dedicated motor tasks. The central subnucleus of the solitary tract contains the pattern generator for swallowing and conveys direct synaptic information to HMs and related motoneurons (Amri and Car 1988; Barrett et al. 1994). The pre-Botzinger complex, a respiratory

rhythm generating region in brainstem, has direct contact with HMs (Funk et al. 1993; Smith et al. 1991).

Thus, HMs are the target for various transmitters (amino acids, amines, peptides). The largest part of premotor neurons are GABAergic, glycinergic, or glutamatergic (Li et al. 1997). Glutamate, GABA, and glycine acting on ionotropic receptors mainly participate in fast transmission of input signals. The modulation of glutamatergic transmission on HMs has been extensively studied (Bellingham and Berger 1994, 1996; Singer et al. 1996). However, the role of glutamate as well as glycine and GABA on synaptic integration and interaction with intrinsic membrane properties of HMs are still poorly investigated (Poliakov et al. 1996, 1997). Establishing of the role of glutamate in synaptic signaling is complicated, due to the presence of both ionotropic (NMDA and non-NMDA types) and metabotropic receptors (mGluR) on HMs (Hay et al. 1999; Martin et al. 1993; Monaghan and Cotman 1985; Shaw et al. 1992). However, the functional role of NMDA, non-NMDA, and mGluR activation remain unknown. Both glycine and GABA activate Cl^- permeable channels (O'Brien and Berger 1999; Singer et al. 1998), thus producing inhibitory action on HMs. No study has been centered to distinguish the consequence of these two receptor activation on HMs excitability.

Noradrenergic input to the nXII comes from neurons in three pontine regions, nucleus subcoeruleus, A7 and A5 cell groups (Aldes 1990; Aldes et al. 1992). The raphe pallidus, obscurus, and magnus are the main regions containing 5-HT-positive neurons projecting to the nXII (Li et al. 1993; Manaker and Tischler 1993; Manaker et al. 1992). The raphe nuclei also contain premotor neurons positive for several neuropeptides. Substance P-like immunoreactive neurons projecting to nXII are in the caudal raphe and Met-enkephalin-like immunoreactive premotor neurons are in the caudal raphe and medial reticular formation (Henry and Manaker 1998).

2.5.2. Modulation of HMs by metabotropic receptors. Activation of metabotropic receptors may modulate input signals (via presynaptic targets) as well as intrinsic membrane properties, thus determining the generation of output signals. Activated metabotropic receptors initiate second messenger cascades that may have multiple effects, many of which can utilize the same signal transduction mechanisms, or affect the same target, such as a specific type of channel (Hille 1992).

The modulation of HMs by activation of norepineprine (NE) and serotonin (5-HT) has been investigated (Bayliss et al. 1995; Berger et al. 1992; Parkis et al. 1995; Talley et

al. 1997). Both NE and 5-HT acts directly by depolarizing HMs (Berger et al. 1992; Parkis et al. 1995; Talley et al. 1997). In addition, 5-HT markedly reduces mAHP, presumably via a reduction in N- and P-type Ca^{2+} currents (Bayliss et al. 1995; Berger et al. 1992). A presynaptic reduction of glutamatergic and glycinergic synaptic transmission by activation of 5-HT_{1B} receptors has been observed (Singer et al. 1996; Umemiya and Berger 1995b). The increased excitability of HMs by NE and 5-HT is compatible with the fact that release of NE and 5-HT is increased during the normal waking state (Jacobs and Azmitia 1992) and make these neurons ready to respond to excitatory input. On the contrary, HMs become more resistant to the same input during sleep when NE and 5-HT release is decreased.

In the CNS the action of ACh, liberated at cholinergic synapses, is mediated by muscarinic and nicotinic receptors. Activation of muscarinic receptors can result in either excitation or inhibition due to modulation of ongoing currents. Although this mechanism is indirect and slow, it can still be a powerful effect, because of background K^+ and Cl^- currents. HMs use ACh as their muscle transmitter, but they also possess high levels of muscarinic receptors as revealed by autoradiographic studies (Rotter et al. 1979; Walmsley et al. 1981). The medullary reticuler formation is a likely source of cholinergic input to nXII (Connaughton et al. 1986). The cholinergic terminals lack conventional postsynaptic specializations (Connaughton et al. 1986). These findings suggest a direct action of ACh on HMs, although studies demonstrating this effect are lacking. A presynaptic reduction by carbachol and muscarine of glutamatergic transmission on HMs has been reported (Bellingham and Berger 1996).

3. Simulation study of motoneuron properties

3.1. Modelling as tool for neuron investigation

Membrane conductances are usually characterised by protocols designed to describe them using a combination of electrophysiological, pharmacological and kinetic tools. However, all these experimental approaches have limitations. For example, sensitivities to various drugs and the time scale for activation/inactivation may overlap amongst different conductances. Even in the ideal case of a totally selective pharmacological block of a certain conductance, data should be interpreted with caution, since neurons can utilise various mechanisms to compensate for the lack of such a conductance. Computer simulations of neuronal activity can thus provide a

useful adjunct to experimental work, as they offer the reconstruction of integrated electrical behaviour and predict certain properties.

Hodgkin and Huxley introduced a remarkably successful quantitative description of action potentials (Hodgkin and Huxley 1952). The success of the Hodgkin-Huxley (HH) model of the squid axon has been due to the system simplicity, as its components (Na^+ and K^+ conductances) have been well separated and parameters have been easily evaluated from voltage clamp experiments. More recent techniques revealed that the assumptions of the HH model were essentially correct if reinterpreted in the light of current knowledge about ion channels (Hille, 1992) and remain the most widely used description of voltage-dependent conductances (Borg-Graham 1998). Extension of HH model to neurons leads to several complications (large number of conductances, difficulties in isolating them, imperfect space and voltage clamp). Moreover, there is increasing evidence that the simple HH kinetic model is inadequate for certain neuronal currents, thus prompting a revision of kinetic schemes (Clay 1998; Klemic et al. 1998; Schoppa and Sigworth 1998).

3.2. Motoneuron models

Several motoneuron properties have been studied using computer simulations (Baldissera and Gustafsson 1974a; Baldissera and Parmiggiani 1979; Kernel and Sjoholm 1972, 1973; Lüscher and Larkum 1998; Powers 1993; Safronov et al. 2000). Baldissera and Gustafsson (1974a), Baldissera and Parmiggiani (1979), Kernel and Sjoholm (1972, 1973) have attempted to reproduce the firing adaptation pattern of cat spinal motoneurons. They have included the Na^+ and K^+ conductances taken from axon studies (Frankenhaeuser and Huxley 1964; Hodgkin and Huxley 1952) and have adjusted them to fit motoneuron firing. In addition, the current underlying Ca^{2+} sensitive AHP has been modeled and included into the model motoneuron. In this way spike frequency adaptation affecting only the few first interspike intervals has been reproduced. This result confirms the experimental finding that mAHP alone is not able to produce all ranges of adaptation (Sawczuk et al. 1995, 1997; Viana et al. 1993b) and invites the search for other mechanisms involved in spike frequency adaptation.

A motoneuron model has been developed to relate biophysical features of cat spinal motoneurons to motoneuron discharge behaviour (Powers 1993). It has included realistic voltage dependency for the K^+ currents and a low-threshold Ca^{2+} conductance

(found in α- motoneurons of spinal cord) plus a function describing the threshold change during repetitive firing as indeed observed in experiments (Barrett et all. 1980, Schwindt and Crill 1980a,c, 1982). In this model an AP of fixed waveform occurs whenever the membrane potential exceeds a specified threshold value. This simplification speeds simulations, but, on the other hand, it could underestimate the development of K^+ and Ca^{2+} conductances during the AP and the resulting changes in AP shape. The model has been able to replicate some characteristics of repetitive discharge behaviour of real motoneurons, such like first interspike and steady-state frequency-current intensity (f-I) relations, relation between total membrane current and membrane voltage (I-V), and bistable discharge of motoneurons.

Safronov et al. (2000) have simulated the generation of action potentials in the two compartment spinal cord motoneuron by using experimental data on Na^+ and K^+ channel densities in the soma and in the remaining part of neuron (the axon and the dendritic tree; Safronov et al. 1999; Wolff et al. 1998). This model confirms the experimental observation that soma itself has low density of Na^+ channels and unable to generate an AP.

4. AIMS OF THE STUDY

As discussed in the previuos sections, the motoneuron is one important cell model to study patterns of normal motor behaviour and its dysfunctions. In particular, rat HMs have recently attracted much attention due to their survival in *in vitro* conditions which allow detailed studies of many cellular properties and mechanisms in a well controlled experimental environment. Understanding their membrane conductances and their interplay in generating repetitive firing may help to clarify the excitability and operation of these cells and their special vulnerability to certain pathologies.

The aim of the present study was to investigate the mechanisms responsible for the control of excitability of HMs, particularly the pattern of repetitive firing. For this purpose the experiments were designed to isolate and characterize the membrane voltage activated conductances. Further, the question how these currents control HMs behavior and particularly their repetitive firing was addressed by means of experiments performed under current clamp conditions and computer simulations.

METHODS

1. Slice preparation and identification of the cells

Experiments were carried out using brainstem slices obtained from 0 to 9 day old rats. Thin slices were prepared following the procedure described earlier by Viana et al. (1994). The brainstem was isolated from neonatal rats and placed into modified ice-cold Krebs solution (see below). A tissue block containing the lower medulla was then fixed (with insect pins) onto an agar block inside a Vibratome chamber filled with ice-cold Krebs solution (bubbled with 95% O_2- 5% CO_2) to obtain 200 μm thick slices. Slices were first transferred to an incubation chamber for 1 h at 32°C under continuous oxygenation and subsequently maintained at room temperature for at least 1 h before use.

Brainstem slices placed in a small recording chamber were viewed with an infrared video camera to identify single HMs within the nXII. The nXII was clearly visible through a Zeiss Axioscope microscope under x10 magnification. Magnification x40 allowed to visualize single HMs, which usually had fusiform soma with 1 to 3 major dendrites. In some experiments neurobiotin (0.2%) was injected into HMs through the recording patch pipette. The motoneurons so prepared had large soma (30- 60 μm diameter) with 3-6 stem dendrites extended out into surrounding nXII. Motor axons followed the route of the XII cranial nerve and usually terminated as a black dot.

2. Solutions and drugs

2.1. Slice cutting and maintenance. For slice preparation and maintenance (mM): NaCl 130, KCl 3, $NaHCO_3$ 26, Na_2HPO_4 1.5, $CaCl_2$ 1, $MgCl_2$ 5, glucose 10, L-ascorbic acid 0.4 (290-310 mOsm).

2.2. Current clamp recordings. For current clamp recordings extracellular solution [A] contained (mM): NaCl 140, KCl 3, $CaCl_2$ 2, $MgCl_2$ 1, HEPES 10, glucose 10. Patch pipette solution [B] contained (mM): K-methyl-SO_4 110, KCl 20, NaCl 10, $MgCl_2$ 2, HEPES 10, EGTA 0.5, ATP-Mg 2.

2.3. Ca^{2+}-dependent K^+ current voltage clamp recordings. The same solutions (extracellular [A] and patch pipette [B]) as in current clamp experiments were used to record Ca^{2+}-dependent K^+ currents.

2.3. Voltage activated K^+ current voltage clamp recordings. For the voltage-activated K^+ current recordings the same extracellular solution [A] as in current clamp experiments was used. The patch pipette solution [C] contained (mM): K-gluconate 110, KCl 20, NaCl 5, $MgCl_2$ 2, $CaCl_2$ 1, HEPES 10, EGTA 10, ATP-Mg 2.

2.4. Voltage activated Na^+ (I_{Na}) current voltage clamp recording. Initial extracellular solution [D] for recording of I_{Na} contained: cholineCl 60, TEACl 60, NaCl 20, KCl 3, $CoCl_2$ 2, $MgCl_2$ 2, HEPES 10, glucose 10, 4-AP 5. In several experiments cholineCl was replaced with NMDG 60 mM (solution [E]) or sucrose 120 mM (solution [F]) to keep the same osmolarity. Several patch pipette solutions were used depending on the experiment. Standard patch pipette solution [G] to record I_{Na} contained (mM): CsCl 120, NaCl 10, KCl 3, HEPES 10, EGTA 10, MgATP 2. High intracellular NaCl solution [H] was similar to [G], except that NaCl and CsCl concentrations were 40 and 90 mM, respectively. In experiments with high Na^+, the standard solution [A] used in CC experiments was utilized, with added 20 nM TTX.

2.5. pH and osmolarity. All extracellular solutions were buffered to pH 7.4 with NaOH or KOH and were adjusted to have osmolarity in the 300-310 mOsm range. All patch pipette solutions were buffered to pH 7.2 with KOH or CsOH and were adjusted to have osmolarity in the 280-290 mOsm range.

2.6. Liquid junction potential. All potential values were corrected off-line for the liquid junction potential (V_j) between external and internal solutions (Barry and Lynch 1991; Neher 1992). V_j was measured with a 3 M KCl-agar bridge (Neher 1992) for all extracellular and patch pipette solution combinations used in experiments and were as follows: between [A] and [B] (or [C]): 10 mV; between [D] and [G]: 7.7 mV; between [E] and [G]: 4.5 mV; between [F] and [G]: 5.5 mV; and between [F] and [H]: 4.4 mV.

2.7. Drugs. I_{Na} was blocked by tetrodotoxin (TTX; 1-2 μM) in most voltage clamp (VC) experiments. In some experiments QX-314 (5-10 mM) was added to the pipette solution to block I_{Na} and I_h (Perkins and Wong 1995). Alternatively, CsCl (4 mM) was added extracellularly to block I_h. Extracellular $CaCl_2$ was replaced by the same amount of $CoCl_2$ (Ca-free-Co solution) or $CdCl_2$ (200 μM) was added to block Ca^{2+} currents and Ca^{2+} dependent K^+ currents. When TEA or 4-AP was added to the recording solution in concentrations larger than 5 mM, an equivalent concentration of NaCl was removed. To minimize the interference from spontaneous synaptic activity,

experiments were done in the presence of kynurenic acid (2 mM), strychnine (1 μM), and bicuculline (10 μM). In all experiments drugs were applied via the bathing solution (continuously superfused at 2-5 ml/min). Stock solutions of the agents were made in distilled water and frozen in small vials (1 ml) volume. The final concentration was obtained by dissolving an amount of the stock into the recording solution. When drugs were tested for their effects as blockers of certain K^+ currents (under voltage clamp) or K^+ mediated conductances (under current clamp), usually drugs were continuously applied for at least 5-10 min to achieve apparent equilibrium conditions; thereafter, data were acquired and stored for further analysis.

The following drugs were used: muscarine chloride (muscarine); carbamylcholine chloride (carbachol); atropine methylnitrate; apamin; 4-amino pyridine (4-AP); tetraethylamonium, chloride salt (TEACl); N-(2-aminoethyl) biotinamide hydrochloride (neurobiotin); bicuculline methiodide (bicuculline); strychnine nitrate (strychnine); 4-hydroxyquinoline-2 carboxylic acid (kynurenic acid); (±)1-aminocyclopentane-1S,3R-dicarboxylic acid (t-ACPD); caffeine; 1-[(5-[p-nitrophenyl]furfurylidene)-amino]hydantoin) sodium salt (dantrolene); ryanodine; N-(2,6-dimethylphenylcarbamoylmethyl) triethylammonium bromide (QX-314).

3. Recording techniques

The conventional whole-cell patch-clamp recording technique (Hamill et al. 1981) was employed. Briefly, with this technique, first described by Neher and Sakmann (1976), a small heat-polished pipette is pressed against the cell membrane, forming an electrical seal with resistance of the order of 50 MΩ. The following gentle suction, applied to the pipette interior, leads to the increase in seal resistance to 1-10 GΩ. The high resistance of so called "giga-seal" reduces the background noise and allows a patch of membrane to be voltage-clamped without the use of an additional microelectrode.

An EPC-7 patch-clamp amplifier was used for voltage clamp experiments and, alternatively, an Axoclamp-2B amplifier was utilized for current clamp experiments. The first one was not suitable to current clamp experiments, since compensation of pipette resistance was not available in current clamp operation mode. Moreover, it has been shown that most of the amplifiers designed for voltage clamp experiments give distortions in fast occurring events like action potential (Magistretti at al. 1996). For

voltage clamp experiments patch electrodes had 3-5 MΩ DC resistance while those pulled for current clamp experiments had 10-18 MΩ. Seal resistance was usually higher than 2 GΩ. After seal rupture series resistance, R_s, (5-15 MΩ) was routinely monitored and compensated (usually by 40%, range 20-60%) in voltage clamp experiments. The voltage clamp recordings were performed only when R_s stabilized and the cells were chosen for analysis if changes in R_s did not exceed 10%. For the sample of cells used for measurements of K^+ current kinetics and steady state properties the average voltage error found at the largest depolarized potential employed (+20 mV) was 7.2±0.5 mV (range 4.3-9.6 mV). For the Na^+ current at potentials where it was maximal (between –20 and 0 mV) the same voltage error was 4±1 mV (range 3.5- 5 mV). The maximal time constant of membrane voltage change due to presence of R_s was 120 μs in experiments when Na^+ current was recorded and 150 μs when K^+ current were recorded. The bridge was balanced routinely in current clamp experiments. Voltage and current pulse generation and data acquisition were performed with a PC running pClamp 6.1 software. Currents elicited by voltage steps were filtered at 3 kHz and sampled at 5-10 kHz.

Evoked synaptic currents. Excitatory postsynaptic currents were evoked by electrical stimulation (5-100 V, 0.1-0.2 ms, 0.1-0.2 Hz) of the reticular formation lateral to the border of nXII with an insulated bipolar platinum wire electrode. The stimulus intensity was adjusted to have an evoked postsynaptic current of consistent amplitude (100-200 pA). These experiments were performed in strychnine (1 μM) and bicuculline (10 μM) to isolate glutamatergic inputs.

4. Data analysis.

Cell input resistance (R_{in}) was calculated from small (5 mV or 10 pA) hyperpolarizing voltage or current commands or from the linear portion of the I-V line (ramp test) near the cell resting potential (V_{rest}).

To quantify the spike AHP its peak amplitude (from baseline), area, time constants for monoexponential rise and decay were measured. As these measurements are largely influenced by membrane potential, the cell resting potential was kept at the same level by intracellular current injection throughout the recording session.

To measure the amplitude and decay time constants of tail currents, these were fitted with a mono or biexponential function. The initial 5 ms record after the end of the

voltage step was discarded from fitting to avoid contamination by uncompensated capacitance transients. Tail current amplitude was then obtained by extrapolating fitted curves back to the end of the voltage step.

Sigma Plot and Clampfit software were used for exponential fitting of membrane currents and for linear regression analysis of experimental data. Data are presented as mean ± standard error. Data were analyzed statistically using Student's *t*-test or ANOVA test. Significance was accepted when $p< 0.05$.

On- and off-line leak subtraction protocols were utilized in VC experiments described below. On-line current leak subtraction was performed during the recordings of I_{Na} currents with the Clampex module of Pclamp6 acquisition program, which uses the "p/N correction" protocol (Armstrong and Bezanilla 1974). Otherwise, off-line leak correction was utilized using the procedure incorporated in Clampfit module.

5. Analysis of kinetic and voltage dependence of ionic currents

The voltage dependence of a conductance activation and inactivation was examined by measuring the current peak conductance (g_{peak}) obtained by dividing the current peak amplitude (I) by the driving force using the following equation:

$$g = \frac{I}{V - E_{rev}} \tag{1}$$

where g is conductance, I- current, V- membrane potential, and E_{rev}- current reversal potential. Then g_{peak} was normalized (g_{norm}) to the maximum conductance, g_{max}:

g_{norm} values were plotted against membrane potentials to give the activation (or

$$g_{norm} = \frac{g_{peak}}{g_{max}}. \tag{2}$$

inactivation) curve. These experimental points were fitted with the Boltzmann equation,

$$g_{\infty}(V) = \frac{1}{1 + \exp\left(\frac{V_{0.5} - V}{s}\right)} \tag{3}$$

where, $V_{0.5}$ – the potential of half activation (inactivation) and s – the slope factor.

Inactivation time constant (τ_h) was calculated from the current decay. At more negative potentials τ_h was evaluated using two-pulse protocol as time constant of recovery from inactivation.

Activation time constant (τ_a) was calculated in several ways.

1. From the exponential fit to the rising phase of I_{Kslow} (20 to 100 % of the peak).

2. From the current time-to-peak for I_{Na} and I_{Kfast}. It has been demonstrated that when the current reaches maximum (that is dI/dt=0; Bonifazzi et al. 1988):

$$t_p = \tau_a \cdot \ln\left(1 + \left(\frac{3 \cdot \tau_h}{\tau_a}\right)\right), \tag{4}$$

where t_p is the measured time-to-peak, τ_h – inactivation time constant evaluated from the current decay, and τ_a is the activation time constant.

3. From exponential fitting of the tail current at hyperpolarized potentials, when the first two procedures were not available.

Thus, estimated τ_a (τ_h) was plotted versus membrane potential and its voltage dependence was obtained by fitting of experimental points with the following expression:

$$\tau = \frac{1}{\exp\left(\frac{A+V}{B}\right) + \exp\left(\frac{C+V}{D}\right)} + E \tag{5}$$

where A, B, C, D, and E are free parameters obtained from fitting procedures. Fitting parameters used in the simulations are summarized in Table 1.

6. Computer simulation

6.1. Description of model. The HM was simulated by a single compartment model and the principal equation for specifying how transmembrane voltage varied with time was given by:

$$\frac{1}{C_m} \cdot \frac{dV}{dt} = I_{inj} - I_{leak} - I_{Na} - I_{Kslow} - I_{Kfast}, \tag{6}$$

where C_m is the cell capacitance, t is time, I_{inj} is the injected current, and I_{leak}, I_{Na}, I_{Kslow}, and I_{Kfast} represent leak, Na^+, and two K^+ currents. I_{leak} was implemented in the simulation by the following equation:

$$I_{leak} = \frac{1}{R_{in}} \cdot (V - E_{leak}), \tag{7}$$

where R_{in} is the neuron input resistance and E_{leak} is the reversal potential for the leak current. Kinetic models of the ionic currents were obtained by following methods proposed by Hodgkin and Huxley (1952). In brief, the Na^+ current was assumed to obey Ohm's law and was described by:

$$I_{Na} = g_{Na,\max} \cdot m^3 \cdot h \cdot (V - E_{Na}), \tag{8}$$

where $g_{Na,max}$ is constant and represents the maximum Na^+ conductance, m is the activation variable, h is the inactivation variable, and E_{Na} is the Na^+ equilibrium potential. Variables m and h are functions of voltage and time and are expressed by this general form:

$$m = m_\infty + (m_0 - m_\infty) \cdot \exp\left(-\frac{t}{\tau_m}\right), \tag{9}$$

where m_0 is the value of m at t= 0, m_∞ is activation steady-state value, and τ_m, time constant. m_∞ and τ_m were obtained from the experiments as described in the previous section. Change of m with the time was described by the following differential equation:

$$\frac{dm}{dt} = \frac{m_\infty - m}{\tau_m}. \tag{10}$$

Similar expressions were utilized for h, related to I_{Na} inactivation.

I_{Kslow} and I_{Kfast} were described as follows:

$$I_{Kslow} = g_{Kslow,\max} \cdot n^4 \cdot (V - E_K) \tag{11}$$

and

$$I_{Kfast} = g_{Kfast,\max} \cdot a \cdot b \cdot (V - E_K), \tag{12}$$

where $g_{Kslow,max}$ and $g_{Kfast,max}$ are maximal conductances underlying I_{Kslow} and I_{Kfast}, respectively, n is I_{Kslow} activation variable, a is I_{Kfast} activation variable, b is I_{Kfast} inactivation variable, and E_K is K^+ equilibrium potential.

The I_{Na} slow inactivation voltage dependence was taken from neocortical neuron model (Fleidervisch et al. 1996). S, variable for this mechanism, was defined by:

$$S = \frac{0.001 \cdot \exp\left(\frac{-85 - V}{30}\right)}{0.001 \cdot \exp\left(\frac{-85 - V}{30}\right) + 0.0034 \cdot \left(1 + \exp\left(\frac{-17 - V}{10}\right)\right)} \tag{13}$$

τ_S was 200 ms, that was near to values obtained experimentally from HMs.

Fast transient Na^+ and delay rectifier K^+ conductances, were taken from respiratory neuron model (Rybak et al. 1997) to create the model of fast spiking neuron. Transient Na^+ and sustained K^+ currents were expressed in the same way as I_{Na} and I_{Kslow} of HMs in eqs. (8) and (11), respectively. Activation and inactivation variables m, h, and n were expressed through α and β, forward and backward reaction rates, described by:

$$\alpha_m = \frac{0.091 \cdot (V + 38)}{1 - \exp\left(\frac{-V - 38}{5}\right)} \tag{14}$$

$$\beta_m = \frac{-0.062 \cdot (V + 38)}{1 - \exp\left(\frac{V + 38}{5}\right)} \tag{15}$$

$$\alpha_h = 0.016 \cdot \exp\left(\frac{-V - 55}{15}\right) \tag{16}$$

$$\beta_h = \frac{2.07}{1 + \exp\left(\frac{17 - V}{21}\right)} \tag{17}$$

$$\alpha_n = \frac{0.01 \cdot (V + 45)}{1 - \exp\left(\frac{-V - 45}{5}\right)} \tag{18}$$

$$\beta_n = 0.17 \cdot \exp\left(\frac{-V - 50}{40}\right) \tag{19}$$

6.2. Numerical methods. Most of the simulations were carried out with a home written program using MatLab software run under Windows 95/NT operating system of PC type computers. The Euler method with a fixed time step of 100 or 10 μs was used for numerical simulations. Control simulations were run on Unix computers using an implicit Runge-Kutta four-step integration method written in FORTRAN programming language.

Maximal conductances underlying the currents were chosen to produce repetitive firing during current injection. Reversal potentials were chosen to match experimental

conditions and were given (in mV) by: $E_{leak} = V_{rest} = -70$, $E_{Na+} = 50$, $E_{Kslow} = E_{Kfast} = E_{K+} = -90$ mV. R_{in} and C_m, set to match those obtained experimentally, were 200 MΩ and 50 pF, respectively. The units used in the model were time in milliseconds (ms), voltage in milliVolts (mV), current in nanoAmperes (nA), conductance in microSiemens (μS), and capacitance in nanoFarads (nF). The fitting parameters describing voltage dependence and kinetics of the currents and used in simulations are summarized in the Table 1.

Table 1. Voltage and kinetic parameters used in the HM model.

Current	$V_{0.5}$[a], mV	s[a], mV	A[b]	B[b]	C[b]	D[b]	E[b]
I_{Na} activation	-30[c]	3.4	42	-9.3	15	7.9	0.78
I_{Na} inactivation	-44[c]	-8.7	100	-17	26	3.0	2.4
I_{Kslow} activation	-25	19	170	-36	-28	9.5	12
I_{Kfast} activation	-28	16	93	-5.2	-3.6	36	1.2
I_{Kfast} inactivation	-93	-11	80	-5.4	-250	65	21

[a] $V_{0.5}$ and s values were obtained by fitting activation and inactivation plots with the Boltzamann equation (eq. (3)).

[b] A, B, C, D, and E are eq. (5) fitting parameters to time constant plots.

[c] In most simulation experiments $V_{0.5}$ values of I_{Na} activation and inactivation were shifted to –40 mV and –65 mV, respectively, to eliminate large "window current" and to obtain repetitive firing of model HM.

RESULTS

1. Firing characteristics of HMs

The HM firing characteristics were studied by injecting depolarizing and hyperpolarizing current pulses into current clamped HMs (patch-clamp whole cell configuration). A neuron was considered healthy if it had resting membrane potential more negative than –55 mV, was able to fire an action potential (AP) with overshoot (usually 20-30 mV), and responded with a train of AP to a long depolarizing current step. Average resting potential (V_{rest}) and input resistance (R_{in}) were –68.8±0.7 mV and 240±90 MΩ, respectively (n= 59 cells).

1.1. Basic properties of repetitive firing

A typical example of responses to 1 s long current step of increasing intensity (200 to 500 pA; current amplitude indicated near each trace) is shown in Fig. 1A. Current steps of ≥200 pA elicited a train of APs. The HM fired at higher frequency with increasing current intensity as exemplified by f-t relation in Fig. 1B. In fact, the HM fired with apparently constant frequency in response to 200 pA current step (open circles), while in response to stronger current the first 1- 4 spikes occurred at higher frequencies (see first 1- 3 points in f-t relations of AP trains elicited by 300, 400, and 500 pA current steps). After this, firing frequency was constant during the remaining time period. Intracellular stimulation rarely exceeded 400- 500 pA, since with high current steps cells fired few spikes only (see for example the HM in Fig. 11A). Note also appearance of late slow adaptation in the AP train evoked by current step of 500 pA in Fig. 1A and B.

The relation between spike discharge frequency and injected current (f-I relation) was further investigated to determine the excitation-frequency transduction properties of these cells. An example of instantaneous firing frequency (1/ interspike interval) *versus* injected current plot is shown for the first six interspike intervals (Fig. 1C). The curve of first interspike interval was sigmoidal (see also examples in Fig. 11D and 13D), while the plots for subsequent interspike intervals were almost linear without secondary range firing and overlapped to a large degree. This last result simply confirms the presence of fast initial adaptation only within a moderate range of current injection amplitude. The f-I

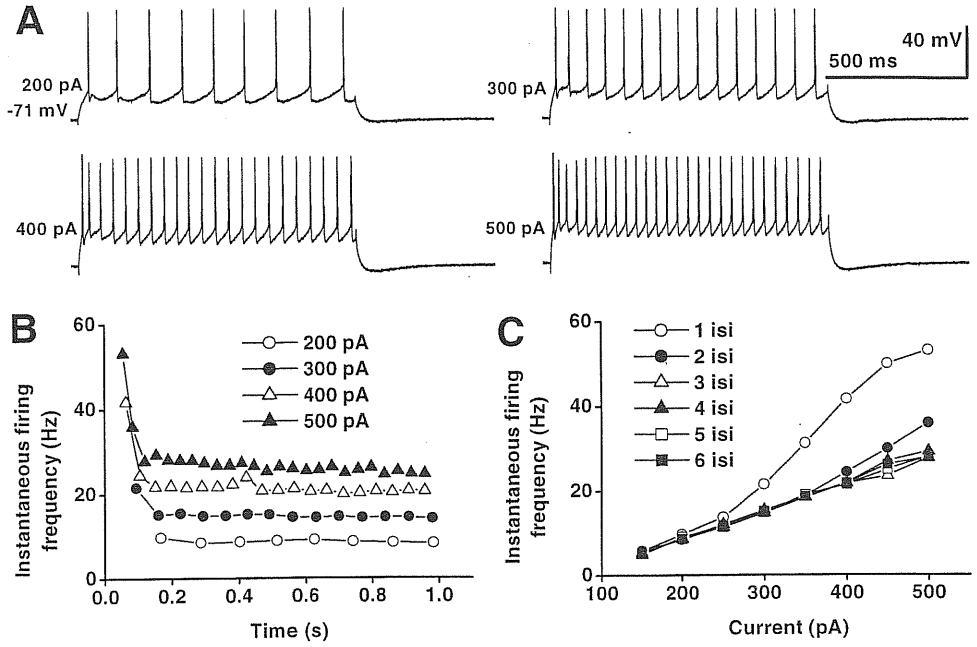

Figure 1. Repetitive firing properties of neonatal HMs. A: responses to 1 s current step of 200 (open circles), 300 (closed circles), 400 (open triangles), and 500 pA (closed triangles) intensity. Values at the start of each trace are the current step intensities. V_{rest} = -71 mV. B: plot of instantaneous firing frequency versus time (same current steps of the same HM as in A) for four different current steps. Note the initial fast decrease in firing frequency. Initial adaptation during 500 pA current step is followed also by slower decline of firing frequency. C: f-I relations for first (open circles), second (closed circles), third (open triangles), fourth (closed triangles), fifth (open squares), and sixth (closed squares) interspike intervals. Note that f-I plots for second and subsequent interspike intervals almost overlap.

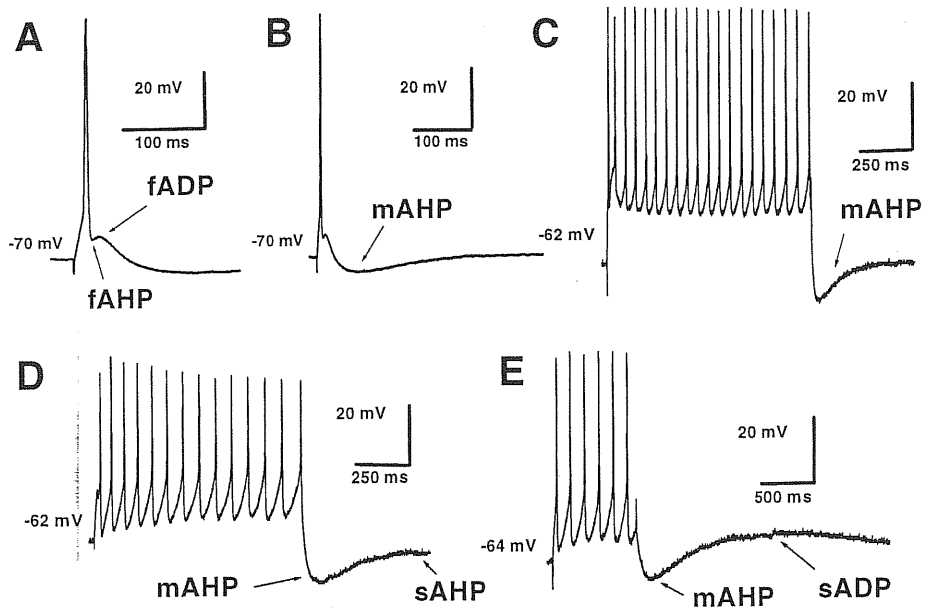

Figure 2. HMs possess different types of afterpotential. All traces are obtained under current clamp conditions. A and B: same action potential (evoked by short depolarizing current step; 5 ms, 0.5 nA) shown on different time-scale. Note the presence of three types of afterpotentials: fAHP, fADP and mAHP. C: repetitive firing evoked in response to a long depolarizing step (2 s, 200 pA). mAHP can be observed at the termination of current step (different cell from A-B). D: example of a neuron (9% of all recorded cells) in which sAHP follows the mAHP (evoked by current step of 1 s duration and 200 pA intensity). E: example of a neuron which, in response to current step injection (400 ms, 200 pA), generates sADP after the mAHP. This behavior was observed in 40% of cells. Values at the start of each trace are resting membrane potentials.

relation for instantaneous frequency of the first interval rose more steeply than that for the subsequent five intervals discharge. The average slope calculated for the first spike doublet or at steady state discharge (usually calculated as average of last 3 to 5 intervals) evoked by 50- 300 pA was 98± 7 or 57± 2 Hz/nA, respectively (n= 37 cells). A rebound hyperpolarization was present at the end of the every current step (Fig. 1A). The cell in Fig. 1 is representative of the most commonly observed firing pattern in control solution: in fact, out of a group of 59 motoneurons which were able to fire repetitively, 37 had exclusively very fast adaptation (lasting up to 50 ms and affecting the first 2-5 spikes only), while 17 cells showed no measurable adaptation and 5 possessed also slower adaptation lasting ~200 ms.

1.2. AP and its afterpotentials

The single AP usually elicited by a short current step (usually 0.5 nA, 5 ms) had a threshold of -43± 2 mV, an amplitude of 59± 5 mV (measured from threshold to peak), and a duration of 3.1± 0.7 ms (measured at threshold level; n= 37 cells). The AP raising and falling rates were 72± 2 mV/ms and 58± 2 mV/ms, respectively. The Na^+ channel blocker TTX (0.5 μM) completely blocked single or trains of APs (data not shown). Some general characteristics of the AP afterpotentials elicited by intracellular current injection are presented in Fig. 2. Fig. 2A shows that, in analogy with the report by Viana et al. (1993b), the decay phase of a single AP (evoked by a short current pulse) comprised a fast afterhyperpolarization (fAHP) and a fast afterdepolarization (fADP). These early afterpotentials were followed by a medium afterhyperpolarization (mAHP) which undershot the baseline for about 250 ms (Fig. 2B, same cell). An analogous mAHP (about 300 ms long) was also observed at the end of a spike train induced by a 2 s current pulse (200 pA; see Fig. 2C, different cell from A-B). In few cells only (9% of total recorded cell number) a slow afterhyperpolarization (sAHP) (lasting 2-5 s) appeared after the mAHP (Fig. 2D; see also Viana et al. 1993b). In a larger group of cells (~40%) the mAHP was followed by a slow afterdepolarization (sADP; 1-3 s long; Fig. 2E).

1.3. HM responses to hyperpolarizing current steps

Fig. 3A shows the membrane potential response to a series of hyperpolarizing current steps. This response was characterized by an initial sag and a rebound depolarization at the end of the pulse. The degree of depolarizing sag was quantified as $((V_{peak} - V_{steady\text{-}state})/V_{peak})$ (Viana et al. 1994). The average degree value was 0.36± 0.03 (n= 22 cells), which differs from the result by Viana et al. (1994), who found that this value (expressed in %) for intracellulary recorded neonatal HMs is 13 %. The initial sag increased at increasing hyperpolarizing pulse strength. Only with very small hyperpolarizations (< 50 pA) the sag was absent.

CsCl (4 mM) added to the solution completely abolished both sag and rebound responses (Fig. 3B). This result suggests that I_h current, found in HMs (Bayliss et al. 1994a), was mainly responsible for the generation of sag and rebound. Occasionally, one (or more) AP appeared at the top of the rebound depolarization (Fig. 3C). The rebound was partially blocked in Ca-free-Co solution, thus, suggesting involvement of low threshold Ca^{2+} currents in generation of rebound.

1.4 Basic properties of mAHP

At V_{rest} the mAHP following a single AP reached peak amplitude of 9.5± 0.7 mV (calculated from V_{rest}) with a monoexponential rise (time constant = 23±2 ms), from which it decayed monoexponentially (decay time constant=150±10 ms). When extracellular Ca^{2+} was replaced by the same concentration of Co^{2+}, the mAHP was abolished (Fig. 4A) but it recovered when standard external solution was reapplied (n=4). The example of Fig. 4B indicates that, under standard recording conditions, the mAHP decreased with membrane hyperpolarization until it disappeared at –94 mV membrane potential. The inset to Fig. 4B is the plot (for two HMs) of the relation between membrane potential and mAHP amplitude, yielding an extrapolated reversal potential of –94 mV, which coincides with the calculated equilibrium potential for K^+ on the basis of the Nernst equation. This result suggests that the mAHP is a response due to increased permeability to K^+. As the mAHP was fully and irreversibly blocked by 100 nM apamin without concomitant suppression of the fAHP (Fig. 4C; similar data were observed on 9

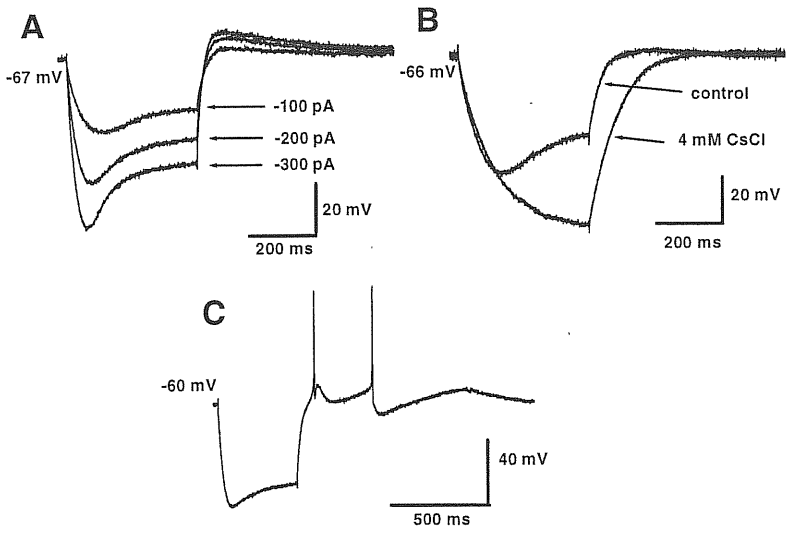

Figure 3. HMs inward rectification under hyperpolarization. A: responses to 400 ms current step of 100, 200, and 300 pA. Note the sag during hyperpolarization and rebound at the termination of hyperpolarizaing current step. B: sag is completely blocked by 4 mM CsCl. Traces in control and CsCl solutions are superimposed. C: example of a neuron, which fires two APs during the rebound.

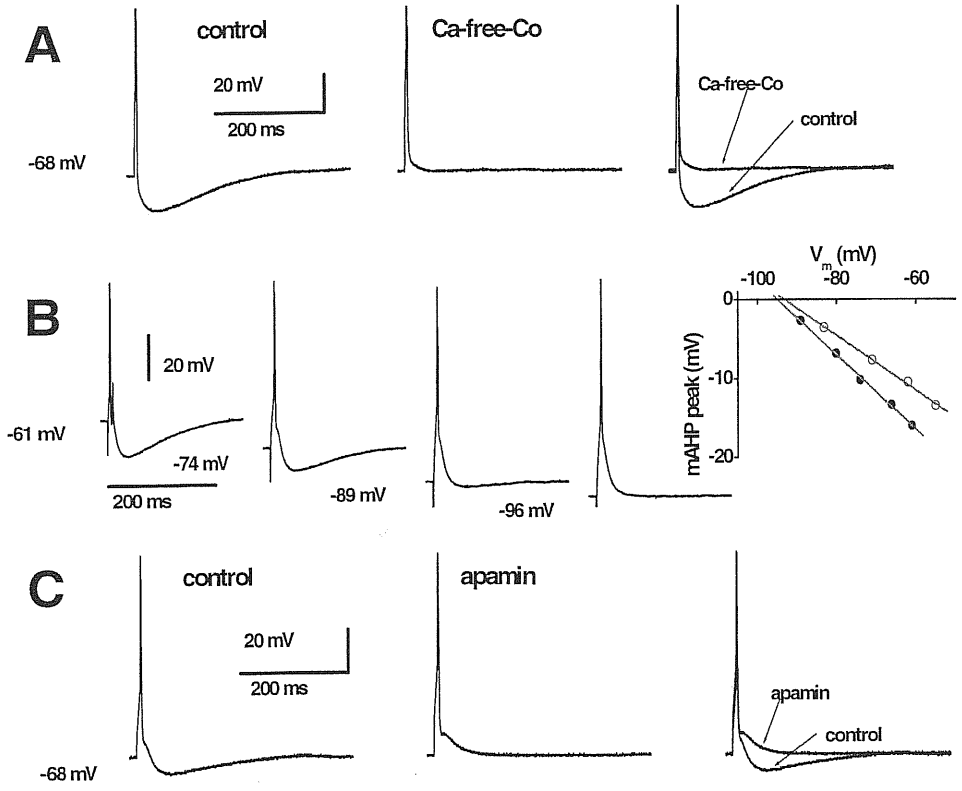

Figure 4. mAHP is Ca^{2+} dependent, reverses at E_K^+, and is sensitive to apamin. A: mAHP after a single spike (control) is blocked by replacing extracellular Ca^{2+} with the same amount of Co^{2+} (Ca-free-Co). B: mAHP amplitude is voltage dependent as it decreases at more negative membrane potential. Inset: reversal potential of the mAHP for two cells estimated from the extrapolated intercept of the linear regression of mAHP amplitude plotted against membrane potential. C: mAHP after a single spike (control) is completely blocked by 100 nM apamin. In A and C (right) traces are superimposed to aid comparison.

cells), it seems likely that the K^+ conductance responsible for generating the mAHP was mediated by SK Ca^{2+}-activated channels (Sah 1996).

1.5. Depression of mAHP by agents acting on ACh receptors

The cholinergic agonist carbachol largely attenuated the mAHP as exemplified in Fig. 5A. On average 50 μM carbachol reduced the mAHP to 37±4 % of control (n=17 cells). The action of carbachol developed quite slowly, taking about 5 min to manifest fully, was completely reversible on washout and was dose dependent. In fact, 10 μM carbachol decrease the mAHP to 76± 5% in 4 cells while 100 μM concentration reduced it to 20± 10% in 2 cells. Note that carbachol depressed the peak amplitude of the mAHP without affecting its rise or decay timecourse (changes in τ_{rise} and τ_{decay} were 90± 10% and 81± 9%, respectively; n=17 cells). The action by carbachol was not accompanied by any significant change in spike amplitude (90±2 %), duration (107±6 %) or threshold (99±6 %).

The carbachol inhibitory action on the mAHP was prevented by 10-15 min pretreatment with 10 μM atropine (n=7 cells), a selective antagonist on muscarinic ACh receptors (Fig. 5B). The mAHP, however, retained its sensitivity to apamin (100 nM; Fig. 5B), indicating distinctive modes of action for carbachol and this toxin in inhibiting the mAHP. Note that on average atropine *per se* increased the mAHP by 29± 7% (n= 7). The selective muscarinic receptor agonist muscarine (50 μM) also produced HM depolarization (10±4 mV) and attenuated the mAHP (Fig. 5C; on average to 40± 20%; n=3).

Together with the depression of the mAHP carbachol (10-100 μM) also produced a dose dependent, slowly developing and reversible depolarization of all HMs tested. An example of such depolarization by 50 μM carbachol is shown in Fig. 6A. During washout of carbachol the membrane potential took several minutes to return to resting value. On average, a 50 μM concentration induced a mean depolarization of 12±1 mV (Fig. 6B) without significant change (96± 4%) in R_{in} (n=17 cells; Fig. 6C). The carbachol depolarization persisted in the presence of TTX, thus suggesting that it had a direct action on HMs (11± 2 mV; n=3; Fig. 6D). Muscarine, applied at the same concentration as

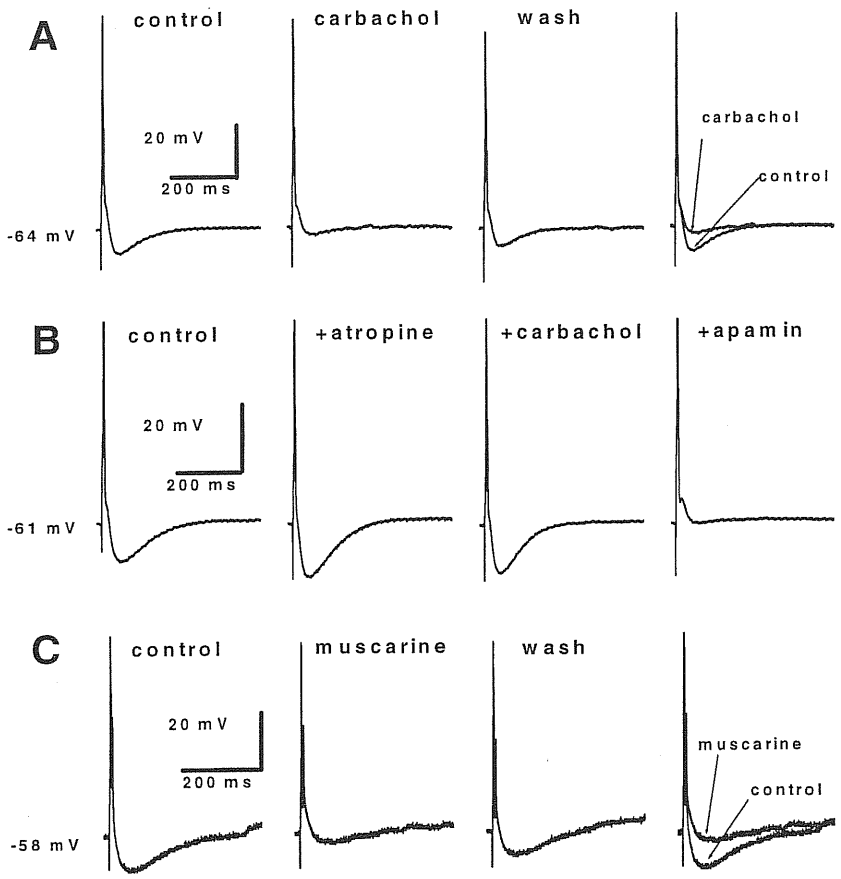

Figure 5. mAHP is depressed by muscarinic receptor agonists. A: mAHP after a single AP (control) is attenuated by 50 μM carbachol and recovers on washout. B: 10 μM atropine increases the mAHP amplitude by 42% and prevents the mAHP depression by 50 μM carbachol. Note however that subsequent application of 100 nM apamin (in atropine plus carbachol solution) completely blocks the mAHP. C: mAHP is reversibly attenuated by application of 50 μM muscarine. Note that the depolarizing effect of carbachol or muscarine was offset by steady current injection to maintain the cell at resting potential.

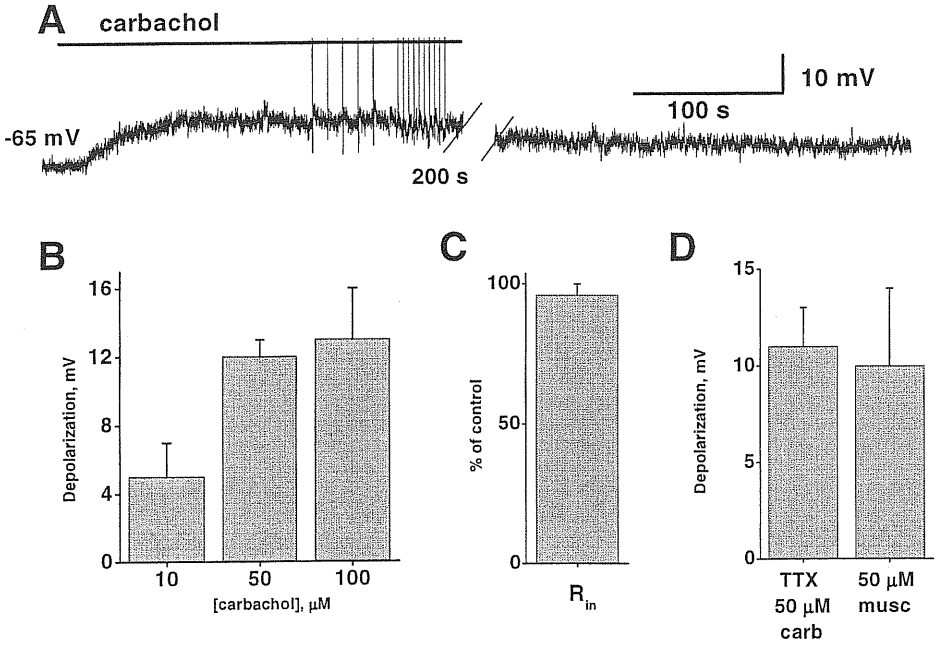

Figure 6. Carbachol reversibly and dose dependently depolarizes HMs. A: example of membrane potential trace showing depolarization due to carbachol (50 µM). B: dose dependence of carbachol depolarization. C: Input resistance (R_{in}) does not change during application of 50 µM carbachol. D: Carbachol acts directly on HMs since the depolarization persists in the presence of TTX. Muscarine (50 µM) also depolarizes HMs by a similar degree, thus suggesting that carbachol operates via activation of muscarinic acetylcholine receptors. Atropine (10 µM) supresses carbachol responses (not shown).

carbachol (50 μM) produced membrane depolarization of similar extent (Fig. 6D; 10± 4 mV).

1.6. mAHP involvement in repetitive firing

The duration and magnitude of the mAHP would predict this response to be a potent regulator of the discharge properties of HMs, particularly in view of a similar role of the mAHP in firing adaptation of hippocampal cells (Storm 1990). It was thus surprising to observe that long current pulses evoked repetitive firing of HMs with slight adaptation only despite the mAHP presence (see Figs. 1 and 2). One possibility for the rather modest (or even absent) process of firing adaptation might be that the action of the mAHP was contrasted by co-activation of other conductances. To reveal the influence of the mAHP on spike firing, the selective blocker apamin (100 nM) was applied and AP trains were evoked as depicted in Fig. 7A. In the presence of apamin the firing properties of the cell were radically transformed with a large rise in frequency affecting both the early and late AP in the train (see Fig. 7B). Effects similar to those of apamin were also observed by applying Ca^{2+}-free-Co^{2+} solution (n=4; not shown). Furthermore, in apamin solution firing adaptation was manifested as indicated by the continuous decline in firing frequency over time (compare timecourse of filled and open circle graphs in Fig. 7B).

A f-I relation is shown for the first and last interspike interval (Fig. 7C). While in control solution the difference between these values was small and skewed towards large injected currents, in apamin solution there was a much more substantial difference throughout the injected current range. The f-I relation slope calculated for the first interspike interval (100±10 Hz/nA) and for steady state firing (58.1±0.7 Hz/nA) evoked by 50-200 pA currents increased, in apamin solution, to 320±20 Hz/nA and 160±20 Hz/nA, respectively (n= 12 cells).

Application of carbachol (50 μM) also increased firing frequency of HMs in response to current injection (Fig. 7D). Spike frequency adaptation was manifested in the presence of carbachol (Fig. 7E), leading to a stronger separation between early and late firing frequencies (Fig. 7F).

In presence of 100 nM apamin, carbachol (50 μM) had little effect on firing properties (Fig. 8A) as quantified in Fig. 8B where data points for apamin or carbachol tests

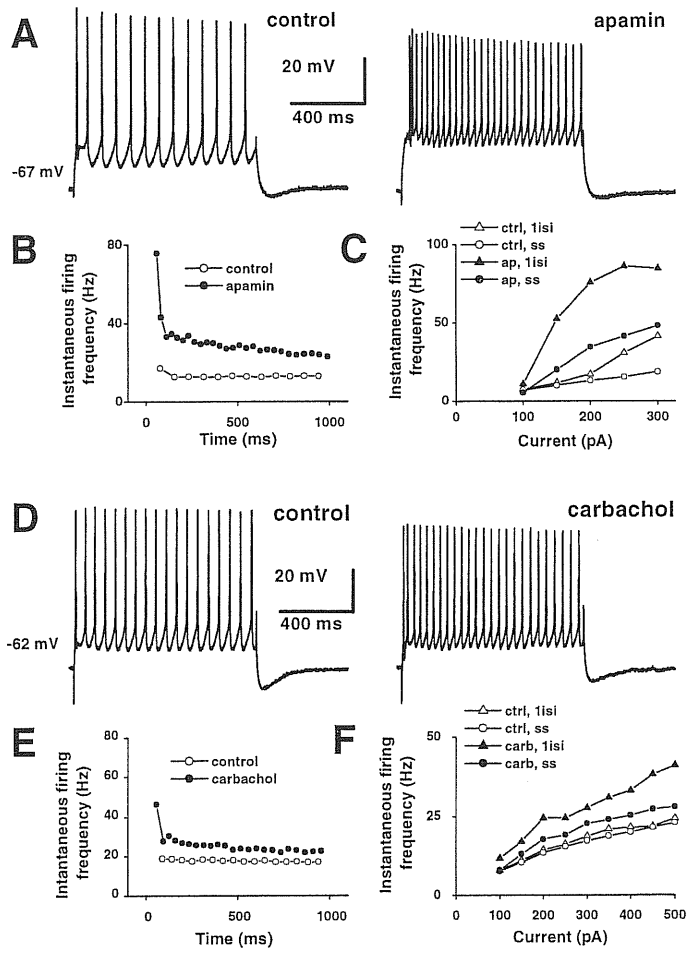

Figure 7. Effect of mAHP block by apamin or carbachol on repetitive firing properties of neonatal HMs. A: responses to the current step (1 s, 200 pA) injected into a HM in standard solution (left) or in 100 nM apamin solution (right). Note large increase in firing frequency. B: plot of instantaneous firing frequency versus time (same HM responses as in A) before (open circles) and after (closed circles) application of apamin. Note that slight, early spike frequency adaptation in control is replaced by two phases of spike frequency adaptation in apamin solution. C: initial (1 isi; triangles) and steady state (ss; circles) f/I relations (same neuron as in A and B) before (open circles and triangles) and after apamin (closed circles and triangles) application. D: spike trains elicited by current step injection (1 s, 300 pA) in control or in 50 μM carbachol solution. Note increase in firing rate. E: plot of instantaneous firing frequency against time (same responses as in D) before (open circles) and after carbachol (closed circles) application. F: initial (triangles) and steady state (circles) f-I relations (same neuron as in D and E) before (open circles and triangles) and after carbachol (closed circles and triangles) application. Note that the depolarizing effect of carbachol was offset by steady current injection to maintain the cell at resting potential.

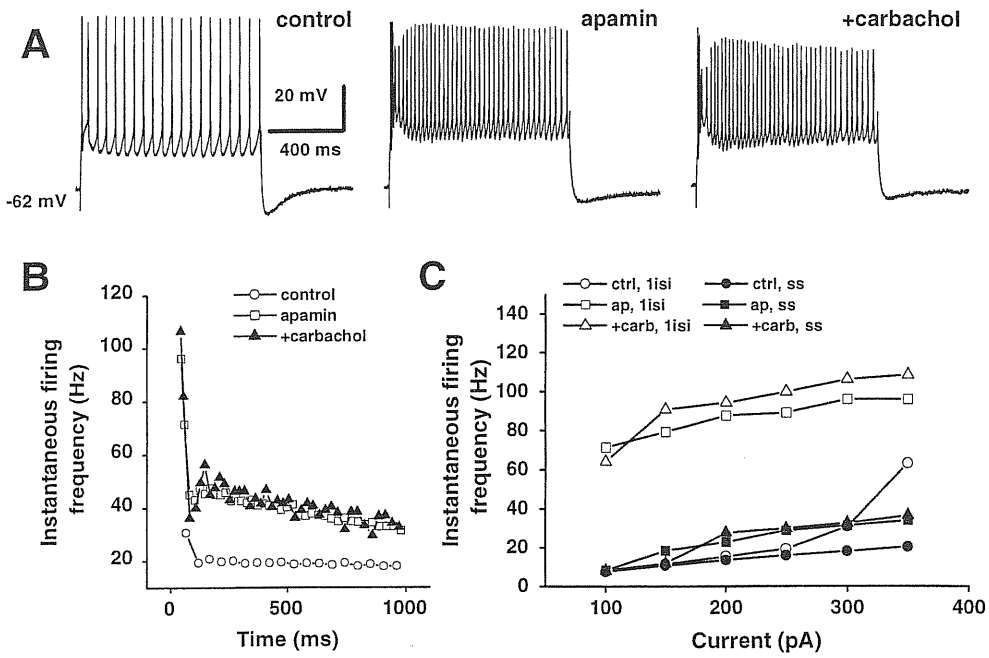

Figure 8. Carbachol affects repetitive firing properties of HMs via an apamin sensitive conductance. A: responses to current pulse (1 s, 300 pA) injection in control solution, in presence of 100 nM apamin, and during co-application of 100 nM apamin and 50 μM carbachol. B: plot of instantaneous firing frequency versus time (same responses as in A) for control (open circles), apamin (open squares), and co-application of apamin and carbachol (closed triangles). C: initial (1 isi; open circles, squares, and triangles) and steady state (ss; closed circles, squares, and triangles) f-I relations of the same neuron as in A and B for control (circles), apamin (squares), and co-application of apamin and carbachol (triangles). Note that the depolarizing effect of carbachol was offset by steady current injection to maintain the cell at resting potential.

overlap. The analysis of f-I plots (Fig. 8C) indicates strong similarity between the effects of apamine and carbachol on the AP frequency rise and firing adaptation. Nevertheless, despite occlusion by apamine of carbachol effects on firing, this latter substance was still able to depolarize HMs (8± 2 mV; n=5). The present data suggest that muscarinic receptor activation could differentially modulate membrane potential and firing properties of HMs.

1.7. Effect of agents interacting with intracellular Ca^{2+} on mAHP and repetitive firing

Several experiments were done with patch pipettes containing 1 mM BAPTA. This agent is known to be an effective chelator of intracellular Ca^{2+} and, thus, used to investigate Ca^{2+} dependent neuronal processes (Schwindt et al. 1992a; Velumian and Carlen 1999). Indeed, out of 6 cells recorded with a patch electrode filled with 1 mM BAPTA and held at –68 mV, four showed no mAHP and two showed a rather small mAHP (3 and 1.5 mV, respectively). An example of a single AP evoked under these conditions is shown in Fig. 9A (left trace). Note the absence of mAHP, while fAHP and prolonged fADP were seen clearly. Further application of 100 nM apamin demonstrated that there was a slight, residual apamin-sensitive conductance masked by a much stronger depolarizing conductance (Fig. 9A). Intracellular BAPTA clearly changed repetitive firing pattern as shown in Fig. 9B. After the initial fast adaptation, also present in control cells (see Fig. 1 and 5), a slower, almost continuous decline in firing frequency emerged during the whole current application, thus exhibiting a strong, late adaptation (Fig. 9B). This second adaptation phase is evident in f-t plots of corresponding spike trains (Fig. 9C). Moreover, f-I plots of first to fifth interspike intervals were clearly separated (Fig. 9D). The train of spikes in all HMs recorded with patch pipettes containing BAPTA (1 mM) was always followed by a long lasting (1-2 s) sAHP (Fig. 9B). sAHP conductance was not investigated in details, but preliminary experiments demonstrated that it was not sensitive to apamine (up to 200 nM) and was blocked by Cd^{2+} (0.2 mM). It seems that Ca^{2+} dependent channels different from those generating mAHP were involved.

Intracellular Ca^{2+} stores participate in the control of mAHP in several types of neuron (Davies et al. 1996; Sah and McLachlan 1991). Agents modulating release of Ca^{2+} from intracellular stores, such as caffeine, dantrolen, and ryanodine were tested on HMs. It has

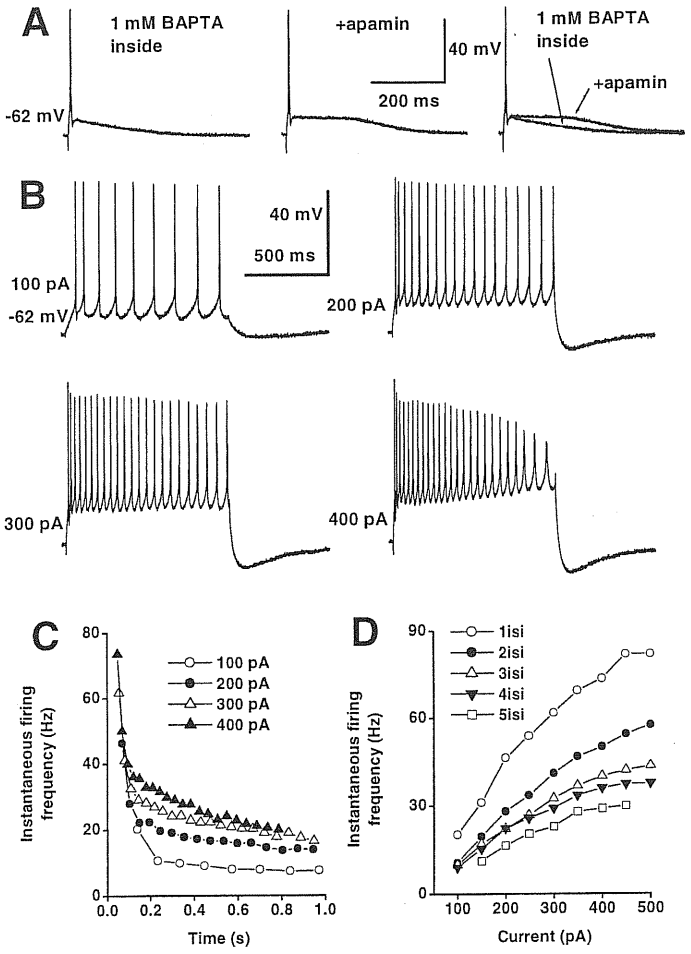

Figure 9. Intracellular BAPTA abolishes mAHP and unmasks strong spike frequency adaptation. A: a single spike and its afterpotential recorded with a pipette containing 1 mM BAPTA. The spike was evoked by a short current step (2 nA, 5 ms). Note prolonged fADP and absence of mAHP in left trace. Trace in the midle was recorded in apamin (100 nM) solution. Note that fADP was prolonged even more. On the right, both traces are superimposed. B: typical responses to long current steps (1 s) recorded with a pipette containing 1 mM BAPTA. Current step amplitude is indicated on the left. Note evident interspike interval prolongation during the response. C: f-t relation for the same cell as in A and B. Note the clear presence of two spike frequency adaptation phases. D: f-I relation corresponding to first (open circles), second (closed circles), third (open triangles), fourth (closed triangles), and tens (open squares) interspike interval. Note clear separation of plots not seen in cells recorded with patch pipettes without BAPTA.

been demonstrated that long lasting application of caffeine discharges the Ca^{2+} stores (Kostyuk and Verkhratsky 1994). Caffeine (10 mM) produced a multiphasic change in HM membrane potential as shown in example trace in Fig. 10A. First, a slowly developing hyperpolarization (3±1 mV) appeared and was followed by a slow depolarization (3.8± 0.5 mV from the V_{rest}) which persisted until the caffeine was washed out (n= 7 cells). The hyperpolarizing phase was not seen when the neuron was pretreated with apamin (n= 2 cells), thus suggesting that Ca^{2+} released by caffeine activated Ca^{2+} dependent K^+ (presumably SK) channels. R_{in} increased during the depolarizing phase by 21± 7 % (p= 0.05; n= 7). In parallel to membrane depolarization, caffeine (10 mM) significantly increased mAHP amplitude by 50± 10 % (p= 0.03; n=7) as depicted in the example in Fig. 10B. Single spikes were elicited in control and in caffeine containing solutions. Caffeine enhanced amplitude of mAHP, which later was completely abolished by apamin (Fig 10). Treatment with caffeine also led to decrease in firing frequency as depicted and quantified in Fig. 11A and C. The first interspike interval and steady state f-I relation slopes in the 150- 300 pA range decreased from 161 to 120 and from 61 to 45 Hz/nA in the sample cell, respectively (Fig. 11D). Dantrolene (30 μM), an agent blocking Ca^{2+} sequestration by intracellular stores (Kostyuk and Verkhratsky 1994), also significantly enhanced mAHP area by 60± 10% (p= 0.04; n= 6), even if amplitude was increased moderately, but not significantly (30± 10 %; p> 0.05). On three HMs ryanodine (20 μM) was applied through bath perfusion. However, despite a slight prolongation of decay phase of mAHP, ryanodine had no significant effect on HMs.

Part of the depolarization by carbachol was sensitive to caffeine. Carbachol (50 μM) was applied to five HMs bathed in caffeine solution (10 mM) and held at V_{rest}. In these conditions carbachol depolarized by 6± 1 mV only (n=5), that is nearly half of the effect standard solution (see Fig. 6B). This result suggested that caffeine and carbachol could utilize the same mechanism of membrane depolarization and that their co-application led to response occlusion.

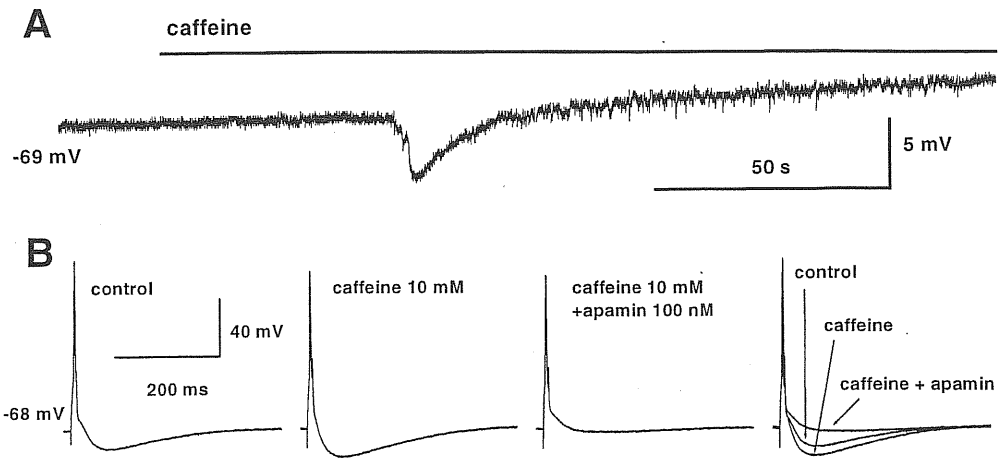

Figure 10. Caffeine effects on membrane potential and mAHP. A: example of membrane potential trace showing two phases of caffeine (10 mM) action. B: Single APs evoked by short current steps (2 nA, 5 ms). mAHP is enhanced in caffeine (10 mM) solution. Apamin (100 nM) abolishes mAHP. On the right the traces obtained in control, caffeine, and apamin are superimposed. Cell V_{rest} = –68 mV. Note that depolarizing effect of caffeine during evoking of mAHP was offset by steady current injection to maintain the cell at resting potential.

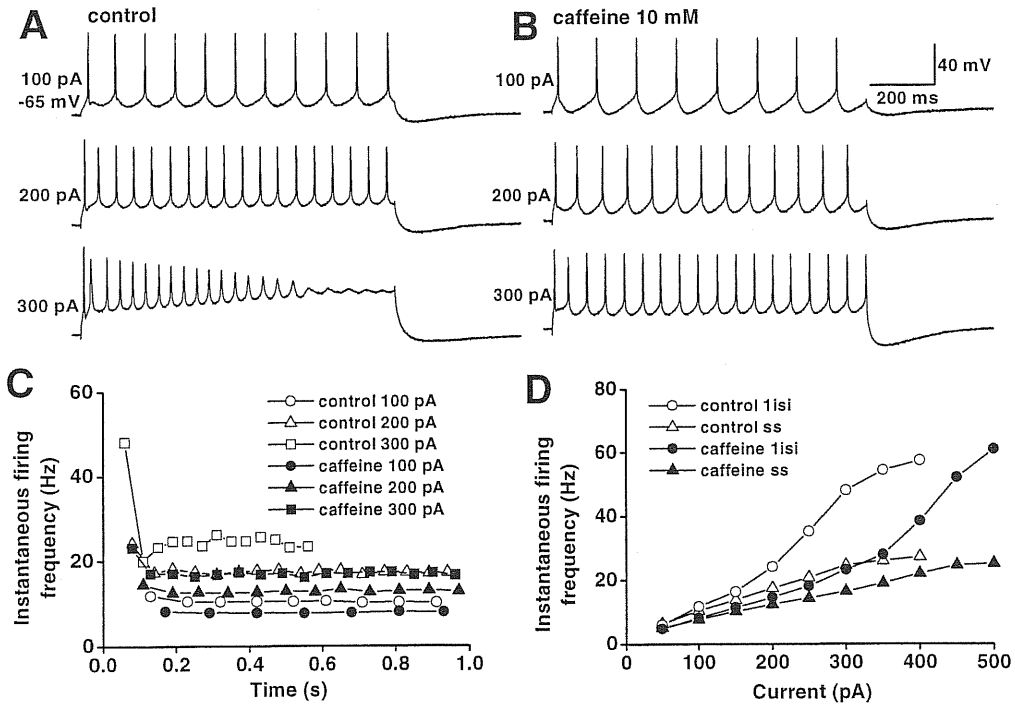

Figure 11. Caffeine decreases repetitive firing frequency. A and B: responses to 100, 200, and 300 pA current steps (1 s) in control (A) and 10 mM caffeine containing (B) extracellular solutions. Values at the start of each trace represent current step intensity. C: f-t plot for the same traces as in A and B. Note that plots in control and in caffeine are have similar forms: the only difference is that those in caffeine are shifted downward for the same injected current. D: f-I plot for the same neuron as in A, B, and C. Note slope decrease by caffeine. Note that depolarizing effect of caffeine was offset by steady current injection to maintain the cell at resting potential.

1.8. Modulation of HMs by activation of mGluRs

1.8.1. Postsynaptic effects of t-ACPD. Although mGluRs are largely present in nXII (Hay et al. 1999), the functional consequences of their activation on HMs are not yet known. In the present experiments, bath application of *t*-ACPD (50 μM), a mGluR agonist, produced a slowly developing depolarization (on average 12± 3 mV; n=7 cells) as is exemplified in Fig. 12A. The depolarization was accompanied by a significant increase in R_{in} (20± 10 %; $p< 0.05$; Fig. 12 B and C). In addition, there was strong increase in baseline noise (insets to Fig. 12A), which was partially diminished by application of ionotropic receptor blockers, such like bicuculline, strychnine, and kynurenic acid. Depolarization by *t*-ACPD persisted also in presence of TTX, thus, suggesting a postsynaptic activation of mGluRs (n=3). Fig. 13A and B show HM responses to a 0.4 s current step (200 pA) in control (A) and *t*-ACPD (B) solutions. No evident change was seen in the AP train. In fact, control or *t*-ACPD f-t plots (Fig. 13C) of AP trains elicited by 200 and 600 pA current step (0.4 s) were almost completely overlapping. The f-I relation indicated that only the first interspike interval frequency was reduced in *t*-ACPD solution. First spikes of the trains of Fig. 13A and B are depicted on a faster time scale in Fig. 14A. Application of *t*-ACPD resulted in a significant increase in spike delay (156± 6 % of control; $p= 0.02$; n=7; Fig. 14B), while spike amplitude (87± 10 %; $p= 0.06$; Fig. 14C), spike duration (120± 10 %; $p= 0.06$; Fig. 14D), and threshold (96± 3 %; $p= 0.07$; Fig. 14E) were not significantly changed. The amplitude and area of mAHP measured after single spike elicited by short current step (2 nA, 5 ms) were also unchanged (110± 20 %, $p> 0.05$ and 130± 20 %, $p> 0.05$, respectively) during treatment with *t*-ACPD.

1.8.2. Presynaptic depression of excitatory synaptic transmission. Since t-ACPD induced strong baseline noise (Fig. 12A), which in part was due to increased synaptic activity, the effect of mGluR activation on evoked glutamatergic excitatory postsynaptic currents (eEPSCs) was tested. eEPSCs were evoked under voltage clamp conditions by stimulating the reticular formation zone lateral to nXII. Voltage clamp was chosen to avoid voltage dependent effects, which would otherwise appear during strong depolarization of HM membrane by t-ACPD. eEPSCs were recorded in the continuous presence of bicuculline (10 μM) and strychnine (1 μM). They were blocked by TTX (0.5 μM; Fig. 15A) or kynurenic acid (2 mM; Fig. 15B), an antagonist of glutamate receptors,

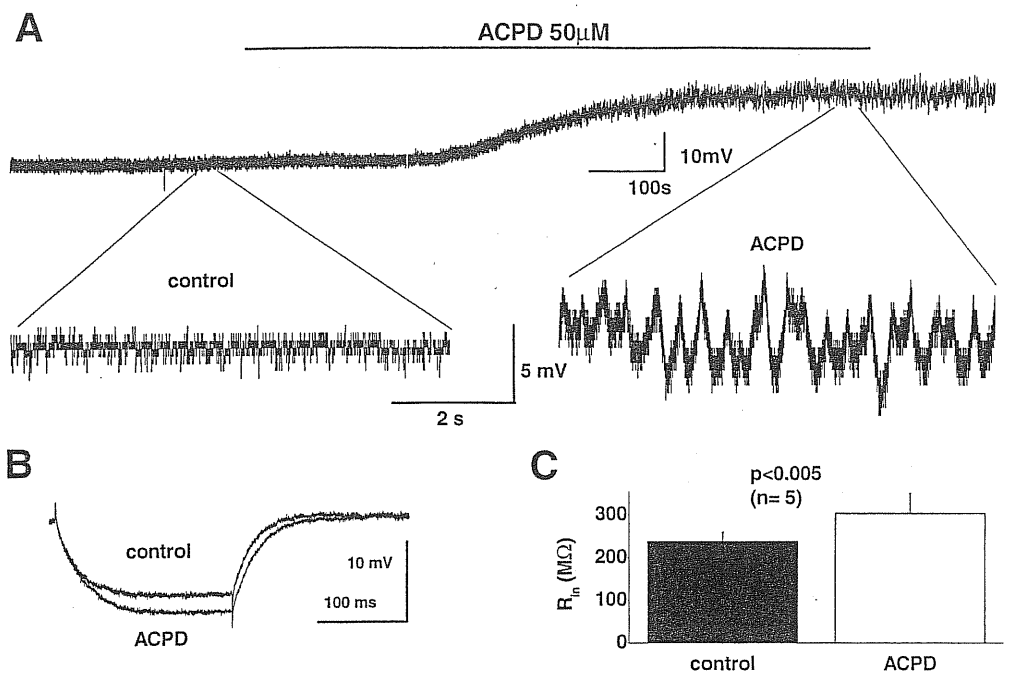

Figure 12. Activation of mGluR depolarizes HM. A: bath application of 50 μM t-ACPD (indicated by bar above the trace) produces a slowly developing depolarization. Two insets show traces taken during control and during t-ACPD treatment as indicated (faster time scale). Note membrane noise increase in t-ACPD. B: negative current steps (50 pA, 200 ms) delivered to calculate R_{in} changes (different cell). In t-ACPD the same current step evokes larger voltage response. C: on average, t-ACPD increases R_{in} as summarized in the plot.

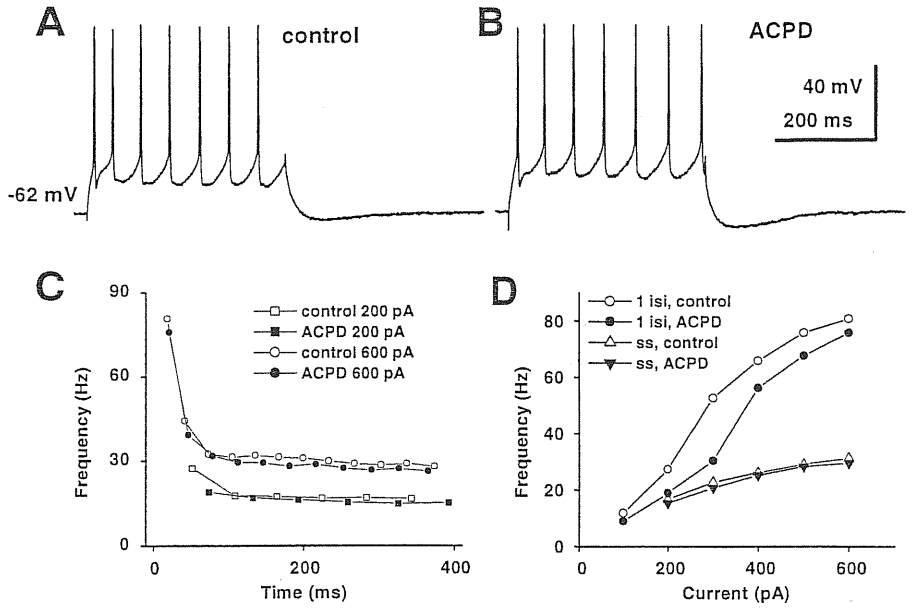

Figure 13. Activation of mGluR by t-ACPD does not influence repetitive firing. A and B: responses to 200pA current step (400 ms) in control (A) and 50 μM t-ACPD solution (B). C: instantaneous firing frequency ploted versus time for the same cell, as in A and B, spike trains elicited by 200 (squares) and 600 pA (circles) current steps (400 ms). Note that plots for control (open symbols) and t-ACPD (closed symbols) are almost overlapping. D: first interspike interval (1isi) and steady-state (ss) f-I relations before and after t-ACPD. Note that the initial firing f-I curve (1isi) is shifted rightward in t-ACPD, while that of steady-state (ss) is unchanged.

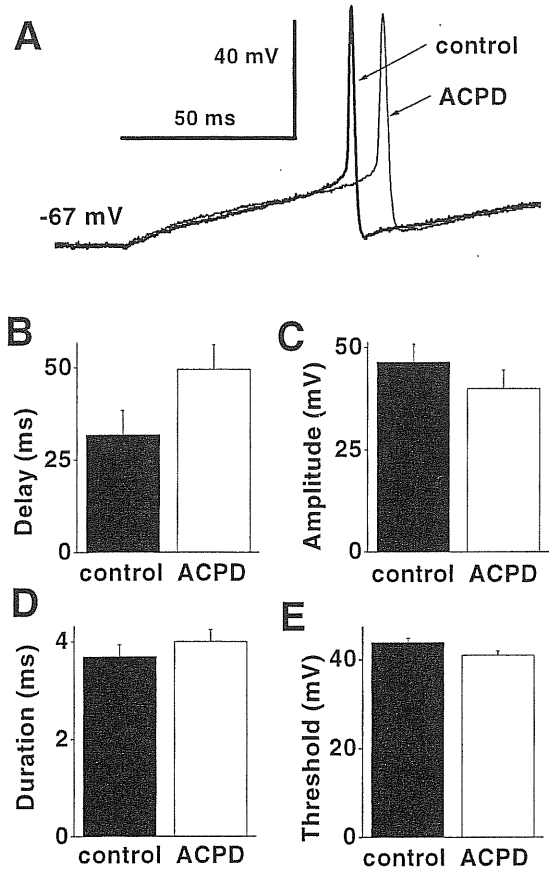

Figure 14. t-ACPD prolongs AP latency. A: first spikes of the trains showed in Fig. 13 A and B superimposed at faster time scale. Note increased delay of spike elicited in t-ACPD as also quantified for 7 cells in B. C, D and E: t-ACPD does not change the spike amplitude (C), duration (D), and threshold (E).

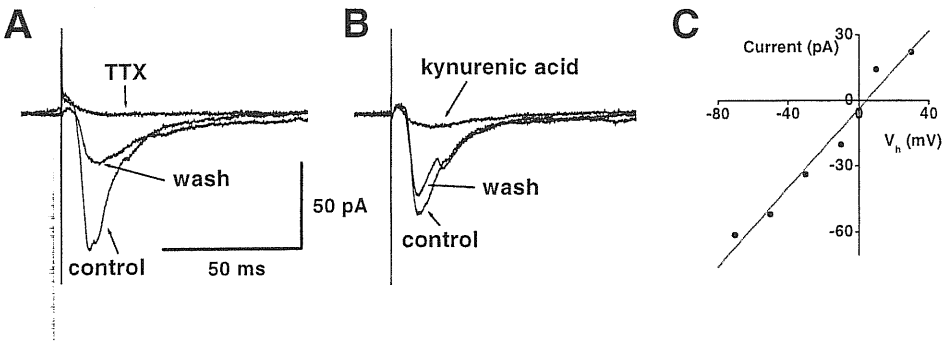

Figure 15. Characteristics of evoked glutamatergic postsynaptic currents. A: evoked current is abolished by TTX (0.5 μM). B: evoked current is markedly reduced by kynurenic acid (2 mM), an antagonist of glutamate receptors. C: I-V plot of evoked currents in a single neuron. Evoked currents reverse at membrane potential near 0 mV.

and reversed at membrane potential near 0 mV (Fig. 15C).

Paired eEPSCs were evoked continuously at 0.1 Hz in control, t-ACPD (50 μM), and washout solutions (Fig. 16A). t-APCD (50 μM) reduced the peak amplitude of the first and second eEPSCs to 38±3% ($p<0.05$) and 40±2% ($p<0.05$), respectively (n= 10 cells). In general, the amplitude recovered during washout of t-ACPD (Fig. 16A, right trace). In addition, t-ACPD produced an inward current, as seen from the downward shift of baseline (Fig. 16A, middle). The time course of t-ACPD effect on both first and second eEPSCs can be followed in Fig. 16B. On average, the peak amplitude of the current evoked by the second stimulus was usually larger than that evoked by first stimulus in control (Fig. 16A and B). This phenomenon was quantified by the ratio of second eEPSC peak amplitude to first one and referred to as paired pulse facilitation (PPF), which is plotted in Fig. 16C. PPF was 1.29±0.05 in control and was significantly increased in t-ACPD to 1.51±0.03 (n= 10; $p<0.05$) as exemplified in Fig.16C and D.

2. VOLTAGE AND CA^{2+} DEPENDENT CURRENTS IN HMS

2.1. Basic characteristics of HMs under voltage clamp conditions

Voltage clamp recordings were obtained from 86 neurons with 51±5 pF somatic capacitance and 300±100 MΩ input resistance (R_{in}). Nine motoneurons in nine distinct slices were injected with neurobiotin in order to check if there was any substantial dye coupling among these cells. After histological processing no significant staining of cells adjacent to injected motoneuron was detected. These results suggest that HMs were not strongly coupled, a condition which would have made difficult to perform voltage clamp studies.

In standard solution membrane currents elicited by depolarizing voltage commands comprised multiple components. An example is shown in Fig. 17A where depolarizing steps (10 mV increments from -70 mV holding potential; V_h) evoked fast inward currents (apparent threshold = -50 mV) followed by slower outward currents (apparent threshold = -20 mV). The fast inward current was blocked completely by 1 μM TTX (Fig. 17B), suggesting that it was a voltage-activated Na^+ current (I_{Na}). Although not shown in Fig. 17 most cells also displayed a slower and smaller inward current which was blocked by Cd^{2+} (0.2 mM) or by replacing Ca^{2+} with Co^{2+}, indicating that it was mostly carried by

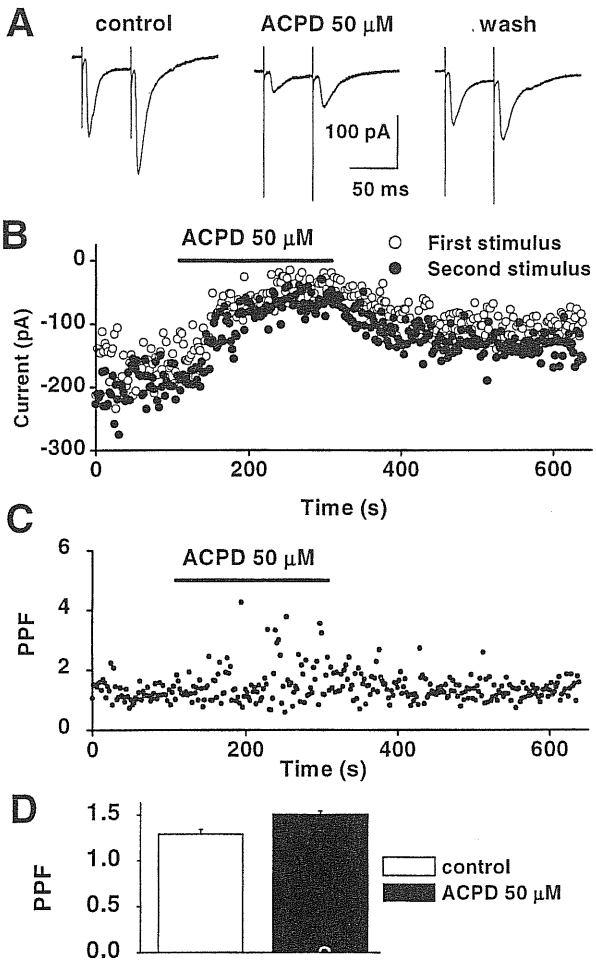

Figure 16. Activation of mGluR depress evoked glutamatergic currents. A: current evoked by paired stimuli is depressed in t-ACPD solution and recovers during it washout. Traces are averages of 10 consecutive evoked responses. B: plot of time course of t-ACPD effect. Both first (open circles) and second (closed circles) stimulus response amplitude is plotted versus time. t-ACPD application period is indicated by the bar above. C: paired pulse facilitation (PPF) as ratio of first stimulus response amplitude to second stimulus response amplitude is plotted versus time. t-ACPD application period is indicated by the bar above. D: histograms of PPF in control or in t-ACPD solution. T-ACPD significantly enhances PPF ($p<0.05$; $n=10$).

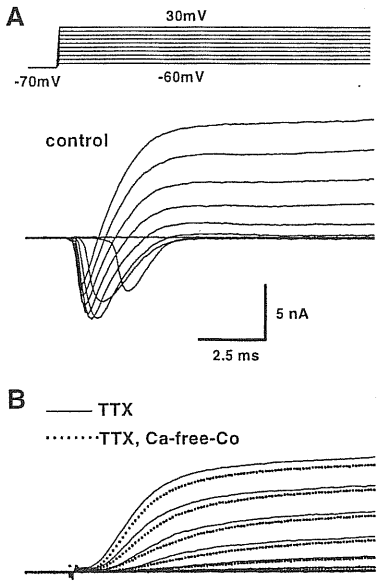

Figure 17. Depolarization elicited membrane currents of HMs. A, membrane currents elicited by application of depolarizing voltage steps (10 mV increments) from -70 mV V_h (schematized in upper panel) in normal solution (control). Pulses (at 10 s intervals) were 1 s long but only the initial 10 ms traces are shown. Note inward current followed by outward current. All traces are leak subtracted. B, membrane currents elicited by the same voltage protocol applied to the same cell bathed in a solution containing 1 μM TTX (solid line traces) or in a solution containing 1 μM TTX and nominally zero Ca^{2+} replaced by Co^{2+} (2 mM) (dotted line traces). Note suppression of inward current while outward current persists.

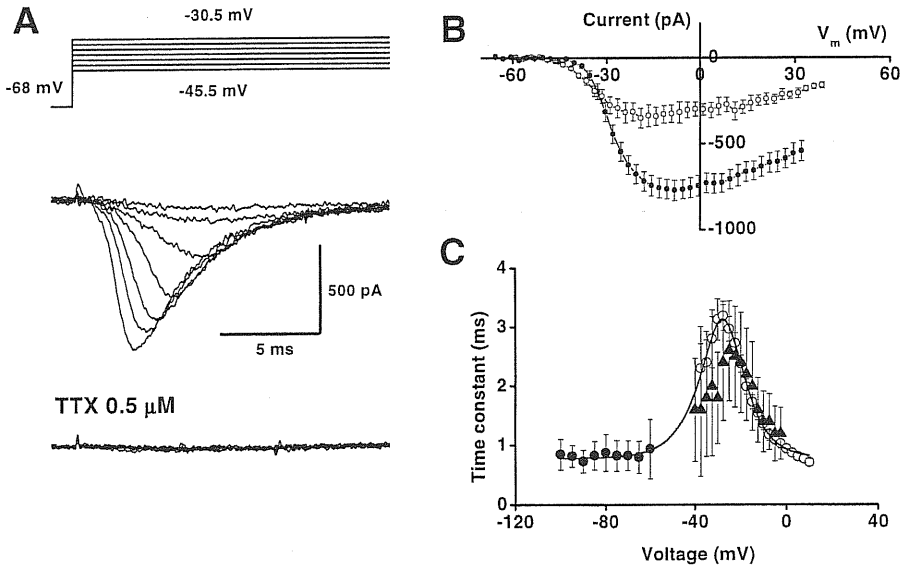

Figure 18. I_{Na} recorded from HMs. A: I_{Na} elicited by depolarizing voltage steps from –45.5 to -30.5 mV. This current is completely abolished by TTX (0.5 μM; lower traces). B: current-voltage (I-V) relation of I_{Na} in choline (black circles; n= 10 cells) or NMDG (open circles; n= 7) containing solutions. C: activation time constants, τ_a, in NMDG solution (open circles; n=7 cells) or in high-Na^+ solution with 20 nM TTX (closed triangles; n= 3 cells) calculated with eq. (4) and plotted versus membrane voltage. Closed circles represent deactivation time constants in NMDG solution as estimated from monoexponential fitting of I_{Na} tail currents (n= 4). Line represents eq. (5) fitting of graph points for data obtained in NMDG solution.

Ca^{2+}. As the properties of voltage dependent Ca^{2+} currents and channels of HMs have been systematically investigated by Umemiya and Berger (1994a, 1995a), they will not be further reported here.

The outward current, clearly detected in TTX medium (Fig. 17B), was partly diminished (for instance by 11 % at 0 mV) in Ca-free-Co solution or by extracellular application of Cd^{2+} (not shown). This outward component was more strongly depressed (40±8 % at 0 mV; n=3 cells) by the K^+ channel blocker TEA (20 mM; not shown). These preliminary observations suggested that the outward current was presumably due to K^+ efflux via several conductances, mainly voltage and partly Ca^{2+} activated. Ca^{2+}-dependent K^+ currents were very small by comparison with Ca^{2+}-independent K^+ currents (Fig. 17 B) presumably because of the presence of the strong Ca^{2+} chelator EGTA (10 mM), which is known to suppress the Ca^{2+} dependent AHPs (Viana et al. 1993b). For this reason EGTA was reduced in patch pipette solution when Ca^{2+} dependent K^+ currents were recorded.

2.2. Voltage dependent Na^+ current

In standard solution the I_{Na} was too fast to be adequately voltage clamped (Fig. 17A; also see Takahashi 1990, for problems to clamping I_{Na} in motoneurons). Thus, an attempt was made to record I_{Na} after a strong reduction in the extracellular Na^+ concentration or in presence of a small dose of TTX (20 nM) to decrease I_{Na}. These manoeuvers made it possible to record apparently voltage clamped I_{Na} and to obtain a detailed kinetic description of this current.

The example of Fig. 18A shows a family of I_{Na} currents elicited by voltage steps from –45.5 to –30.5 mV by 5 mV increments in low-Na^+ (20 mM NaCl) solution, in which 120 mM of external NaCl was replaced by 60 mM TEACl and 60 mM cholineCl. I_{Na} was completely blocked by 0.5 µM TTX as demonstrated in Fig. 18A (lower traces). No TTX resistent inward current was observed.

I_{Na} appeared to be under voltage clamp control for various reasons. There was no latency jitter, the current activation phase become steeper with increasing voltage, and the descending phase of the current-voltage (I-V) curve declined continuously without discontinuous breaks (Fig. 18B; closed circles; n=10 cells).

In neurons maintained at –65mV V_h, I_{Na} activated at an apparent threshold of – 45 mV

(Fig. 18B; closed circles) and reached a maximum peak at about –10 mV. Reversal potential (E_{Na}) of I_{Na} was estimated from the projected intersection of the I-V (voltage range 0 to 30 mV) with the voltage axis. A value of 110 mV was obtained, which was far from that calculated with the Nernst equation (15 mV). This fact led to the conclusion that either the cells were poorly clamped or there was another ion substantially permeating Na^+ channels (for example choline). When another large cation NMDG was used instead of choline to replace external Na^+, the E_{Na} estimated from this I-V gave a value of 80 mV (Fig. 18B; open circles; n= 7), still far from the expected one. However, the amplitude of I_{Na} in NMDG solution was reduced by half compared with I_{Na} recorded in presence of choline (Fig. 18B). This result suggests that care should be taken with the choice of this "impermeant" cation to replace Na^+ as choline had apparently the ability to permeate through Na^+ channels of HMs. Although it might have been anticipated that a large cation like choline would have had minimal permeability through Na^+ channels, it is worth noting that significant permeability to choline of Na^+ channel has actually been reported on squid axon (Hironaka and Narahashi 1977).

Further attempts were made to improve clamp efficiency of I_{Na}. One approach consisted in reversing the I_{Na} direction by increasing internal Na^+. This method should have helped to decrease the size of I_{Na} and, thus, to improve clamping. Therefore, high Na^+ (40 mM) patch pipettes were used, while the extracellular Na^+ concentration was 20 mM (with 60 mM NMDG). This Na^+ concentration ratio gave E_{Na} of –15 mV as calculated with the Nernst equation. A set of current traces elicited by depolarizing voltage commands to potentials between –30 and +30 mV from –65 V_h is shown in Fig. 19A. At membrane potential positive to 0 mV, I_{Na} changed direction as seen from appearance of a fast transient outward current at these potentials. An average I-V of 4 cells is plotted in Fig. 19B. E_{Na} estimated from this plot was 5 mV. However, closer inspection of traces recorded in these conditions revealed that occasionally I_{Na} was multiphasic at positive potentials. An example of such a current trace (elicited by voltage step to 20 mV) is depicted in Fig. 19C. The current following the capacitative artifact had three components. A fast, transient inward current, I_{sp}, and an outward current, I_{Na}, both sensitive to TTX. I_{sp} had the same amplitude at all potentials where it was present and was presumably an action current generated at a distal, unclamped part of the neuron.

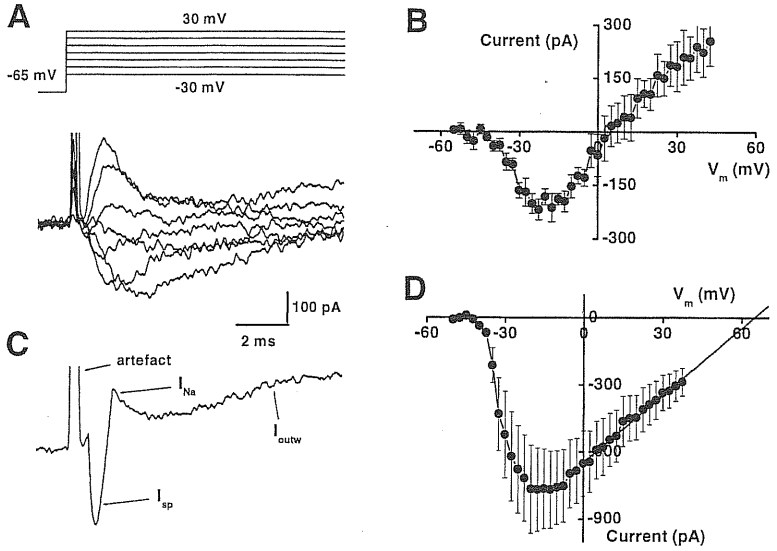

Figure 19. I_{Na} reverses during recording with a high Na^+ containing pipette. A: I_{Na} elicited by depolarizing voltage steps as depicted in upper panel. Recording pipette contains 40 mM Na^+ (20 mM Na^+ in extracellular solution). Note that I_{Na} reverses at positive membrane potentials. B: average I-V relation of I_{Na} recorded in high intracellular Na^+ conditions (n= 5 cells). C: an example of membrane current trace (elicited by voltage step to 20 mV), which exhibits two components of TTX sensitive Na^+ current, I_{Na} and I_{sp}, seen immediately after artifact. A slow outward current, I_{outw}, is the current also depicted in Fig. 20. D: average I-V relation of I_{Na} recorded in standard solution (150 mM extracellular Na^+ and 10 mM intracellular Na^+) containing 20 nM TTX to partially block I_{Na} (n= 5).

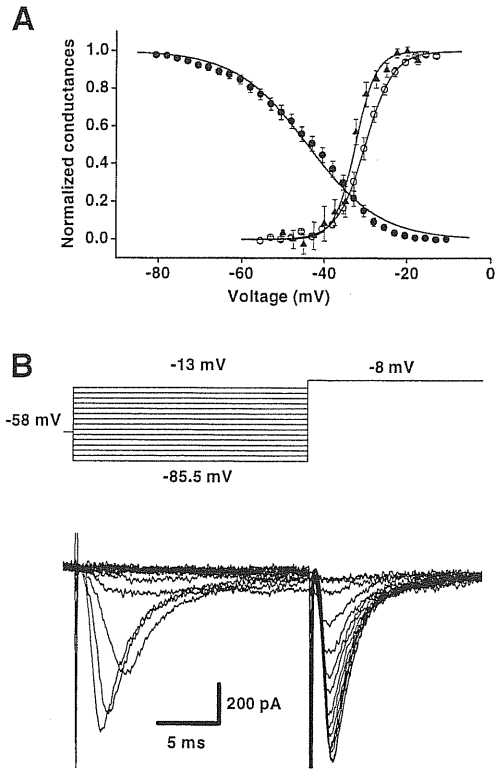

Figure 20. Voltage dependence of I_{Na} activation and inactivation. A: I_{Na} activation (open circles) and inactivation (closed circles) curves obtained in NMDG solution. Experimental points obtained by dividing I_{Na} peak by its driving force (V_m-E_{Na}) and by normalizing them by the maximal conductance. Lines represent Boltzmann equation fits; the potentials for half activation and half inactivation were –30.2± 08 and –44.1±0.3 mV, respectively, while the slope factors were 3.4± 0.7 and –8.7±0.3 mV, respectively (n= 7). Closed triangles represent data obtained in high Na^+ solution containing 20 nM TTX. B: a set of I_{Na} traces elicited by a test voltage step to –8 mV after conditioning prepulse from –85.5 to –13 mV for 20 ms.

This current, present at positive potentials also in choline and NMDG solutions, contaminated the I_{Na} and did not allow plotting reliable I-V curves at these positive potentials. The slow outward current, I_{outw}, insensitive to TTX and present also in previous experiments, will be described below. Further experiments were performed in standard extracellular Na^+ (high-Na^+) solution containing 20 nM TTX to block Na^+ channels partially. An average I-V plot (n= 3 cells) of I_{Na} current is shown in Fig. 19D. The E_{Na} estimated from this I-V was 64 mV, near to that calculated with the Nernst equation (61.5 mV).

Voltage dependence and kinetics of I_{Na} (recorded in NMDG containing extracellular solution) were next examined. The time-to-peak, t_p, was measured to estimate the activation time constant, τ_a, which was analytically calculated from eq. (4) and plotted *versus* membrane potential in the Fig. 18C (open circles; n=7). This plot indicates the strong voltage dependence of the I_{Na} activation process. Similar τ_a plot was obtained for I_{Na} recorded in high Na^+ solution (Fig. 18C; closed triangles; n= 3 cells). The deactivation time constant at more negative membrane potentials was evaluated by exponential fitting of decaying I_{Na} tail currents recorded at repolarized membrane potentials (range –60 to –100 mV) after activation of I_{Na} by short voltage steps to –10 mV for 3- 4 ms in NMDG solution. Decay time constants were averaged and plotted *versus* membrane potential (Fig. 18C, closed circles; n=4). Both activation and deactivation time constants in the plot in Fig 18C were fitted by the eq. (5).

The voltage dependence of I_{Na} conductance activation was examined by calculating the I_{Na} peak conductance (g_{peak}) obtained by dividing the I_{Na} peak amplitude by the driving force using eq. (1). E_{Na} used in these calculations was that calculated with Nernst equation (15 mV for given solution). Normalized conductance values (eq. (2)) were thus plotted against membrane potentials to give the activation curve (Fig. 20A; open circles). These experimental points were fitted with the Boltzmann equation (eq. (3)), which indicated half activation of I_{Na} at -30.2±0.8 mV with a 3.4±0.7mV slope factor (n= 7 cells). The conductance was activated at potentials positive to -50 mV and was virtually fully activated at -10 mV. The voltage dependence of I_{Na} recorded in high Na^+ solution (Fig. 20A; closed triangles) activated half maximally at –32.6± 0.3 mV with a 2.5± 0.2 mV slope factor (n= 3 cells).

The protocol to study steady-state inactivation of I_{Na} is depicted in Fig. 20B in which the motoneuron membrane potential was conditioned (for 20 ms) to different potentials (in the range from –85.5 mV to -13 mV) and then depolarized to the fixed test potential of -8 mV which corresponded to full activation of I_{Na} (see Fig. 20A). Traces in Fig. 20B show that, with progressively more depolarized prepulses, I_{Na} disappeared. I_{Na} peak was measured and the underlying g_{peak} calculated and normalized to g_{max} (eq. (3) and (4)). The inactivation curve was generated by plotting g_{norm} *versus* the conditioning step potential (Fig. 20A; closed circles) and fitted with the Boltzmann equation. Half inactivation was estimated at –44.1± 0.3 mV with a –8.7± 0.3 mV slope factor (n= 7 cells). The conductance inactivation was complete at -20 mV and was completely removed at -80 mV.

Once activated the I_{Na} inactivated exponentially to zero with a single voltage dependent time constant. An example of the monoexponential fitting of I_{Na} is shown in the Fig. 21A. Currents elicited by voltage steps to –22.5, -15, -7.5, and 0 mV from –65 mV V_h decayed with 2.68, 2.15, 1.79, and 1.62 ms time constants, respectively, in NMDG solution. Excellent fitting with a single exponent indicated the presence of only one component of I_{Na} in neonatal HMs. Moreover, such a good fit might be an additional sign of good voltage clamp of I_{Na}. The averaged inactivation time constants obtained in NMDG (closed circles) and high Na^+ (open triangles) solutions were plotted against the membrane potential in the Fig. 21B. Data obtained in two different solutions were very similar and thus indicated that the use of low Na^+ solution did not changed I_{Na} characteristics.

The kinetics of recovery from inactivation is of special interest since it can limit the firing frequency of AP in motoneurons (Powers et al. 1999). In the present study, the I_{Na} recovery from inactivation at four different potentials was investigated using the two-pulse protocol shown in Fig. 21D. I_{Na} was activated and subsequently inactivated by a long (20 ms) voltage pulse from of –58 mV to –13 mV. A second test pulse to –13 mV was then applied to the membrane with increasing delay to check for the cell ability to generate I_{Na}. The ratio between the peak amplitude evoked by the second and first voltage pulses was plotted against the time interval between the two pulses. In Fig. 21E there are examples of such plots for two V_h –58 (Ea) and –78 mV (Eb). The experimental points

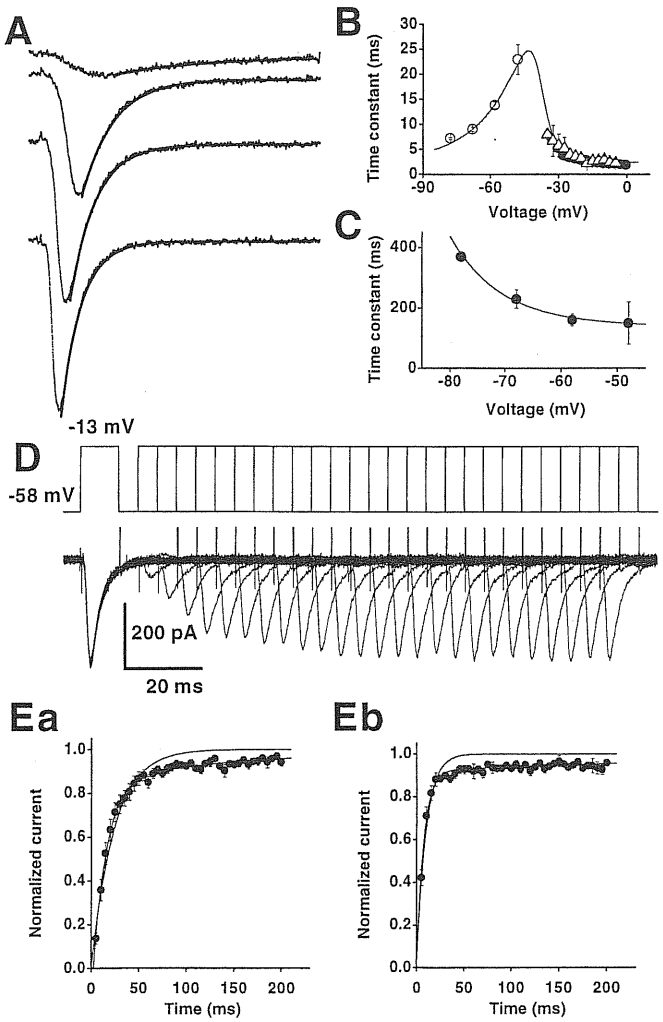

Figure 21. Inactivation kinetics of I_{Na}. A: I_{Na}, recorded in NMDG solution, decay phase fitted monoexponentially with time constants of 2.7, 2.2, 1.8, and 1.6 ms for currents elicited by depolarizing steps to –22.5, -15, -7.5, and 0 mV, respectively. B: inactivation time constants (closed circles) and fast time constants of recovery from inactivation (open circles) plotted versus membrane potential. Line represents fitting of experimental points with eq. (5). Open triangles represent inactivation time constant of I_{Na} recorded in high Na^+ solution containing 20 nM TTX. C: plot of time constants of slow recovery from inactivation versus membrane potential. D: current traces elicited by two pulse protocol to study the process of I_{Na} recovery from inactivation in NMDG solution. E: plots of experimental points obtained by the protocol shown in D. Data points represent the normalized amplitude of I_{Na} evoked by second pulse at different intervals after first pulse for sojourns at –58 (Ea) or –78 mV (Eb). The lines represent fits with one or two exponentials. The best fit is obtained with two exponentials (time constants of 13.9± 0.7 and 160±20 for –58 mV).

were obtained by averaging data from 6 cells. The examples of Fig. 21E show fitting with single or double exponentials. Since monoexponential fitting failed to describe the late phase of recovery, two exponents were found to be adequate for fitting both fast and slow phases of recovery from inactivation. At a potential of –58 mV the fast and slow time constants were 13.9±0.7 and 160±20 ms (n= 6 cells), respectively. Fast and slow time constants were plotted against V_h in the Fig. 21B (open circles) and in the Fig. 21C (closed circles), respectively. Both inactivation and fast recovery time constants were fitted with eq. (2) to describe the voltage dependence of inactivation time constants.

In solutions containing low Na^+, choline (or NMDG), TEA, and 4-AP together with I_{Na} an unidentified outward current (I_{outw}; Fig. 22A), elicited by the same voltage protocol as depicted in Fig. 18A was recorded. I_{outw} was resistant to 500 nM TTX, a dose which completely blocked I_{Na} (Fig. 22B). An average I-V is plotted in Fig. 22C. The identity of this current remains unclear.

2.3. Voltage dependent outward K^+ currents

2.3.1. Slow transient outward current (I_{Kslow}). The delayed transient outward current (I_{Kslow}) was routinely investigated in Ca-free-Co solution containing TTX (1 μM) and Cs^+ (4 mM). The example of Fig. 23A shows a set of current traces generated by steps to potentials between -30 mV and +20 mV following a 500 ms long conditioning step (prepulse) to -50 mV from -70 mV V_h. The test command to -20 mV was clearly above threshold for eliciting a slowly developing outward current, which did not decline during the 1-s pulse. Larger steps generated currents of larger amplitude and faster peaking response. Some decline in current amplitude emerged for responses generated by pulses to positive membrane potentials. Preliminary trials showed that the conditioning step (200-500 ms) to -50 mV did not influence the slow current development but it removed the contaminating presence of a faster current (described below). For this reason, whenever the slow current was studied in isolation, a 400 ms prepulse to -50 mV was always applied before depolarizing test steps. We also checked that extracellular application of Cs^+ did not influence I_{Kslow} since this monovalent cation can block a variety of K^+ channels in other cells (Rudy 1988). Thus, comparing the steady state I_{Kslow} amplitude (evoked by +20 mV steps) in Cs^+ free solution with the one obtained after the

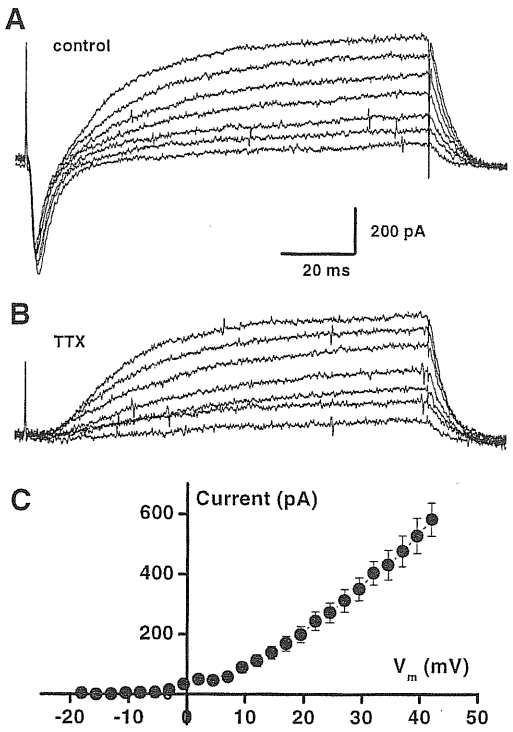

Figure 22. An unidentified I_{outw} current recorded from HMs. A: set of membrane current traces elicited with similar voltage protocol as in Fig. 16. Note the presence of two components, I_{Na} and I_{outw}, of distinct kinetics and flow directions. B: I_{Na} is blocked by TTX (500 nM), while I_{outw} is TTX resistant. C: average I-V relation of I_{outw} (n= 10 cells).

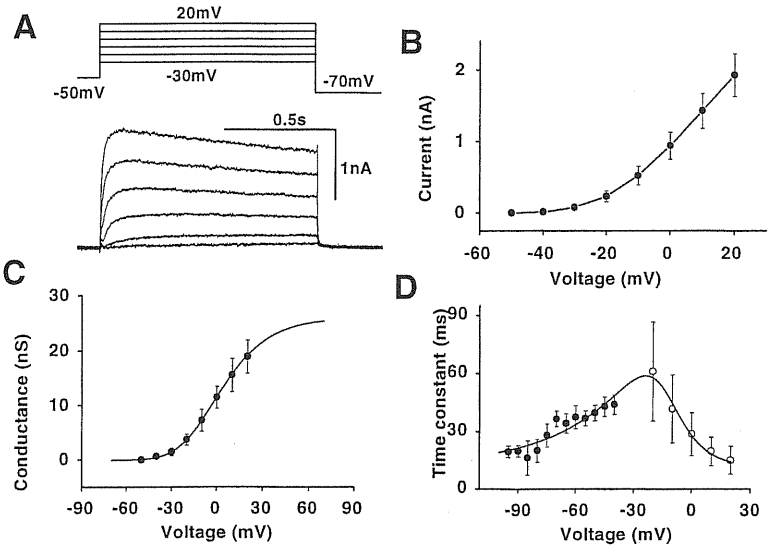

Figure 23. HMs possess a slow transient outward current (I_{Kslow}). A, I_{Kslow} elicited by depolarizing voltage steps from -30 mV to 20 mV with conditioning step to -50 mV for 400 ms. B, I-V relation of I_{Kslow} (n=15 cells). C, plot of I_{Kslow} chord conductance *versus* membrane voltage for the same group of cells. Line represents Boltzmann equation fit; the potential for half activation and slope factor were -25±10 mV and 19±3 mV, respectively. D, graph of I_{Kslow} activation time constant (open circles; estimated by fitting the current activation phase with a single exponential) and deactivation time constan (closed circles) *versus* membrane voltage (n=8 cells). Line represents eq. (5) fitting of graph points.

addition of Cs^+ (4 mM) indicated that there was no significant change (3±8 %; n=4; p=0.7 with ANOVA test)

The average I-V relation (n=15 cells) for I_{Kslow} is shown in Fig. 23B. I_{Kslow} activated at membrane potentials positive to -50 mV. Its amplitude monotonically increased with increasing depolarization within the tested potential range of -50 to +20mV. The dependence of I_{Kslow} chord conductance (*g*; expressed in nS) on membrane potential is shown in Fig. 23C. After measuring the peak of I_{Kslow}, the values for *g* were calculated according to the eq. (1). The values of *g* grew for potentials positive to -50 mV and showed an average increment of 3.9±0.4 nS/mV. Fitting these data according to the Boltzmann equation (Fig. 23C line) yielded an average slope of 19±3 mV; the *g* maximum value was estimated as 26±1 nS as it occurred at a potential level (+60 mV) outside the range tested in the present experiments.

Fig. 23D shows a plot for the voltage dependence of I_{Kslow} activation (open circles) in which the current rising phase could be fitted monoexponentially: it is clear that it had a slow onset, which for example at 0 mV had a time constant of 30±10 ms. Once I_{Kslow} reached its peak, it remained at a plateau or gradually declined for test depolarizations positive to -10 mV. For example, I_{Kslow} decline had a time constant of 4.2±0.4s at +20mV membrane potential (n=3 cells). The deactivation properties of I_{Kslow} were studied using the time constant of tail currents at the end of depolarizing voltage commands. Deactivation time constants were plotted in Fig. 23D (closed circles). In this case the deactivation time constant was in the range 20-60 ms within -110 and -40 mV (n=7 cells). These data therefore indicate that I_{Kslow} had rather slow kinetic characteristics which made it unsuitable to control motoneuronal excitability within a narrow time frame and prompted a more systematic search for a faster outward current component hitherto undescribed in these cells.

2.3.2. Fast transient outward current (I_{Kfast}). Any hypothetical fast outward current (I_{Kfast}) might have been largely masked by the use of relatively depolarized V_h values since this appears to be the case for the fast outward current of other central neurons (Rogawski 1985; Rudy 1988). In order to demonstrate its existence in HMs a subtraction procedure as detailed in Fig. 24A, B was utilized. In fact, a family of outward currents consisting of an initial, rapid peak followed by a slower component was obtained (Fig. 24A) when the

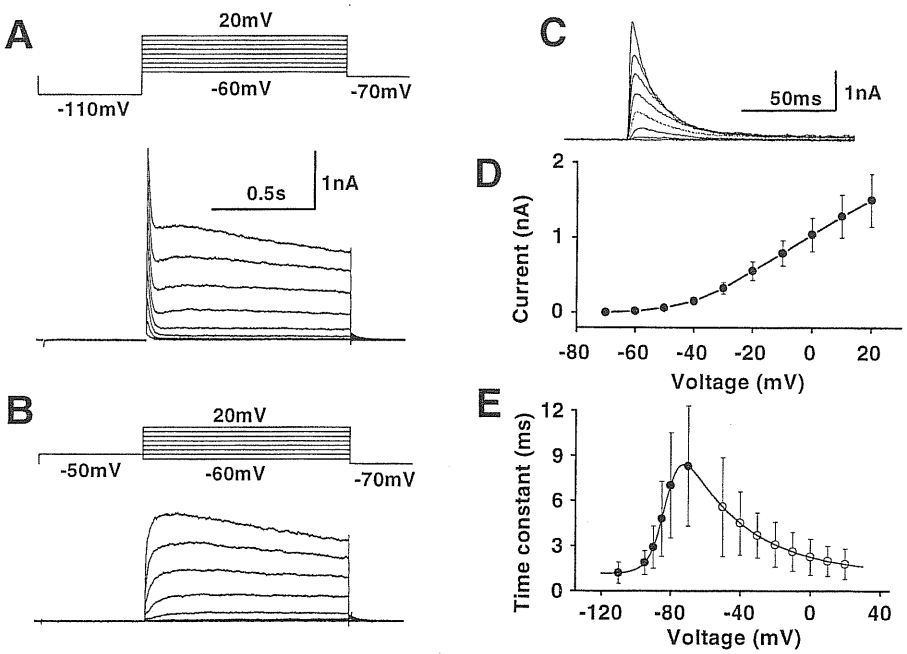

Figure 24. HMs possess a fast transient outward current (I_{Kfast}). A and B, two sets of outward current traces evoked by a series of depolarizing voltage steps from -60 mV to 20 mV preceded by either a hyperpolarizing voltage step to -110 mV (A) or a depolarizing voltage step to -50 mV (B) for 400 ms. C, I_{Kfast} isolated by subtracting current traces in B from those in A. D, I-V relation of I_{Kfast} (n=8 cells). E, plot of I_{Kfast} activation (open circles) and deactivation (closed circles) time constant *versus* membrane potential. Line represents eq. (5) fitting of graph points.

1 s depolarizing test steps were applied immediately after a hyperpolarizing prepulse (to -110 mV). An analogous protocol was subsequently repeated on the same cell with only one difference, namely, instead of a hyperpolarizing prepulse, a depolarizing one (to -50mV; Fig. 24B). In the latter case the outward current typically consisted of I_{Kslow} only (see also Fig. 23). After point-to-point subtraction of the current traces obtained with depolarized prepulses from those obtained with hyperpolarizing prepulses, a transient and rapid outward current (I_{Kfast}) could be demonstrated in isolation (Fig. 24C). I_{Kfast} grew to a peak and inactivated in less than 200 ms (Fig. 24C). It was also investigated whether the presence of 4 mM Cs^+ in the bathing solution might have affected I_{Kfast} development. Comparing the peak amplitude of I_{Kfast} (induced by steps to +20 mV) before and after adding Cs^+ showed that there was no significant change (7±9 %; n=3; p=0.8) suggesting that this cation did not interfere with I_{Kfast} recording.

The peak current-voltage (I-V) relation for I_{fast} is shown in Fig. 24D. The threshold for activation of I_{Kfast} was approximately -60 mV with a monotonic increase in I_{Kfast} amplitude as the test depolarization increased. The I_{Kfast} activation time constants were calculated from time-to-peak using eq. (4) and were plotted against the membrane potential in Fig. 24E (open circles). The activation time constant decreased with increasing depolarization, suggesting voltage dependence of the current activation process. The activation time constant was 6±3 ms at -50 mV and 2±1 ms at +20mV (n=5 cells). Deactivation properties of I_{Kfast} were obtained by measuring the time constant of decay of tail currents (e.g. Fig. 27) at potentials between -105 and -65 mV (plotted in Fig. 24E, closed circles) since at less negative level the inactivation process became predominant. In this case deactivation was in the range 1-9 ms (range 4-38ms; n=6 cells).

The activation and inactivation properties of I_{Kfast} g were next examined. For activation the peak conductance (g_{peak}) was simply determined by dividing the I_{Kfast} peak amplitude by the driving force (eq. (1)) and then normalized (g_{norm}) to the maximum conductance, g_{max} (eq. (2)). The latter value was obtained from chord conductance-voltage plots, which indicated g saturation at +20 mV.

For 9 cells the normalized conductance (g_{norm}) values were thus plotted against membrane potentials to give the activation curve (Fig. 25A; filled circles). These experimental points were fitted with the Boltzmann equation, which indicated half

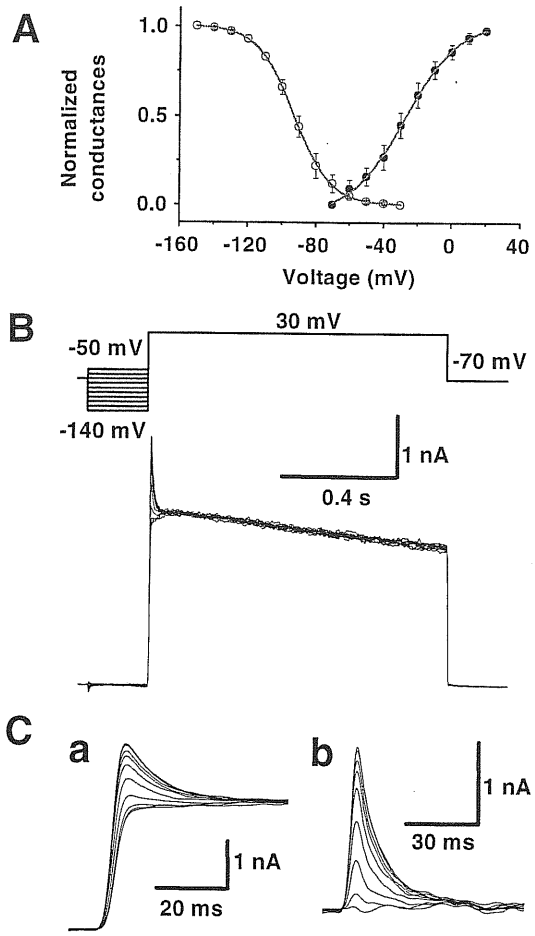

Figure 25. Voltage dependence of activation and inactivation of I_{Kfast}. A, activation (filled circles) and inactivation (open circles) curves for I_{Kfast}. Experimental points were obtained dividing I_{Kfast} peak by its driving force (V_m-E_{rev}) and normalizing them by the maximal conductance g_{max} taken as 1. Lines represent Boltzmann equation fits; the potentials for half inactivation and half activation were -92.9±0.2 mV and -27.6±0.9 mV, respectively, while the slope factors were 10.8±0.2 mV and 16±1 mV for inactivation and activation, respectively (n=9 cells). B, a set of outward currents elicited by a test voltage step to 30 mV after conditioning pre-pulses from -140 mV to -50 mV for 200 ms. C a, same set of current traces on a faster time scale. C b, individual I_{Kfast} responses were isolated by subtracting the current trace obtained after the depolarizing prepulse to -50 mV from the current traces shown in C a.

activation of I_{Kfast} at -27.6±0.9 mV with a 16±1mV slope. The conductance was thus activated at potentials positive to -70 mV and was virtually fully activated at +20 mV.

The protocol to study steady-state inactivation of I_{Kfast} is depicted in Fig. 25B in which the motoneuron membrane potential was conditioned (for 200 ms) to different potentials (in the range from -140 mV to -10 mV) and then depolarized to a fixed test potential of +30 mV which corresponded to full activation of I_{Kfast} (see Fig. 25A). The faster timebase records of Fig. 25Ca show that, with progressively more depolarized prepulses, I_{Kfast} disappeared. For full isolation of I_{Kfast} the current trace after a prepulse to -50 mV (when I_{Kfast} was absent) was subtracted from all the other traces. I_{Kfast} could thus be measured separately (Fig. 25C b) and the inactivation curve was generated as described for I_{Na} (Fig. 25A; open circles) and fitted with the Boltzmann equation. Half inactivation was estimated at -92.9±0.2 mV with a -10.8±0.2 mV slope (n=9 cells). The conductance inactivation was complete at -50 mV and was completely removed at -140 mV. When activated I_{Kfast} inactivated completely or to a small residual current (Fig. 25C).

It seemed useful to characterize how quickly I_{Kfast} inactivation could develop as this property may influence the firing characteristics of the cell. This result was obtained by measuring the time constants of single exponential decay of I_{Kfast} (Fig. 26A). In these examples the values were 86, 75, and 61 ms at -40, -20, and 0 mV membrane potentials, respectively. These observations allowed to plot the average time constants of inactivation *versus* membrane potential (Fig. 26B, open circles; n=7 cells). Inactivation was found to be dependent on voltage since the decay time constant was twice faster at +20 mV than at -40 mV.

Recovery of I_{Kfast} from inactivation was studied using a two pulse protocol as shown in Fig. 26C. A conditioning step (1 s) from -110 mV V_h to +10 mV was first employed to inactivate I_{Kfast} completely and then, after a sojourn at -110 mV for 10-1000ms, a test pulse to +10 mV was subsequently applied. Note that after progressively longer sojourns at -110 mV the amplitude of I_{Kfast} gradually returned to control value. The I_{Kfast} peak (normalized with respect to the initial control amplitude) was plotted *versus* time (Fig. 26D; open circles). Fig. 26D also shows that on 3 cells similar data were obtained when the initial V_h and sojourns values were -110 mV or -90 mV (open circles and filled circles, respectively). In both cases the time course of recovery from inactivation was

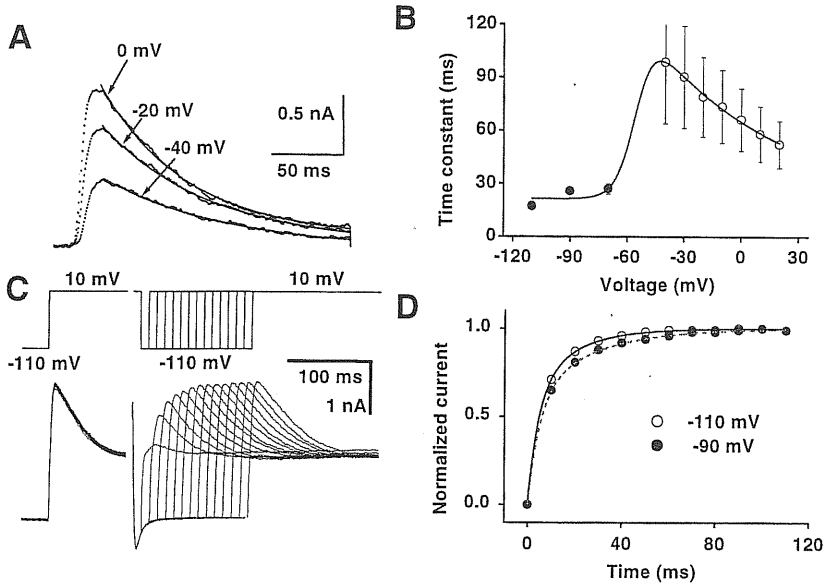

Figure 26. Inactivation kinetics of I_{Kfast}. A, I_{Kfast} traces isolated as described in Fig. 22 C. The decay phase was fitted monoexponentially with time constants of 86 ms, 75 ms, and 61 ms for currents elicited by depolarizing steps to -40 mV, -20 mV, and 0 mV, respectively. B, plot of inactivation time constant (open circles) and fast time constant of recovery from inactivation (closed circles) *versus* membrane voltage (n=7 cells). Line represents eq. (5) fitting to graph points. C, current traces elicited by two pulse voltage protocol to measure time course of I_{Kfast} recovery from inactivation. D, plots of data obtained with a protocol similar to the one shown in C; the experimental points represent the normalized amplitude of I_{Kfast} (ordinate) evoked by the second pulse at different intervals (expressed in ms; abscissa) after first pulse for sojourns to -110 mV (open circles) or -90 mV (closed circles) (n=3 cells). The time course for recovery was well fitted by two exponentials with time constants of 4.4±0.6 and 17±2 ms for -110mV and 5.1±0.2 and 25.8±0.9 ms for -90 mV.

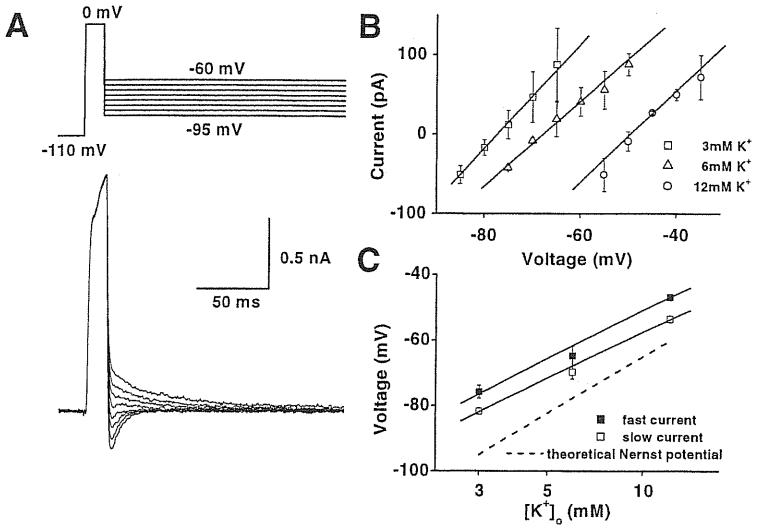

Figure 27. Ionic properties of outward currents. A, tail currents of I_{Kfast} (bottom) elicited by voltage steps to different potentials from -95 mV to -60 mV after a depolarizing step to 0 mV for 15 ms (top). The membrane was hyperpolarized to -110 mV for 400 ms prior to the test pulse to remove inactivation of the transient outward current. B, plot of average tail current amplitude as a function of membrane voltage in the presence of 3 (n=11), 6 (n=3), and 12 mM (n=3) extracellular K^+. C, plot of the reversal potential as a function of the extracellular K^+ concentration. Closed squares for I_{Kfast}, open squares for I_{Kslow}. Dashed line represents theoretical K^+ equilibrium potential calculated from the Nernst equation.

well fitted by two exponentials (Fig. 26D). The time course for recovery was well fitted by two exponentials with time constants of 4.4±0.6 and 17±2 ms at -110mV and 5.1±0.2 and 25.8±0.9 ms at -90 mV, indicating a slight voltage dependence for this process. Fast time constant of recovery was plotted *versus* V_h in Fig. 26B (closed circles). In conclusion, recovery from inactivation was less dependent on membrane potential that the process of inactivation itself.

2.3.3. Ionic properties of outward currents. The ionic selectivity of I_{Kfast} and I_{Kslow} was studied with tail current analysis. Voltage steps to 0 mV from -70 mV V_h with or without a prepulse to -110 mV (for 200-500 ms) were applied to evoke these currents. When the current reached its peak (200 ms for I_{Kslow} and 15 ms for I_{Kfast}) the membrane potential was stepped to different voltages and tail currents were recorded. An example of I_{Kfast} tail currents recorded at membrane potentials from -95 mV to -60 mV is shown in Fig. 27A. In this cell the tail current reversed at -80 mV. The mean reversal potential of I_{Kfast} tail currents was -75±2 mV (n=11 cells) while the corresponding value for I_{Kslow} tail currents was -81±1 mV (n=11 cells).

Average I_{Kfast} tail currents plotted *versus* membrane voltage in 3 (n=11 cells), 6 (n=3), or 12 (n=3) mM external K^+ concentrations are presented in Fig. 27B. A compensatory reduction in NaCl was effected whenever K^+ was raised. The results indicate that the tail current reversal potential, E_{rev}, moved to more positive values when the external K^+ was increased and that there was an approximately parallel, rightward shift of these plots. The E_{rev} dependence on the external K^+ concentration is shown in Fig. 27C for both I_{Kslow} (open squares) and I_{Kfast} (closed squares). The theoretical E_{rev} for K^+ at three K^+ concentrations was calculated with the Nernst equation and is shown as a dashed line in Fig. 27C. From these data it is apparent that E_{rev} for both outward currents moved together with changes in external K^+ concentration, suggesting that I_{Kslow} and I_{Kfast} were predominantly K^+ currents. Nevertheless, as the observed values differed from the calculated one, at least three factors could have accounted for the deviation: (1) K^+ accumulation in the extracellular space; (2) a degree of membrane permeability to other ions such as Na^+; (3) imperfect voltage clamp conditions. The first possibility seemed unlikely because the tail current amplitude of I_{Kfast} or I_{Kslow} at -50 mV (to maximize its size) did not change during 2 Hz test pulses, a condition which should have enhanced any

K^+ accumulation. The second possibility was explored by 50 % replacement of external NaCl with the presumably impermeant NMDG: in this case the tail E_{rev} of I_{Kfast} shifted in the negative direction by 5±1 mV (n=3 cells). This result suggests a measurable contribution by Na^+ to the transient outward currents. Using the Goldman-Hodgkin-Katz equation (Hille, 1992) the permeability ratio of K^+ to Na^+ (P_K/P_{Na}) was calculated. For the Na^+ and K^+ concentrations of the patch pipette and extracellular solutions the permeability ratio values of 1/0.01 (92/1) and 1/0.02 (50/1) were obtained for I_{Kslow} and I_{Kfast}, respectively. These data suggest that the contribution by Na^+ permeability to the transient K^+ currents was relatively small and that the deviation of the outward current E_{rev} from the one calculated for a pure K^+ mediated response was perhaps also due to the difficulty to obtain isopotential conditions for a large cell with dendritic arborization in a slice preparation.

2.3.4. Pharmacological dissection of I_{Kfast} and I_{Kslow}. Two well known K^+ channel antagonists, TEA and 4-aminopyridine (4-AP), were tested. Application of 10-30 mM TEA (n=6 cells) readily depressed I_{Kslow} as indicated by the example in Fig. 28A a,b in which the whole set of outward current traces (elicited by the same protocol shown in Fig. 23A) recorded in control solution (Ca-free-Co, TTX, Cs^+) was attenuated by 20 mM TEA. Fig. 28A c shows the I-V curve related to the same data indicating that there was a consistent depression (by 70±3 %) of I_{Kslow} at various test potentials. This effect was reversible after 15-20 min washout. I_{Kfast} was comparatevely resistant to 10-30 mM TEA: in fact, I_{Kfast} amplitude at +20 mV slightly increased by 1.1±0.2 times (n=4 cells).

I_{Kfast} was preferentially blocked by 4-AP. An example is shown in Fig. 28B in which I_{Kfast} elicited by a depolarizing step to 20 mV after a conditioning step to -110 mV was recorded in Ca-free-Co solution containing TTX (1 μM), TEA (20 mM), and Cs^+ (4 mM). Increasing concentrations of 4-AP (1, 2, and 3 mM) were cumulatively added to the external solution. The peak amplitude of I_{Kfast} was not decreased by 1 mM 4-AP although the current decay became faster (33 ms time constant in control and 21 ms time constant in presence of 1 mM 4-AP) as could be expected from use dependent block of these channels by 4-AP. This result is also consistent with findings by single Kv1.4 channel recordings, which have demonstrated little or no change in the fast kinetics of opening and closing within bursts, but shorter mean burst duration and reduced

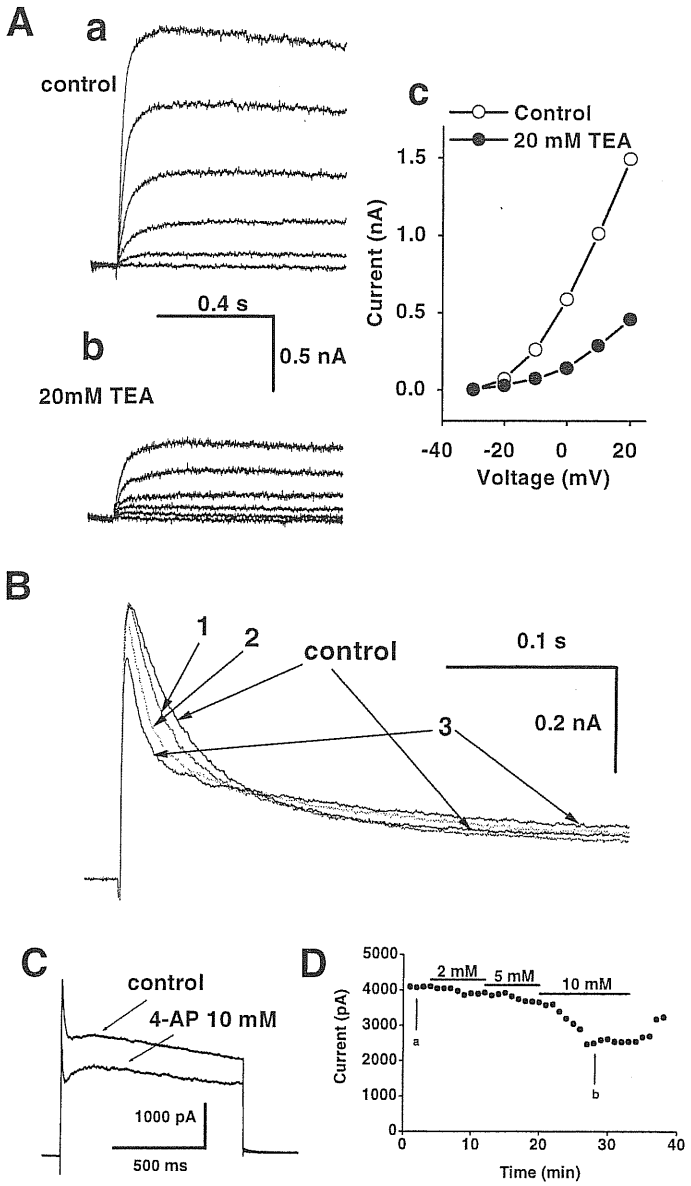

Figure 28. Pharmacological properties of I_{Kslow} and I_{Kfast}. A: current traces obtained by depolarizing voltage steps (same protocol as in Fig. 21.) in control (containing TTX, Ca-free-Co, Cs^+) solution (A a) and in the presence of TEA (20 mM) (A b). A c: I-V relation of I_{Kslow} in control (open circles) solution or in the presence of 20 mM of TEA (closed circles) for the same cell shown in A a-b. B: 4-AP preferentially blocks I_{Kfast}. Current traces (elicited by voltage step to 20 mV) were recorded in a solution containing TTX, TEA (20 mM), Ca-free-Co and different concentrations of 4-AP (0, 1, 2, and 3 mM). All records are from the same cell. C: current traces elicited by voltage steps (same protocol as in B) in control (containing TTX, Ca-free-Co, Cs^+) solution and in presence of 4-AP (10 mM). Note, that both, I_{Kfast} and I_{Kslow}, were reduced by this high dose of 4-AP. D: time course of I_{Kfast} block by 4-AP (2, 5, and 10 mM) for the same cell shown in C.

probability of channel opening by depolarization (Yao and Tseng 1994). At 2 or 3 mM concentration 4-AP diminished I_{fast} peak by 6 and 19 %, respectively, together with a progressive reduction in current decay (13 and 10 ms time constants). Nevertheless, the late component of I_{Kfast} remained relatively unaffected. Even very high concentrations of 4-AP (up to 10 mM) were unable to block I_{Kfast} completely as shown in Fig. 28C. Fig. 28 D shows, on the same cell, the time course of peak outward current depression by incrementing concentrations of 4-AP. At concentrations higher than 6 mM 4-AP also depressed (by 28 % in 7 mM 4-AP solution) I_{Kslow}. At 5 mM concentration 4-AP depressed I_{Kfast} and I_{Kslow} by 37 and 6 %, respectively. An example is shown in Fig. 28C in which membrane current was elicited by a depolarizing step to 20 mV after a conditioning step to -110 mV and recorded in Ca-free-Co solution containing TTX (1 μM) and Cs^+ (4 mM) before and after addition of 4-AP (10 mM). The peak amplitude of I_{Kfast} and I_{Kslow} were decreased by 4-AP.

2.4. Membrane current sensitive to apamin and carbachol

Apamin sensitive membrane currents were investigated under voltage clamp conditions. Outward membrane currents were recorded by delivering depolarizing voltage steps (1 s duration) in the range –40 mV to 20 mV from –50 mV V_h in the presence of TTX. This protocol generates a heterogeneous voltage dependent outward current, a typical example of which is shown in Fig. 29A. The outward current did not inactivate during the 1 s long voltage steps and was followed by a tail current. The contribution of the apamin sensitive current to the total membrane current was examined by adding 100 nM apamin to the extracellular solution. Apamin (which did not change leak current) reduced by 36± 1 % the outward current (Fig. 29B; n=10) measured 10 ms before the voltage step termination. Preliminary experiments were performed on four HMs to test if rundown of outward currents could develop during the course of recording. Over a period of time up to 30 min there was no significant decrease (4± 2 %) in current amplitude, suggesting that the apamin sensitive current was a stable cell response. Since all the effects induced by apamin were fully produced within 20 min application, it seems that any outward current reduction was due to pharmacological block and not to current rundown. The apamin sensitive outward current could then be obtained by subtracting the current recorded in

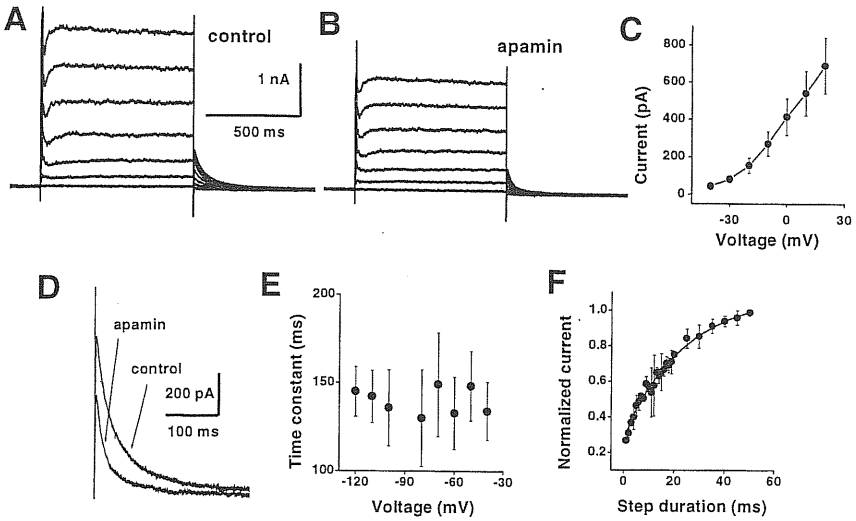

Figure 29. Apamin sensitive current of HMs. All data are from voltage clamp experiments. A: membrane currents elicited by application of depolarizing voltage steps between -40 to +20 mV (10 mV increments) from -50 mV holding potential in control solution containing TTX. B: set of membrane current traces elicited by the same voltage steps in the same neuron as in A after application of 100 nM apamin. Note reduction in steady state outward current. C: average I-V relation (n= 5 cells) of apamin sensitive membrane currents obtained after subtracting current traces recorded in apamin solution from those recorded in control solution. Note that the current activation threshold is near -30 mV. D: superimposed tail currents recorded at the end of +20 mV voltage steps as the membrane potential was returned to -50 mV (same neuron as in A and B in control or in the presence of 100 nM apamin). Note shortening of tail current in apamin solution. E: plot of apamin sensitive tail current time constant versus membrane potential. F: plot of apamin sensitive tail current (obtained by subtracting tail currents recorded in apamin solution from those recorded in control solution) versus voltage step (to +20 mV) duration. The time course of apamin sensitive tail current development is well fitted by two exponentials (0.7± 0.1 and 24±3 ms; n= 5 cells). Currents were normalized with respect to the one obtained by a 50 ms depolarizing step.

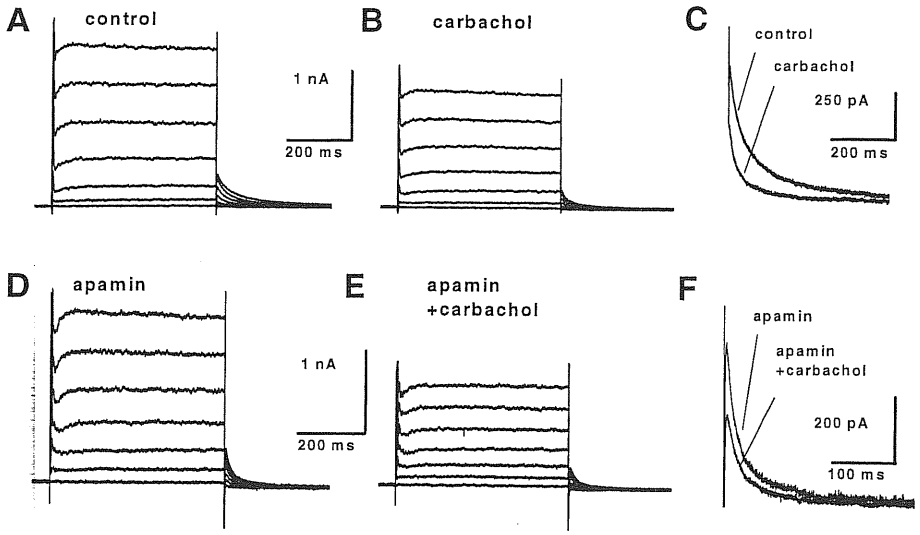

Figure 30. Block of outward currents by carbachol. A and B: membrane currents elicited by depolarizing voltage steps between -40 to +20 mV (10 mV increments) from -50 mV in control solution containing TTX (A) or in 50 μM carbachol solution (B). Note reduction in steady state outward current by carbachol. C: superimposed tail currents recorded at the end of +20 voltage steps (same neuron as in A and B) in control or carbachol solution. Note shortening of tail current by carbachol. D and E: membrane currents elicited with the same protocol as in A and B in solution containing 100 nA apamin (D) or further application of 50 μM carbachol (E). F: tail currents (recorded at the end of +20 mV voltage step; faster time scale) taken from tests shown in D and E. Note reduction in tail current amplitude by carbachol.

apamin solution from the control one. The average I-V relation for the apamin sensitive current is plotted in Fig. 29C. Its apparent activation threshold was -40 mV from which the current grew monotonically with increasing membrane potential.

To characterize the apamin sensitive current deactivation, tail currents following voltage steps to +20 mV in the absence or in the presence of apamin were studied (see Fig. 29D). In control conditions tail currents could be fitted by two exponentials with decay time constants of 24±3 ms and 154±9 ms at -50mV, respectively (n= 11 cells). In the presence of apamin only a fast monoexponential component remained (decay time constant=19± 3 ms; n= 5 cells). After current subtraction, the apamin sensitive tail current was shown to have a monoexponential decay (140±20 ms) which was voltage independent in the range between -40 to -120 mV (Fig. 29E). This observation suggests that deactivation of the apamin sensitive current was relatively slow and unaffected by membrane potential. Apamin sensitive tail currents reversed at -91±1 mV (n= 5) membrane potential, a value very near E_K^+ (-95 mV).

Studying the activation kinetics of the apamin sensitive current was difficult because of its contamination by the concomitant development of other voltage-dependent currents. To partially circumvent this problem we studied the kinetics of generation of the apamin-sensitive tail currents by applying voltage steps of different length. In this case the current flowing at the end of each voltage command should have represented the activation of a certain fraction of apamin sensitive channels for a given membrane potential. The protocol therefore consisted in delivering fixed-amplitude voltage steps of increasing duration (from 1 to 50 ms) in the absence or in the presence of apamin and in measuring the tail currents obtained after current subtraction. The subtracted tail currents were then plotted (Fig. 29F) *versus* the voltage step duration (step command to 20 mV). The time course of tail current development was fitted by two exponentials with time constants of 0.7±0.1 and 24±3 ms (n=5 cells). Note that even 1 ms voltage command was able to generate a measurable fraction of the apamin sensitive current (~20%).

Examples of outward currents recorded before or after adding 50 μM carbachol are shown in Fig. 30A, B. On average carbachol depressed the outward current by 28± 3% (n=6), a phenomenon associated with the generation of an inward current (40±20 pA). Analysis of tail currents (Fig. 30C) indicated that carbachol blocked the slow component

(by 80±10 %) strongly and the fast one (by 35±9 %) weakly (n=6). Nevertheless, 50 μM carbachol in the presence of 100 nM apamin could still reduce the steady-state outward current by 27±1 % (n= 3 cells) as shown in example of Fig. 30D, E. In apamin solution the monoexponentially decaying (20±5 ms) tail current was also depressed in amplitude by 20±10 % (Fig. 30F).

3. Simulation of HM responses

A computer model was set up to simulate the electrical behavior of HMs and to investigate the role of I_{Na}, I_{Kslow}, and I_{Kfast} in generating an AP or in controlling repetitive firing. Since this model did not include the complete set of voltage dependent conductances present in HMs as such data are not yet available, the aim was necessarily restricted to explore the contribution by I_{Na}, I_{Kslow}, and I_{Kfast} underlying conductances to shape the AP and the firing pattern. The kinetic parameters obtained from the present experiments (Table 1, see p. 40) were used as a start-up for the simulation experiments. The first test of the model was to examine how well it could simulate the Na^+ and K^+ currents previously recorded under voltage clamp conditions. Fig. 31 shows simulated membrane currents I_{Na} (A; top traces), I_{Kslow} (B; top traces), and I_{Kfast} (C; top traces), that were elicited by voltage clamp protocols similar to those used in the previously described experiments (see Figs. 18, 23, and 24). The simulated current responses closely resembled those experimentally obtained (Fig. 31A, B, and C bottom traces), including features like time course of activation and inactivation. However, the transient I_{Na} was followed by a persistent Na^+ current in two simulated responses (voltage steps to –40 and –30 mV). This presumably happened because of the presence of a 'window' current occurring when the activation and inactivation curves overlapped (see Fig. 20A). Note also that inactivation of I_{Kslow} was not described in model.

Next, the protocol of brief current pulse injections was simulated to reproduce the AP normally obtained with current clamp experiments. Fig. 32A shows the simulation with 100 ms current pulses injected into the model neuron which initially comprised leak (g_{leak}), Na^+ (g_{Na}) and slow K^+ (g_{Kslow}) conductances only. The maximal values of g_{Na} and g_{Kslow} were 1 μS and 0.5 μS, respectively. The 1 μS g_{Na} maximal value was chosen to reproduce the real HM spike characteristics such like threshold (-43 mV) and rate of rise

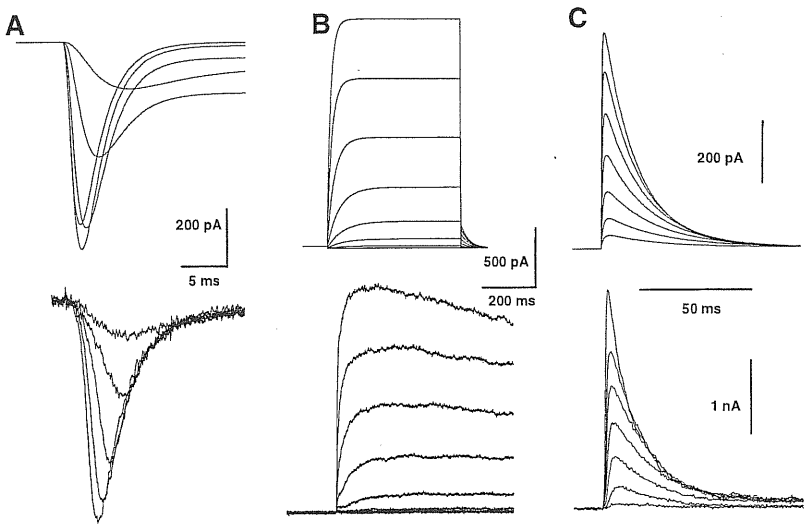

Figure 31. Computer simulations can reconstruct the voltage activated currents normally present in HM. I_{Na} (A), I_{Kslow} (B), and I_{Kfast} (C) as simulated responses (top traces) with the protocols used in real VC experiments. In all three cases V_{hold} = -70 mV and the voltage step increment is 5 mV for I_{Na} and 10 mV for I_{Kfast} and I_{Kslow}. In (C) a conditioning prepulse (to –100 mV) is applied for 500 ms. Bottom traces are experimentally obtained current traces. Note that average values were used for simulations, thus some differences in currents kinetics and amplitudes could be noted when compared with single cell current traces.

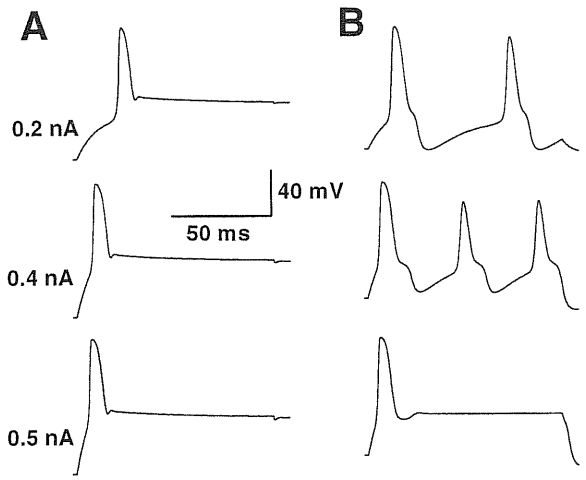

Figure 32. Simulation of HM including Na^+ and slow K^+ conductances. A, current pulses of varying intensities (indicated on the left to every response) elicit one spike only. Note appearance of the plateau after a single spike, which persists also after termination of 100 ms current step. Standard value of Na^+ conductance (g_{Na}) is used for these simulations (see Table 1). B, simulation results with modified g_{Na}. Repetitive APs appear in response to similar current pulses as in (A).

(62 mV/ms). However, using these parameters only a single spike was elicited at the beginning of each one of the current steps (200, 400, and 500 pA) as the AP was followed by a sustained plateau which persisted even after the termination of the current pulse. Simulations with increased g_{Kslow} (up to 1 μS) led to shortening of the plateau and/or its elimination at the end of current step but could not reveal any repetitive firing during the pulse. At g_{Kslow}= 5 μS the spike was completely abolished. The simulated behavior shown in Fig. 32A was never observed experimentally. In fact, a plateau was found in real HMs only with current > 0.5- 0.8 nA and it terminated immediately after the end of current pulse. Analysis of g_{Na} parameters suggested that "window" Na^+ current could bring the model neuron to generate a plateau state. Shifting the half activation and half inactivation potential values to –40 mV and to –65 mV, respectively, led to disappearance of this plateau in the model neuron (Fig. 32B). These changed g_{Na} parameters were thus used for further simulations. Under these conditions the model could then generate all-or-none APs, the frequency of which increased with the cell depolarization pulse up to block of repetitive firing. Cell repolarization after the end of the pulse also occurred.

The characteristics of simulated single APs were next investigated. A series of computer generated voltage traces (maximal values for g_{Na}= 1μS and g_{Kslow}= 1 μS) are shown in Fig. 33A. The 100 pA current step did not evoke any spike, while stronger pulses elicited APs of 11 ms duration (measured at threshold value). The corresponding value for real HMs was 3.5 ms. This long duration of the simulated AP was partially due to the appearance of a shoulder during the final phase of spike repolarization. However, even when measured at midheight, spike duration was too long (5.5 ms). Fig. 33B shows the result of simulating a response to 300 pA step when maximal g_{Kslow} was 0.1, 0.5, 1, 2, or 5 μS. The increase in the g_{Kslow} progressively reduced the duration of the simulated spike. When g_{Kslow} was 5 μS, duration of simulated spike was 3.5 ms at midheight (10 ms total duration). Fig. 33C presents responses when g_{Na} and g_{Kfast} only were included in the model (maximal g_{Kfast} values were 0.01, 0.05, 0.1, 0.2, or 0.5 μS). The waveform of the simulated AP became narrower with increasing g_{Kfast}, until the AP generation was prevented when maximal g_{Kfast} reached 0.5 μS. Moreover, g_{Kfast} influenced the initial repolarization phase only and could not repolarize the membrane potential back to spike

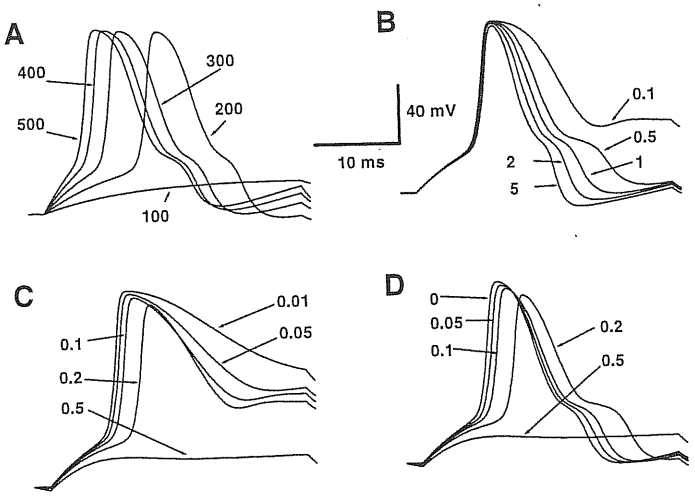

Figure 33. Action potential of model HM has long duration. A, APs evoked by incrementing current step (100 to 500 pA, 30 ms). The latency of AP decreased with increasing current intensity. The current step of 100 pA did not elicit any spike. The peak of the APs was apparently invariable. B, AP elicited by 300 pA current step (50 ms). Decrease in AP duration is due to increasing g_{Kslow} value (0.1, 0.5, 1, 2, and 5 μS as indicated near traces). C, substitution of g_{Kslow} by g_{Kfast} fails to decrease AP duration. AP elicited by similar current step as in (B). g_{Kfast} values expressed in μS are indicated near traces. The AP is completely blocked when the g_{Kfast} reached 0.5 μS value. D, both g_{Kslow} (1 μS) and g_{Kfast} inserted in model HM. Increasing of g_{Kfast} (values indicated near traces) does not further shorten AP. Note increase of AP delay with increasing g_{Kfast}.

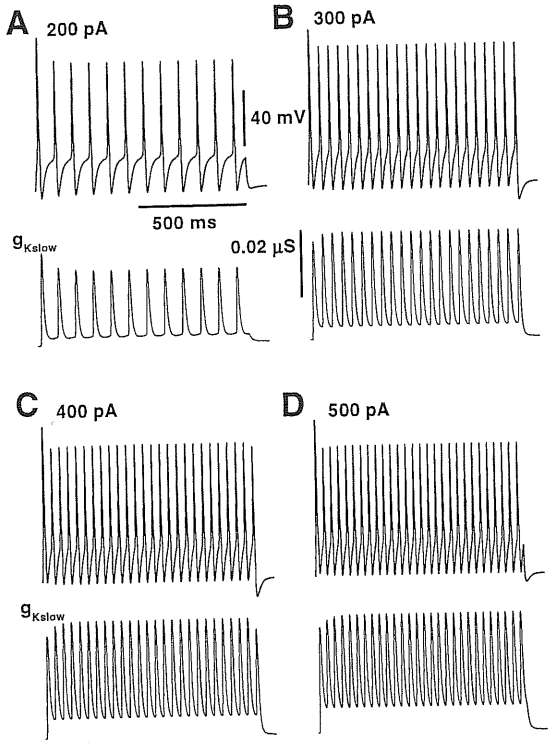

Figure 34. HM model exhibits repetitive firing. Simulated voltage traces as responses to current pulses (200- 500 pA; A- B, respectively; upper traces) and corresponding g_{Kslow} plots (bottom traces in each panel).

threshold. Thus, g_{Kfast} also failed to shorten the spike duration to the experimentally observed values. Next, voltage traces were generated to investigate whether the simultaneous presence of both g_{Kslow} and g_{Kfast} repolarized the membrane potential after an AP. An example is shown in Fig. 33D. Maximal g_{Kslow} was 1 μS and maximal g_{Kfast} was increased from 0 to 0.5 μS. Changing of g_{Kfast} did not have any influence on the duration of AP, while latency increased from 8.8 ms (for g_{Kfast}= 0.05 μS) to 11 ms (for g_{Kfast}= 0.2 μS). When g_{Kfast} reached 0.5 μS, AP was blocked. Similar results were obtained for different g_{Kslow} values (0.5-5 μS).

Discrepancies between behavior of the model and the real HM suggested that neither g_{Kslow} nor g_{Kfast} (separately or together) could repolarize the membrane potential quickly enough to produce an AP as short as the real one. This conclusion is perhaps unsurprising if the AP duration (3.5 ms experimentally measured) is compared with the time constants of I_{Kslow} (tens of ms; Fig. 23D). However, it is surprising that the relatively fast activating I_{Kfast} (Fig. 24E), which is only ~3 times slower than I_{Na} (Fig. 18C), could not play a major role in shortening APs. Preliminary simulations were performed to test whether the use of first power for I_{Kfast} activation and inactivation variables (a and b, respectively, in eq. (12)) was indeed correct. When the power of the activation variable was raised to two or four, g_{Kfast} was still unable to shorten the AP. Moreover, g_{Kfast} become even more effective to delay and/or to block completely AP. Thus, the formalism described in eq. (12), did not apparently show any substantially wrong assumption and was used for further simulations. Employing this formalism is also useful as it allows comparison with other cells, like hippocampal neurons (Traub et al. 1991; Warman et al. 1994).

The rather small contribution by g_{Kslow} and g_{Kfast} to AP repolarization raised the possibility that these currents were instead involved in the control of repetitive firing. This aspect was therefore further investigated. In response to long (1 s) depolarizing current pulses (200-500 pA), the model HM consisting of g_{Na} and g_{Kslow} (both 1 μS) exhibited repetitive firing as exemplified in Fig. 34. g_{Kslow} was set to 1 μS since this value gave a relatively short AP. Higher values led to voltage responses with a single spike only. Responses to a 100 pA current pulse were below AP generation threshold. The real HMs were able generate repetitive firing with current pulses between 20 to 100 pA (depending also on R_{in}). Addition of a low threshold Ca^{2+} current might presumably

lower AP generation threshold. The simulated neuron fired at frequency of 12 Hz or 22 Hz for 200 or 300 pA steps, respectively (Fig. 34A and B). These frequencies were similar to those of real HMs. In fact, the sample neurons in Figs. 1 or 7 fired at steady state frequencies of ~10 Hz and ~18 Hz in response to similar current pulses. g_{Kslow} plots are depicted under each voltage trace in Fig. 34. These plots represent the g_{Kslow} activated every moment during depolarization. About 0.03 μS g_{Kslow} (3% of maximally available) was activated during first AP for all traces presented. g_{Kslow} did not deactivate completely after termination of AP. Subsequent spikes again activated a similar fraction of g_{Kslow}.

When g_{Kfast} (0.1 μS) was included into model in addition to g_{Kslow}, the 200 pA current step was not able to evoke any AP and higher current steps (300 pA and 500 pA; Fig. 35A) elicited AP trains which fired at lower frequencies (18 Hz for 300 pA step). Increase in maximal g_{Kfast} to 0.2 μS led to further decrease in firing frequency (7 Hz at steady state for 300 pA step). The fraction of active g_{Kslow} or g_{Kfast} was plotted below every voltage trace in Fig. 34 and 35A to illustrate the evolution of these conductances during repetitive firing. A similar degree of g_{Kslow} (about 3% for each current pulse) activated during every subsequent AP in the train and deactivated to the same level between every two spike (Fig. 34 and 35A). A different behavior was exhibited by g_{Kfast}. About 10% of maximally available g_{Kfast} was activated during the first spike of the train (Fig. 35A). During subsequent spikes this portion gradually decreased to about 3%, presumably due to inactivation of g_{Kfast}. Moreover, the firing frequency increased during the AP train in the model cell which included g_{Kfast}. This fact is quantified in the f-I plots of Fig. 36A. The f-I plot of the model cell with g_{Na} and g_{Kslow} only (both with 1 μS maximal values) was almost linear in the range 200- 400 pA and deviated downwards at a higher current step (Fig. 36A; closed circles). Given that the f-I plots for initial and steady state were overlapping, only average f-I plots are shown. Inclusion of g_{Kfast} (0.1 μS) into the model cell produced firing with changing frequency. Initial (closed triangles) and steady state (open triangles) f-I curves are shown in Fig. 36A. They had similar slope but that of steady state was shifted upward indicating that firing frequency increased during AP train (accelerating firing). Inclusion of larger g_{Kfast} (2 μS) into the model gave the same trend but the separation of f-I plots and the overall decrease in firing frequency were stronger (Fig. 36A; open and closed squares).

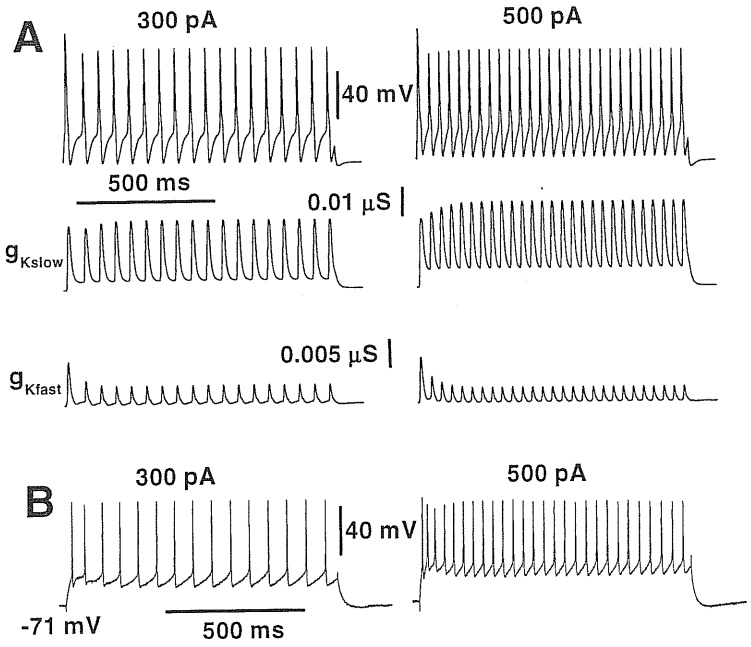

Figure 35. Fast K^+ conductance reduces model HM firing frequency. A: simulated responses to current pulse (1 s, 300 and 500 pA). Voltage trace (upper trace), g_{Kslow} plot (middle trace) and g_{Kfast} plot (bottom trace) are shown. Note large activated g_{Kfast} during first AP and its gradual inactivation during depolarization. B: experimental responses to 1 s current step of 300 and 500 pA intensity (taken from Fig. 1).

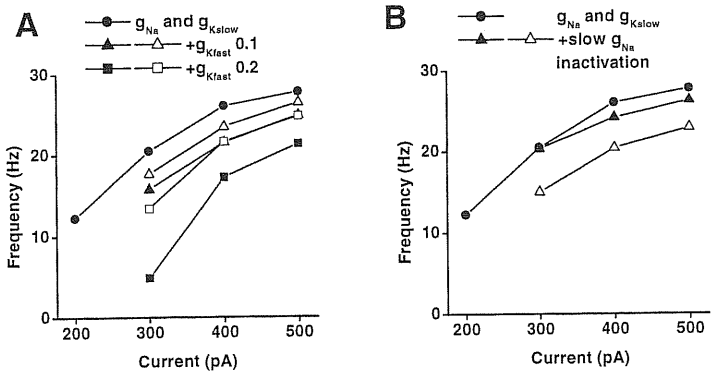

Figure 36. f-I plot of model HM. A, f-I relations for the basic model (g_{Na}= 1μS and g_{Kslow}= 1μS; closed circles) and for models including different g_{Kfast} maximal values- 0.1 μS (triangles) and 0.2 μS (squares). B, f-I relations of basic model (closed circles) and of model with g_{Na} slow inactivation (triangles). In both A and B, steady state and initial firing plots are depicted with closed and open symbols, respectively.

The above described simulations showed that model could be made to fire at frequencies like those of real HMs (see sample traces recorded under control conditions; Fig. 35B). One interesting finding is that the presence of g_{Kfast} could produce accelerating firing as indeed reported for a small population of HMs (Viana et al. 1995). However, simulation results should be considered with caution, because real HMs possess other conductances, such as voltage activated Ca^{2+} and Ca^{2+} dependent K^+ conductances, which were not present in the model neuron. Moreover, the present experiments demonstrated that the mAHP strongly reduced firing frequency. Perfusion of cells with apamin, which blocks the mAHP, strongly increased firing frequency to values (~25 Hz and ~40 Hz, respectively; see for example Fig. 7) higher than those of the simulated neuron. On the other hand, the simulated neuron fired at a constant or accelerating (in presence of g_{Kfast}) rate in contrast to the experimental data (Fig. 1 and 7), especially those obtained in apamin solution (Fig. 7 and 8) when spike frequency adaptation became apparent.

Ideally, the contribution of other conductances should have been tested but the lack of information about kinetics, voltage and/or Ca^{2+} dependencies of other currents present in HMs made it impractical.

For this reasons other mechanisms were explored. In particular, slow inactivation of I_{Na} has been suggested as a candidate for spike frequency adaptation (Fleidervisch et al. 1996; Powers et al. 1999). This mechanism was observed in real HMs and thus was inserted into the HM model (g_{Na}= 1 μS and g_{Kslow}= 1 μS). Time constant of slow inactivation was 200 ms, near the value found in the present experiments. The result of the simulation is shown in Fig. 36B and 37. The model neuron still was able to fire repetitively, but the spike amplitude progressively decreased (Fig. 37). In addition, spike frequency adaptation became manifested and lasted up to about 500 ms. Initial (closed triangles) and steady state (open triangles) f-I plots are shown in Fig. 36B and are shifted downward in respect to the f-I plot of the model cell without g_{Na} slow inactivation. In addition, the steady state f-I is shifted downward with respect to that of initial firing, thus, indicating that firing frequency decreased during depolarization.

One basic difficulty with the present modelling approach was generated by the long duration of single spikes. This artificial condition meant that a larger portion of g_{Kslow} and g_{Kfast} would be activated during a 10 ms (simulated) than a 3.5 (measured experimentally)

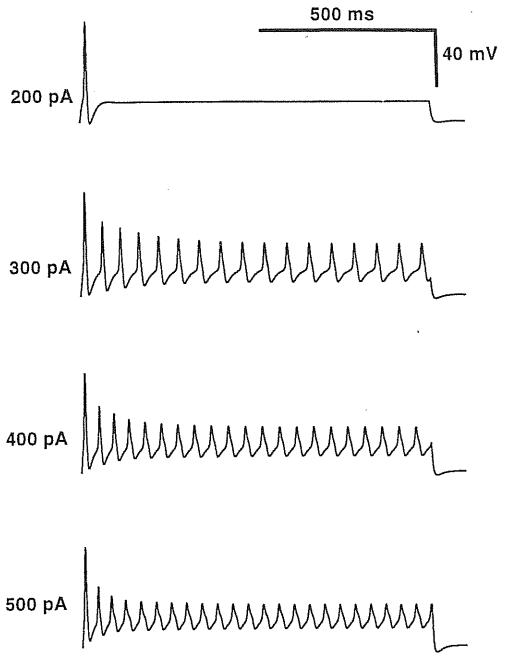

Figure 37. Slow I_{Na} inactivation produces spike frequency adaptation. Simulated responses to current steps (200- 500 pA, 1 s) when slow inactivation of g_{Na} is added to the model. The frequency of repetitive discharge becomes lower. In addition, spike frequency adaptation during the first 300- 500 ms appears. Note strong depression of subsequent AP amplitude.

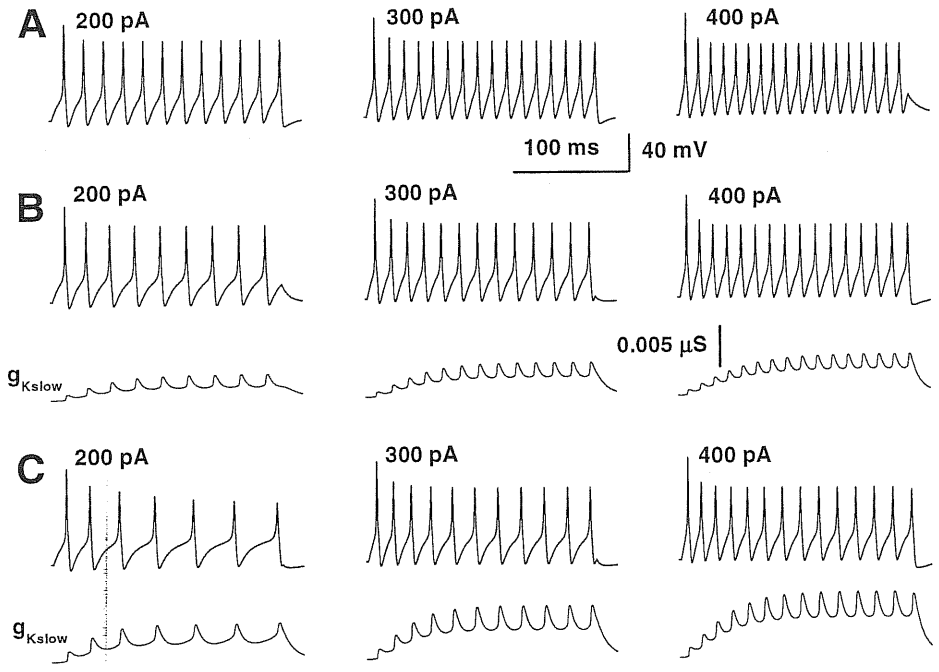

Figure 38. Slow K+ conductance reduces firing frequency in the fast spiking neuron model. A, simulated responses of basic fast spiking neuron model to current pulses (200- 400 pA, 200 ms). B, insertion of 1 µS (B) or 2 µS (C) g_{Kslow} into fast spiking neuron model lowers firing frequency. Note that firing frequency declines during depolarization. During depolarization activated g_{Kslow} is plotted versus time below voltage traces. Note cumulative activation of g_{Kslow}, which might explain the appearance of spike frequency adaptation.

lasting AP. Consequently, the role of these K^+ conductances on firing frequency would be overamplified. In practice, in order to study how much HM g_{Kslow} and g_{Kfast} were capable of controlling firing, single spikes had to be as short as those found in real HMs. A different approach was therefore chosen to address this question. Two conductances, namely a fast transient Na^+ current and a generic K^+ current (both 1 μS), were taken from the standard respiratory neuron model (Rybak et al. 1997) and were inserted into the HM model together with g_{leak}. The choice of these conductances seemed justified since they produced high frequency firing (57 Hz or 72 Hz for 200 pA or 300 pA steps, respectively; Fig. 38A) with short APs (2.5 ms) when neuron was at -70 mV V_{rest}. This approach was simply used to estimate the influence of g_{Kslow} and g_{Kfast} on the qualitative characteristics of the model behavior. Following insertion of g_{Kslow} (1 μS) steady state firing frequency dropped to 42 Hz or 57 Hz (200 pA or 300 pA steps, respectively) with changed pattern of firing, since spike frequency adaptation become evident and lasted for the first 100 ms (Fig. 38B). Adaptation was even more evident when g_{Kslow} was increased to 2 μS (Fig. 38C). Plots of the activated g_{Kslow} during depolarization are shown below the voltage traces in Fig. 38B and C. The percent of g_{Kslow} gradually increased for each subsequent spike, suggesting that accumulation of this conductance could be one mechanism responsible for adaptation. The insertion of g_{Kfast} (0.1 μS or 0.2 μS), instead of g_{Kslow} into the fast spiking model, also led to reduction in steady state firing frequency (66 Hz or 55 Hz, respectively, for 300 pA step; Fig. 39). However, it had the opposite effect on firing pattern since firing gradually accelerated as also found in the previously described simulations. Moreover, the first interspike interval was larger than those at steady state. This was probably due to inactivation of g_{Kfast}, as shown with the time profile plot of this conductance (Fig. 39; corresponding plots below voltage traces).

The following simulations were made when both g_{Kslow} and g_{Kfast} were inserted into the model with values of either 1 μS and 0.1 μS (Fig. 40A), or 2 μS and 0.2 μS (Fig. 40B), respectively. In these exemplified cases, the adaptation pattern prevailed against the accelerating one, while the temporal evolution of those conductances during depolarization is also shown in Fig. 40 (plots below voltage traces). Sample traces recorded in apamin solution (which best approximated the simulated conditions) are depicted in Fig. 40C. Strong firing frequency adaptation emerged in presence of apamin.

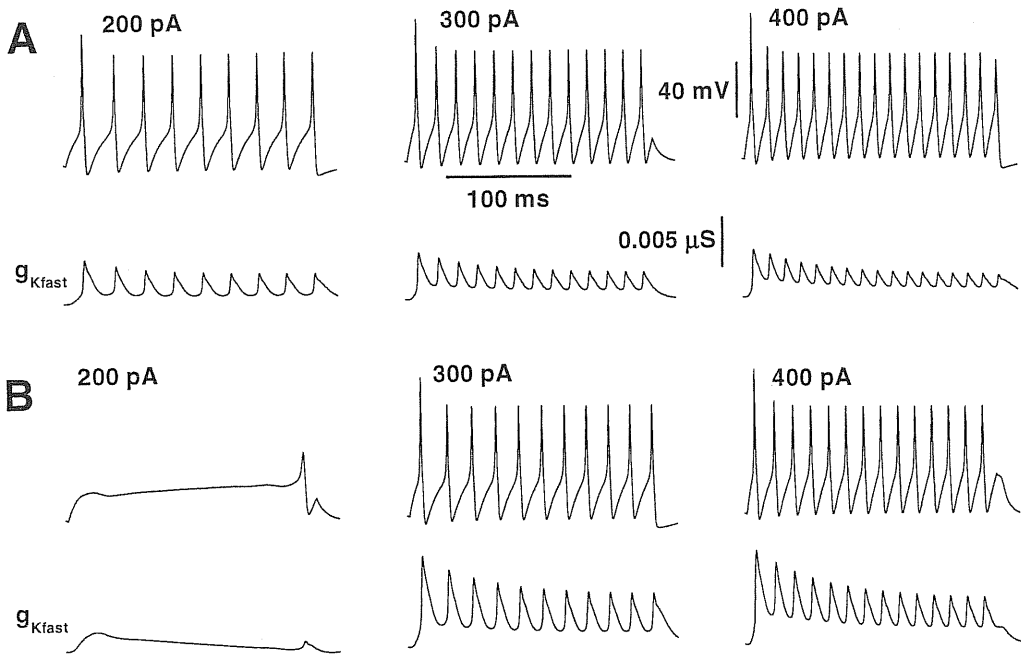

Figure 39. Fast K^+ conductance reduces firing frequency in the fast spiking neuron model. Simulated responses to current steps (200-400 pA, 200 ms) when g_{Kfast} is 0.1 µS (A) and 0.2 µS (B). Voltage traces (upper traces) and g_{Kfast} plots (bottom traces) are depicted. Insertion of g_{Kfast} diminishes firing rate stronger at the beginning of depolarization than at the end, thus producing apparent acceleration of firing. This is probably due to progressive inactivation of g_{Kfast} during depolarization as is clearly seen from g_{Kfast} plots.

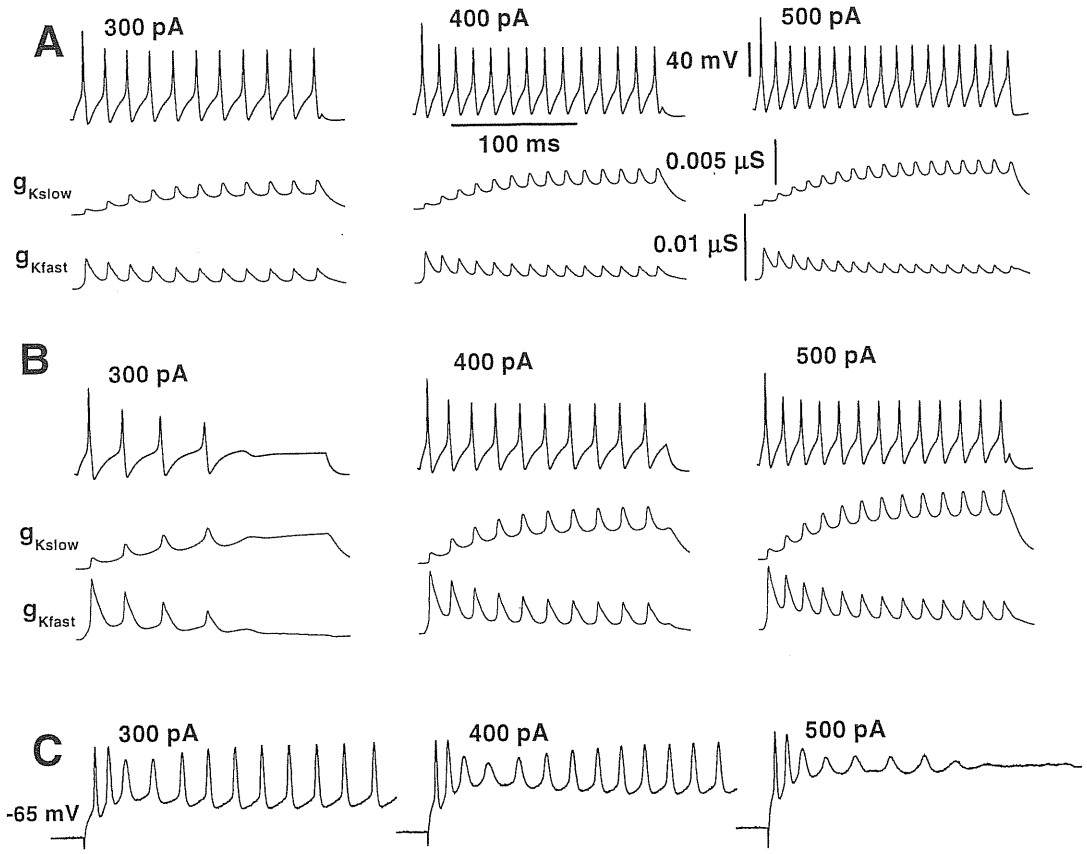

Figure 40. Slow and fast K^+ conductances together slow down firing rate. Simulated responses of fast spiking neuron model to current steps (300- 500 pA, 200 ms) possessing two different sets of g_{Kslow} and g_{Kfast} values: A, g_{Kslow} is 1 µS and g_{Kfast} is 0.1 µS; B, g_{Kslow} is 2 µS and g_{Kfast} is 0.2 µS. For every voltage trace (upper traces) are depicted g_{Kslow} plot (middle trace) and g_{Kfast} plot (bottom trace). Note that conductance behavior during depolarization is similar to that in previous cases when g_{Kslow} and g_{Kfast} were inserted separately. However, frequency decline prevailed in AP trains. C: sample current traces recorded in the presence of apamin (100 nM) are shown to compare simulated and real HM voltage responses.

The results of fast spiking model simulations are summarized in Fig. 41. The basic model f-I plot was linear (closed circles in Fig. 41A, B, and C). g_{Kslow} (1 μS or 2 μS; triangles or squares, respectively; Fig. 41A) shifted f-I plots downwards. Steady state f-I plots (open triangles and squares) were shifted more than those for initial firing (closed triangles and squares), thus indicating the presence of adaptation. Insertion of g_{Kfast} (0.1 μS), instead of g_{Kslow}, shifted f-I plots (Fig. 41B; triangles) in a different fashion as those for steady state (open triangles) were shifted less than those for initial firing (closed triangles). Increasing of g_{Kfast} to 0.2 μS had qualitatively similar, although stronger effects on f-I plots (open and closed squares). Fig. 41C summarizes the simulation results when both g_{Kslow} and g_{Kfast} were inserted into model.

In summary, simulations of model HM with g_{Na}, g_{Kslow}, and g_{Kfast} produced single or trains of AP. The simulated AP did not replicate precisely that recorded experimentally in terms of duration, suggesting that at least another current is involved in single AP repolarization. One possible candidate for this role is the large-conductance non-inactivating Ca^{2+} dependent K^+ current (driven by BK channels). While this current has been suggested to be responsible for the most of the AP repolarization of hippocampal neurons (Lancaster and Nicoll 1987; Storm 1987), its presence and characteristics in HMs are presently unknown.

Simulations using the fast spiking neuron model helped to ascertain the possible role of g_{Kslow} and g_{Kfast}. Insertion of g_{Kslow} into this model produced repetitive firing with adaptation, that is the phenomenon most frequently observed in real HMs under control conditions (Viana et al. 1995) or unmasked after block of mAHP (Viana et al. 1993b; see also Fig. 7). Interestingly, the insertion of g_{Kfast} into the model led to responses with accelerating firing. This type of firing is not usual in HMs as it has been found in a small population of HMs only (Viana et al. 1995). When both g_{Kslow} and g_{Kfast} were inserted together into model, simulations gave adapting firing patterns. This observation shows that the action of these conductances was temporally restricted to modulation of firing pattern, a phenomenon undoubtedly controlled also by other conductances not included into the present, simplified model of HMs.

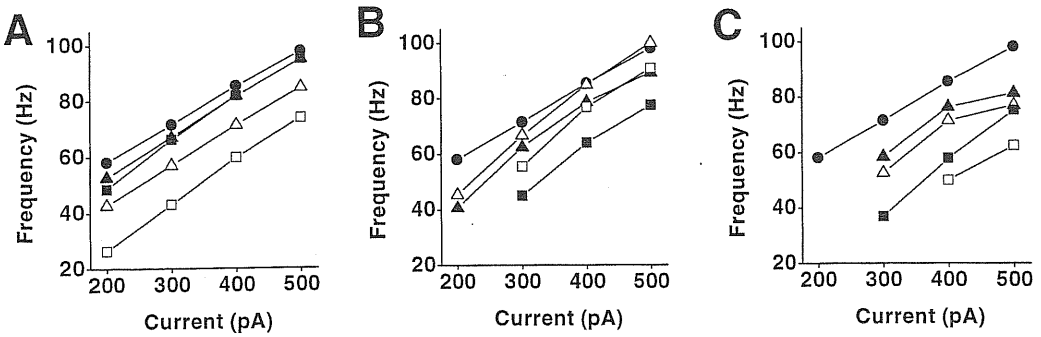

Figure 41. f-I plot of fast spiking neuron model. f-I relation for basic fast spiking neuron model (closed circles) is plotted in A, B and C. In each panel open triangles or open squares indicate steady state plots while filled triangles and squares refer to initial firing. A, f-I plot of model including different g_{Kslow} maximal values- 1 μS (triangles) or 2 μS (squares). B, f-I relations of model including different g_{Kfast} maximal values- 0.1 μS (triangles) or 0.2 μS (squares). C, f-I relations of model including two different sets of g_{Kslow} and g_{Kfast} values- 1 μS and 0.1 μS (triangles), or 2 μS and 0.2 μS (squares), respectively.

DISCUSSION

The present study provided the first macroscopic, quantitative description of three voltage-activated, Ca^{2+}-independent currents, such as fast transient Na^+ (I_{Na}), slow activating K^+ (I_{Kslow}), and fast transient K^+ (I_{Kfast}) in neonatal HMs under voltage-clamp conditions. In addition, a distinct outward current apparently responsible for the mAHP was identified and its modulation by muscarinic receptor activation was demonstrated. The present patch clamp experiments also provided new evidence for the role of the mAHP in spike firing and its regulation by muscarinic receptors. Finally, the present study attempted to integrate available parameters of macroscopic currents into a coherent model, which might help to explain the electrical behavior of HMs.

1. Technical considerations

Analysis of voltage and/or Ca^{2+} activated currents in HMs, like in all mammalian CNS neurons, is fraught with problems. In slice preparations, Na^+ and K^+ membrane currents are large and possibly distributed along dendritic processes of complicated structure and length. These two factors create problems for voltage and space clamp. The introduction of the patch clamp technique (Hamill et al. 1981; Neher and Sakmann 1976) has led to significant progress in voltage clamp studies of many neurons.

In the present study the whole- cell patch clamp technique led to considerable success in recording membrane currents of HMs. The opportunity to vary extracellular and intracellular solutions and the use of low resistance recording pipettes should have minimized voltage errors. Time constant (τ_s) of membrane charging due to the presence of series resistance was 120 μs in the case when I_{Na} was recorded. τ_s was smaller than time constant of I_{Na} activation. Any distortion of I_{Na} was probably evry small since even in the voltage range (from -100 to –60 mV or positive to 0 mV) where the activation time constant was faster, this remained six times larger than τ_s. Activation time constants of I_{Kfast} and I_{Kslow} were at least ten times slower than τ_s, thus distortion of these currents should be minimal.

Space clamp problems are more difficult to assess. However, the study by Viana et al (1994) has suggested that HMs are compact neurons, with an electronic length of 0.99. A

similar result (0.5- 0.85 λ) has been reported for spinal motoneurons (Clements and Redman 1989; Thurbon et al. 1998). The use of thin slices (in which some parts of the dendritic tree might have been cut off) and visual identification of cells (with the possibility of choosing smaller cells) may have reduced space clamp errors, which cannot be completely excluded. In fact, the estimation of I_{Na} reversal potential was made difficult probably due to incomplete clamp of distal parts of HMs. However, the kinetic properties of I_{Na}, the current most vulnerable to poor voltage and space clamp, were similar to those of the spinal motoneuron Na^+ current (see discussion below), which was investigated when space and voltage clamp conditions should have been much better (two electrode or single channel recordings; Barrett and Crill 1980; Safronov and Vogel 1995). Histological staining of single HMs with neurobiotin did not reveal any dye coupling and thus indicated that single HMs were presumably electrically isolated within the network, a condition necessary for effective voltage clamping.

Until recently data regarding firing properties and membrane conductances of HMs have been obtained using intracellular recording with sharp electrodes (Mosfeldt-Laursen and Rekling 1989; Sawczuk et al. 1995, 1997; Viana et al. 1993a,b, 1994, 1995). It is interesting to compare these results with the present ones, because the two recording techniques produce differences in neuronal R_{in} (Spruston and Johnston 1992; Staley et al. 1992). One possible factor leading to these discrepancies can be the membrane shunt created around the sharp electrode. On the contrary, the seal of several GΩ created around the patch pipette leaves the membrane of the neuron relatively undamaged. In recordings with sharp electrodes, part of injected current is dissipated via the shunt. This can explain the differences in current step intensities required to evoke repetitive firing. In the present study the AP trains were evoked with current pulses in the range 50- 700 pA, while current steps of several nA have been injected via sharp electrodes into HMs to have similar f-I curves (Mosfeldt-Laursen and Rekling 1989; Sawczuk et al. 1995, 1997; Viana et al. 1993b, 1995). In sharp electrode experiments some currents flowing via activated conductances can also be deviated via shunt and might not generate changes in current clamp experiments. This is a concern especially for conductances situated in distal parts of dendrites and could explain the fact that inward rectification by hyperpolarization is weak in neonatal HMs recorded with sharp electrodes (Viana et al.

1994), while the same inward rectification was substantially stronger in the present study, when neurons were patch clamped. Although the localization of the I_h conductances in HMs is not yet known, its presence in dendrites of hippocampal neurons has been reported (Magee 1998, 1999).

Nevertheless, patch clamp recordings have limitations too. The large pipette provides less resistance (thus improves voltage clamp conditions), but also washes out enzymes and metabolic products from the neuron cytoplasm. Consequently, many membrane properties are not constant during recording (Robinson and Cameron 2000; Spruston and Johnston 1992) due to phosphorylation/dephosphorylation of membrane proteins (including ionic channels). Since low resistance pipettes were used for voltage clamp experiments (to reduce series resistance and improve voltage clamp) and high resistance electrodes were utilized for current clamp recording (to reduce rundown), strightforward comparisons between the two sets of data requires caution.

Typically, single or repeated APs were followed by a series of depolarizing and hyperpolarizing afterpotentials as examplified in Fig. 2. The fAHP, mAHP and fADP were present in all HMs. A few cells possessed the sAHP (see also Viana et al. 1993b; Nishimura et al. 1989) or the sADP, which has also been observed in facial motoneurons (Nishimura et al. 1989). The HM mAHP was qualitatively similar to the one recorded with sharp electrodes from brainstem (Mosfeldt Laursen and Rekling 1989, Nishimura et al. 1989, Sah and McLachlan 1992, Viana et al. 1993b, Chandler et al. 1994) or spinal (Walton and Fulton 1986, Zhang and Krnjevic 1987) motoneurons. The similarity of voltage pattern demonstrates that HM whole cell patch clamping allowed measuring of voltage response without introducing artifacts inherent to the recording technique.

Adult HMs in brainstem slices show three distinct phases of spike frequency adaptation (Sawczuk et al. 1995, 1997). In most cases HMs of neonatal rats display fast spike adaptation or, in a minority of cases, firing acceleration (Viana et al. 1993b, 1995). The present study found no direct experimental evidence for spike frequency acceleration while fast adaptation was the commonest response (a minority of cells had a regular firing pattern). The differences might be due to postnatal developmental changes (as the present results were obtained from younger rat cells that often show fast adaptation; Viana et al. 1995) or to the recording conditions (sharp *versus* patch electrodes; blind

recording *versus* visually identified motoneurons; large current pulses *versus* weaker ones).

2. *Fast transient Na^+ current*

One of the most problematic membrane currents to be studied accurately is the fast transient Na^+ current (I_{Na}). Its fast activation is strongly distorted by any voltage clamp error. This fact explains the poor understanding of I_{Na} properties in motoneurons (Barrett and Crill 1980; Takahashi 1990). Until now no data were available about the kinetics of macroscopic I_{Na} in motoneurons in a slice preparation and only single channel recordings are available for spinal motoneurons (Safronov and Vogel 1995). Several approaches were utilized in the present study to investigate macroscopic I_{Na}, e.g. strong decrease in extracellular Na^+ concentration (substituted by TEA, NMDG, or choline) or perfusion of HM with very low doses of TTX (20 nM), which partially reduced I_{Na}. I_{Na} recorded under these conditions was apparently clamped and had activation threshold at about –45 mV (half activation –30 mV). I_{Na} activated with time constants of 1- 4 ms, inactivated during depolarization (half inactivation –44 mV), and recovered from inactivation with a biexponential process. These I_{Na} kinetics strongly resemble the kinetics of spinal neuron Na^+ channels. However, the voltage dependence of HMs I_{Na} activation and inactivation was shifted rightwards with respect to that of spinal motoneurons. It is difficult to decide whether these more depolarized values could be attributed to voltage clamp errors. I_{Na} has been recorded in many reduced preparations like acutely isolated neurons or oocytes (Cummins et al. 1994; Fan et al. 1994; Huguenard et al. 1988; Sah et al. 1988; Stühmer et al. 1987) and exhibited large variability of half activation and inactivation values (range –21 mV to –41 mV and –46 mV to -70 mV, respectively). Values for HMs were within this range of values. Nevertheless, simulations of HM spike using these parameters of I_{Na} revealed a plateau state, normally not found experimentally and which disappeared after shifting half activation and inactivation values leftwards by 10 mV and 20 mV, respectively. Note also that I_{Na} was recorded in a Ca^{2+} free extracellular solution of highly reduced Na^+ concentration. This milieu might have interfered with activation and/or inactivation processes of Na^+ channels.

Slow inactivation of I_{Na} has been suggested to be a suitable mechanism for some spike frequency adaptation (Fleidervish et al. 1996; Powers et al. 1999; Rudy 1981). I_{Na} in HMs exhibited two phases of recovery from inactivation (fast one with τ= 10- 20 ms and slow one with τ= 100- 300 ms). Simulations including this property produced trains of AP with firing adaptation lasting hundreds of milliseconds. However, it still is not confirmed experimentally whether this mechanism is indeed utilized for spike frequency adaptation by HMs.

A persistent noninactivating Na^+ current (I_{NaP}) is present in adult facial, hypoglossal, and trigeminal motoneurons (Chandler et al. 1994; Mosfeldt Laursen and Rekling 1989; Nishimura et al. 1989) as well as in other central neurons (Alzheimer et al. 1993a; French et al. 1990; Huguenard et al. 1988; Schwindt and Crill 1980a,b). I_{NaP} activates below spike threshold, and would therefore accelerate subthreshold membrane depolarization to spike threshold. However, this current was not observed in neonatal HMs, since only one fast inactivating component (estimated with exponential fitting of I_{Na} decay during depolarization) was present. A similar result has been obtained on neonatal spinal motoneurons (Safronov and Vogel 1995). It has been demonstrated that I_{NaP} increases with age (Alzheimer et al. 1993b; Huguenard et al. 1988) and, perhaps, HMs at this developmental stage (1- 7 days) have not yet expressed I_{NaP}.

The Na^+ channel from rat brain consists of one major α subunit and two smaller β subunits, β1 and β2 (Catterall 1992). Five different α subunits were cloned from rat brain (Noda et al. 1986a,b) and seem to be differentially distributed among brain regions. The RII subtype is preferentially expressed with RI/RII ratios ranging from 0.07 (in the hippocampus) to 0.17 (in the cerebral cortex), while the RI subtype is preferentially expressed in more caudal areas of the central nervous system with values of RI/RII of 0.98 (for medulla oblongata) and 2.2 (for spinal cord; Gordon et al. 1987). The strict regional expression of these two sodium channel subtypes suggests that they may have distinct functional properties or physiological roles. Immunochemical staining of neurons against Na^+ channels from rat brain showed their preferential localization in the axon hillock (Boudier et al. 1985; Catterall 1981; Wollner and Catterall 1986).

The axon hillock- initial segment of axon has been identified as a site where AP is generated (Araki and Terzuolo 1962; Coombs et al. 1957; Moore et al. 1983). Recently

information about Na^+ channel distribution over the spinal motoneuron membrane has been provided (Safronov et al. 1999). It appears that the soma has very low density of Na^+ conductance (~22 pS/μm^2) and is even unable to generate an AP, while the same value for the axon is about 2400 pS/μm^2 (Safronov et al. 1999, 2000). This fact has been confirmed by both experiments and simulation studies. In contrast, the soma of hippocampal pyramidal neurons in which Na^+ channel densities can reach 30 pS/μm^2, is able to generate spikes (Colbert and Johnston 1996). An even higher density of these channels (~400 pS/μm^2) have been reported in isolated hippocampal cells by Sah et al. (1988). The Na^+ conductance used in present computer simulations was 200 pS/μm^2, that is near the realistic one. However, the HM model consisted only of the soma compartment. This is justified by the lack of information about Na^+ and K^+ conductance density and distribution. More accurate reconstruction of HM excitability characteristics could be obtained when all the necessary information becomes available.

3. *K^+ currents*

In addition to I_{Na} generated by depolarization, multiple K^+ conductances have been suggested to shape AP repolarization and repetitive firing behavior of HMs (Viana et al. 1993b). Molecular biology studies have indicated that rat brainstem nuclei contain mRNA for various K^+ channel subunits, particularly Kv3.3 (and to a lesser degree Kv3.1) which in expression studies generates a sustained, slowly inactivating current (Weiser et al. 1994), and Kv4.2 and Kv4.3 responsible for fast activating and inactivating currents (Serodio and Rudy 1998). It appears likely that HMs possess a repertoire of K^+ currents, which so far have not been systematically analyzed under voltage clamp conditions.

In the present experiments the total outward current could be separated into two broad components. One composed of voltage-activated K^+ currents and a second one of Ca^{2+}-dependent K^+ currents, which are typically responsible for the medium and slow AHP (Viana et al. 1993b).

Voltage-activated K^+ currents were investigated in the presence of TTX to block I_{Na} and in Ca-free-Co solution to eliminate Ca^{2+} currents and any residual Ca^{2+}-dependent K^+ currents. Cs^+ was routinely present in the external solution to block the hyperpolarization activated current I_h (Bayliss et al. 1994a) and did not appear to interfere with the voltage

activated K^+ currents. Under these conditions a slow K^+ current (I_{Kslow}) was generated by 1 s voltage steps from -70 mV V_h (see Fig. 17B), peaking in tens of milliseconds and remaining at a plateau with a slow decline. Hyperpolarizing prepulses allowed unmasking a much faster K^+ current (I_{Kfast}). I_{Kslow} and I_{Kfast} could therefore be distinguished on the basis of the substantial differences in their voltage dependence of activation and inactivation. Ca^{2+} dependent K^+ currents were recorded in the presence of TTX and in normal Ca^{2+} (2 mM) solution. In addition, EGTA concentration in the pipette solution was decreased to avoid reduction of this current due to Ca^{2+} chelation, as shown also by the fact that intracellular EGTA blocks the mAHP (Viana et al. 1993b).

4. I_{Kslow} and I_{Kfast} properties

By its activation kinetics and voltage dependence I_{Kslow} resembled the classical delayed rectifier (I_{Kdr}) first reported for the squid giant axon by Hodgkin and Huxley (1952) and found in many neurons (see for review Rudy 1988; Storm 1990). I_{Kslow} activated at membrane potentials positive to -50 mV, and showed voltage-dependent kinetics of activation. For example, the activation time constant value decreased nearly three-fold from -20 mV to +20 mV. At membrane potentials positive to -10 mV I_{Kslow} inactivated slowly with a time course of seconds. During repolarization at the end of voltage step, I_{Kslow} deactivated with monoexponential time constant. In addition, I_{Kslow} was suppressed by TEA and partly depressed by very high doses of 4-AP.

I_{Kfast} was unaffected by TEA application, a treatment which actually allowed to observe it in isolation with its characteristically faster kinetics. I_{Kfast} resembled the fast transient outward current I_A, first observed in gastropod neurons (Connor and Stevens 1971a). I_{Kfast} was almost completely inactivated near resting potential, since depolarizing voltage steps from -70 mV V_h did not evoke I_{Kfast}. Halfmaximal inactivation was at -93 mV. By membrane hyperpolarization the inactivation of I_{Kfast} was rapidly removed with recovery to 50 % of control amplitude in about 10 ms (see Fig. 26 D). Subsequent depolarization to values positive to -60 mV activated I_{Kfast} (with a time course depending on membrane voltage) which peaked and fully inactivated within 200 ms (at 0 mV the inactivation time constant was 70 ms). I_{Kfast} deactivation after the end of the command pulse was

comparatively faster (19 ms) and showed little voltage sensitivity. In contrast to I_{Kslow}, I_{Kfast} was selectively attenuated after application of 4-AP (up to 5 mM) which, in mM concentrations, is a well established blocker of I_{Kfast} in other nerve cells (Rudy 1988; Storm 1990). The characterization of I_{Kfast} in HMs is thus based on distinct electrophysiological properties and pharmacological sensitivity.

It should be noted that E_{rev} for I_{Kfast} (and also for I_{Kslow}) was relatively near the calculated value for K^+ and was shifted positively (as predicted by the Nernst equation) by raising extracellular K^+ concentration. These observations suggest that both currents were mainly mediated by an increased membrane permeability to K^+. Nevertheless, there was a small but systematic difference between the current E_{rev} and E_K. This was partly due to a slight, yet consistently measurable permeability to Na^+ inherent in both currents and perhaps partly to the difficulty in obtaining complete isopotential conditions in neurons with dendritic arborization.

5. Apamin sensitive current

The outward current selectively inhibited by apamin may be termed I_{AHP} (see Sah, 1996). On HMs this represented about 1/3rd of the total outward current induced by membrane depolarization and deactivated slowly. For 1 s long membrane depolarization to +20 mV (from -50 mV V_h) the cord conductance of I_{AHP} (under apparently steady state conditions) was 7 nS. The corresponding conductance value for the I_{Kslow} (values taken from Fig. 23A) was 14 nS while I_{Kfast} was strongly inactivated at this time point. Thus, during sustained depolarization I_{Kslow} generated a membrane shunt considerably larger than I_{AHP}. Note that in addition to these K^+ currents there was a residual, unidentified outward current sensitive to muscarinic agents. Since the largest component of the total outward steady current was apparently made up by I_{Kslow} (which deactivated with a faster timecourse), it was difficult to study I_{AHP} in isolation. For this reason kinetic parameters pertaining to I_{AHP} were obtained by analyzing the current (and especially its slow tail) obtained after subtraction. The I-V relation of I_{AHP} indicated an apparent activation threshold at about -40 mV; its non-linear voltage dependence in the -40/-10 mV range might have reflected the strong voltage dependence of Ca^{2+} conductance activation (Hille 1992). The time course of I_{AHP} development was bi-exponential. This latter property

probably reflects the multifactorial process underlying I_{AHP} generation and might have been due to phased recruitment of SK channels by increasingly larger amounts of intracellular Ca^{2+} diffusing over a wide cytoplasmic area. It is interesting that I_{AHP} deactivation (observed as monoexponential decay time constant of the apamin sensitive tail current) showed no voltage dependence, thus suggesting that the membrane conductance underlying I_{AHP} was probably voltage independent. I_{AHP} with similar kinetic properties has been described in sympathetic neurons (Cassell and McLachlan 1987, Goh and Pennefather 1987), vagal motorneurons (Sah and McLachlan 1992), trigeminal motoneurons (Chandler et al. 1994) and cortical neurons (Schwindt et al. 1992b).

It is noteworthy that membrane depolarization as short as 1 ms could elicit a measurable I_{AHP}. It is suggested that even very short voltage changes (as brief as a single AP, normally lasting 1-3 ms) can trigger Ca^{2+} entry sufficient to turn on an adequate number of SK channels to generate a mAHP. Similar observations have been obtained with ganglion neurons (Lancaster and Pennefather 1987).

The mAHP was completely blocked by Ca^{2+}-free solution or apamin, and it reversed at membrane potential near the predicted E_K. All these observations indicate that mAHP was due to I_{AHP} activation. Its sensitivity to apamin, a very selective blocker of SK channels (for review see Sah 1996), suggests that I_{AHP} responsible for this phenomenon was probably mediated by SK channels and turned on by Ca^{2+} entry following one (or more) AP. In fact, the lack of effect of apamin on resting potential or leak conductance shows that such a I_{AHP} was inactive at resting levels of intracellular Ca^{2+}. Additional experiments explored the mAHP sensitivity to intracellular Ca^{2+}.

Introducing BAPTA (1 mM), a fast Ca^{2+} chelator, into the HMs strongly reduced mAHP as does also EGTA (10 mM; Viana 1993b). The AP and fAHP were unaffected, but a long sAHP (1-2 s duration) appeared. This result could suggest that the relative distance of Ca^{2+} diffusion might be important in determining the different BAPTA actions on distinct afterpotential components. As SK channels might be located relatively far from Ca^{2+} entry sites, BAPTA would be able to capture Ca^{2+} moving towards these channels. On the other hand, potentiation of Ca^{2+} dependent K^+ currents or sAHP by BAPTA has surprisingly been reported for hippocampal neurons (Engisch et al. 1996; Jahromi et al. 1999; Velumian and Carlen 1999; Zhang et al. 1995). The suggested mechanism for this

potentiation (Jahromi et al. 1999; Zhang et al. 1995) implies that BAPTA increases the pool of diffusible cytoplasmic buffers which reversibly bind and release Ca^{2+} and thereby it facilitates diffusion of Ca^{2+} from sites of entry to sites of action. BAPTA is more suitable for this than EGTA, because BAPTA has K_D similar to that of EGTA, but releases Ca^{2+} 100 times slower (Pethig et al. 1989). Whether this scheme is applicable to HMs is not clear, but it could explain why sAHP was rarely seen in control conditions but was unmasked when BAPTA (1 mM) was present in patch pipette. Very low concentration of EGTA (0.5 mM) in the control pipette solution and possible wash out of endogenous mobile buffers from HMs presumably led to impossibility to observe sAHP under control conditions.

It is interesting to note that an exceptionally low endogenous Ca^{2+} binding ratio of 41 has been reported for HMs (Lips and Keller 1998, 1999). This value is much smaller than the one for cortical (100-135; Helmchen et al. 1996), hippocampal pyramidal (168- 207; Helmchen et al. 1996), or Purkinje neurons (900; Fierro and Llano 1996). Moreover, this property of HMs might account for their high vulnerability to Ca^{2+} dependent excitotoxic damage. In fact, the degenerative motoneuron disease ALS has been shown to affect preferentially HMs as well as some other brainstem motoneuron groups (e.g. trigeminal, facial, and ambiguous; DePaul et al. 1988), which do not contain the Ca^{2+}-chelating protein parvalbumin, while motoneurons containing this protein are more resistant to ALS (Reiner et al. 1995).

During a single AP the increase in intracellular Ca^{2+} concentration which is responsible for generating the mAHP is suggested to originate from transmembrane influx as well as release from internal stores (Sah 1996). This phenomenon is applicable to sympathetic neurons (Davies et al. 1996; Kawai and Watanabe 1989) or vagal motoneurons (Sah and McLachlan 1991). On HMs the Ca^{2+} store depleting agent caffeine (10 mM) largely and persistently enhanced mAHP. Such an observation indicates that on HMs the contribution by Ca^{2+} release from internal stores to the mAHP following each AP was probably very small. Further evidence in support of a minimal role by internal Ca^{2+} release in mAHP generation comes from the experiments with dantrolene or ryanodine, agents which are known to block release of Ca^{2+} from internal stores (Friel and Tsien 1992; McPherson et al. 1991; Ohta et al. 1990; Shmigol et al. 1994; Thayer et al. 1988; Usachev et al. 1993).

While these results collectively indicate that the main mechanism for Ca^{2+} mediated generation of HM mAHP is influx of this divalent cation, future work will be necessary to clarify the process underlying the mAHP enhancement by caffeine or dantrolene.

6. Functional implications of K^+ currents for motoneuronal firing properties

6.1. AP repolarization

I_{Kslow} observed in the present study showed rather slow activation. This slowness is hardly to be attributed to poor clamping conditions. Single, delayed rectifier- like channel recordings from spinal motoneurons have intrinsically slow kinetics (Safronov and Vogel 1995). A similar time course is seen in acutely dissociated hippocampal (Numann et al. 1987) or sympathetic neurons (Goh et al. 1989). Slow kinetics of I_{Kslow} lead to doubts about this current participation in AP repolarization. Nevertheless, it has been reported by Viana et al. (1993b), that TEA (1-10 mM) prolongs AP duration. However, it cannot be excluded that another conductance, e.g. fast Ca^{2+} dependent K^+ current mediated by BK channels could have been blocked by TEA. The last one current is the main AP repolarizing mechanism in hippocampal (Lancaster and Adams 1986; Lancaster and Nicoll 1987; Storm 1987) and sympathetic neurons (Adams et al. 1982). Unfortunately, this current is still uncharacterized in HMs.

It has been previously proposed that 4-AP sensitive K^+ conductances shape the AP of HMs (Viana et al. 1993b) as 4-AP (0.1-0.5 mM) prolongs AP duration. The present experiments suggest that only a very small part of I_{Kfast} could be blocked by 1 mM 4-AP. Thus, it seems plausible that spike lengthening by small doses of 4-AP does not involve depression of I_{fast}. Furthermore, as the resting potential of neonatal HMs is about -70 mV and the spike duration about 1 to 3 ms (Viana et al. 1995; present study), it is likely that at rest level I_{Kfast} is partially inactivated and that any available fraction of I_{Kfast} possesses activation and deactivation kinetics (approximately 10 and 20 ms, respectively) much slower than the spike duration.

For these characteristics one can suggest that I_{Kslow} and I_{Kfast}, rather than controlling the duration of a single AP (which perhaps relies on a distinct Ca^{2+} dependent K^+ current have a role in determining the repetitive firing pattern.

Simulations confirmed that neither I_{Kslow} nor I_{Kfast} were capable of quickly repolarizing the AP. Surprisingly, I_{Kslow} despite its slower kinetics was more effective than I_{Kfast} in producing repolarization. However, with maximal g_{Kslow} equal to maximal g_{Na} (1 μS, that corresponds to conductance density of 200 pS/μm^2 for a neuron with capacitance of 50 pF) the simulated AP had duration of 10 ms. This is a rather high conductance density if compared with the K^+ conductance density in spinal motoneuron soma (20 and 18 pS/μm^2 for K_{DR} and K_A channels respectively; Safronov et al. 2000). This fact raises the question of how K^+ channels are distributed over the HM membrane, since spatial distribution of K^+ conductances may strongly influence their contribution to neuronal excitability. A simulation study by Mainen and Sejnowski (1996) has demonstrated that a set of neurons that share a common set of ion channels and differ only in their dendritic geometry can exhibit an entire spectrum of firing patterns. The heterogeneity of channel distribution over dendritic and somatic membranes can elicit even more complicated firing behavior. K_A channels, generating I_A, have been found to be distributed with increasing density along the hippocampal cell main dendrites (Hoffman et al. 1997). This localization allows these channels to reduce excitatory synaptic events and to limit back propagation of AP into the dendrites. The dendrites of spinal motoneurons posses about one fifth of total I_A, which is mainly situated in the soma (36%) and in the axon (47%; Wolff et al. 1998). Surprisingly, the largest part of I_{KDR} (47%) is located in the dendrites of these motoneurons. This result suggests that similar currents can have different roles in the regulation of neuron excitability not only in view of the variability in the kinetics and/or voltage dependence but also of their compartmental distribution.

6.2. Control of repetitive firing

Previous studies have shown the importance of the mAHP in controlling repetitive firing in different neurons (Kernel and Sjoholm 1973; Baldissera and Gustafsson 1974a,b; Madison and Nicoll 1984; Nishimura et al. 1989; Schwindt et al. 1992b; Viana et al. 1993b; Chandler et al. 1994, Powers et al. 1999). In the present investigation the crucial role of the mAHP (or it underlying I_{AHP}) in firing behavior became immediately apparent after the mAHP was blocked by apamin, carbachol or Ca^{2+} free solution. Very strong firing adaptation was readily manifested as a result. The present results therefore

demonstrate that the mAHP of neonatal HMs had the fundamental property of maintaining a slow firing frequency (with a relatively regular pattern). Whenever the mAHP was present, the duration of membrane potential sojourns at depolarized level became inadequate for full activation or inactivation of other voltage dependent K^+ conductances.

The fact that discharging rate increased and strong spike frequency adaptation appeared when the mAHP was fully suppressed by apamin raises the question of the relative contribution by different conductances to repetitive firing. In the presence of apamin and/or carbachol (which should have also blocked I_M or leak conductance as discussed later), adaptation probably developed because of the kinetic properties of I_{Kfast} and/or I_{Kslow}, especially as the baseline membrane potential, elevated during the spike train, should have facilitated persistent I_{Kslow} activation. Modulation of mAHP by neuromodulators like muscarine, 5-HT (Bayliss et al. 1995) or norepinephrine (Parkis et al. 1995) suggests that HM firing could change during different behavioral states associated with various degree of activity of cholinergic, serotoninergic or noradrenergic pathways. These transmitters might thus act via dynamic alterations in the role of various K^+ conductances to the total outward current.

Only a small part of I_{Kslow} could by activated during the first spike due to its slow kinetics. Nevertheless, since I_{Kslow} deactivated with a time constant (20- 50 ms) longer than first interspike interval (5 to 10 ms, when mAHP was blocked; Figs. 7 and 8), a certain fraction of activated I_{Kslow} would be present at the beginning of the second spike in a train. Likewise, further accumulation of I_{Kslow} would occur during the spike train with summating properties after each successive spike. Analogous considerations may be applied to I_{Kfast} on the basis of the properties of the fast I_A current described by Connor and Stevens (1971a,b).

Unfortunately, direct experimental test of I_{Kslow} and I_{Kfast} participation in the spike frequency adaptation manifested after mAHP block is presently made difficult by the lack of highly selective blockers. For instance, although I_{fast} is sensitive to 4-AP, even a 5 mM concentration of this substance could not block it completely. The same applies to TEA acting on I_{slow}. Along the same line it might be difficult to rely on holding potential

changes to remove I_{fast} inactivation selectively as this approach would also affect the kinetic properties of voltage dependent inward currents.

Computer stimulation studies shed some light on the functional role of I_{Kslow} and I_{Kfast} in HMs. The model HM did not include any mAHP conductance, thus, it was similar to the experimental conditions, when mAHP was blocked by apamin or carbachol. Simulations indicated that, during first AP, about 10% of available I_{Kfast} activated and substantially prolonged the first interspike interval. However, I_{Kfast} inactivated during depolarization, thus gradually reducing its inhibitory contribution. Apparent spiking acceleration emerged in a train of AP until an equilibrium between I_{Kfast} activation and inactivation was reached. On the contrary, accumulation of activated I_{Kslow} in the model neuron led to stronger delay of subsequent spikes within the first 100-200 ms, thus suggesting that slow activation of I_{Kslow} could be a suitable mechanism for early adaptation lasting hundreds of ms as indeed observed in experiments when mAHP was blocked (see Figs. 7 and 8).

7. Effects of muscarinic or mGlu receptor activity on HMs

The mAHP of HMs is a target for neuromodulation by 5-HT or norepinephrine (Bayliss et al. 1995; Parkis et al. 1995). Both substances do not act directly on the mAHP underlying conductance but operate indirectly by either inhibiting Ca^{2+} currents in the case of 5-HT (Bayliss et al. 1995) or reducing leak conductance (and activating an inward current) in the case of norepinephrine (Parkis et al. 1995). The present study shows that the mAHP (and I_{AHP}) is also a target for muscarinic receptor activity. Carbachol or muscarine reduced mAHP amplitude without changing its rise and decay times, suggesting that muscarinic receptors apparently led to inhibition of a fraction of I_{AHP} channels. It should be pointed out that previous studies on cortical neurons have reported that muscarinic receptors usually block the sAHP (Cole and Nicoll 1983, 1984; Schwindt et al. 1988, 1992b) while sparing the mAHP. On the other hand, like in the case of HMs, the mAHP of hippocampal neurons is reduced by carbachol (Storm 1989; Fiszman et al. 1991; Williamson and Alger 1990; Zhang and McBain 1995). It is however clear that in hippocampal cells several conductances participate in the generation of mAHP (Storm 1989) and that one of them, the so called I_M, may be the main target for the blocking action by carbachol on the mAHP (Halliwell and Adams 1982). It seems unlikely that on

HMs I_M was responsible for generating the mAHP since I_M is not Ca^{2+} dependent and has slow activation kinetics (Adams et al. 1982, Brown and Selyanko 1985) which preclude its turning on by a single AP. The present study thus indicates the mAHP as a novel site of action for muscarinic receptors of HMs. Furthermore, atropine enhanced the mAHP amplitude, suggesting that, under the recording conditions of the slice preparation, there was background release of acetylcholine sufficient for partial inhibition of the mAHP.

The present data however indicate that, in addition to I_{AHP}, other K^+ currents of HMs were modulated by muscarinic receptors. In fact, in the presence of apamin when I_{AHP} should have been completely blocked, carbachol could still reduce a component of the sustained outward current. The multiple sites of carbachol action on HMs were confirmed in experiments under current clamp conditions, as reduction in mAHP and membrane depolarization could be differentially occluded by apamin. While block of a variety of K^+ conductances contributes to the carbachol-evoked depolarization (Benardo and Prince 1982; Womble and Moises 1992), it is possible that enhancement of a non-specific cationic current is also a factor leading to membrane depolarization (Colino and Halliwell 1993; McCormick and Prince 1985; Segal 1982). Unlike the case of CA1 hippocampal cells (Figenschou et al. 1996), the present study did not observe any change in action potential duration or threshold in the presence of carbachol.

In addition, muscarinic agonists increase intracellular free Ca^{2+} in hippocampal and symphatetic neurons by causing Ca^{2+} release from intracellular Ca^{2+} stores and by promoting Ca^{2+} influx (del Rio et al. 1999; Felder et al. 1992; Kudo et al. 1988). Indeed, pretreatment of HMs with caffeine, which is known to release Ca^{2+} from internal stores (Kostyuk and Verkhratsky 1994), reduced the depolarizing action of carbachol, thus, suggesting some interaction between caffeine and carbachol.

The excitatory transmitter glutamate, acting on metabotropic receptors, modulates neurons by regulating their intrinsic and synaptic properties (Baskys 1992; Baskys and Malenka 1991; Cochila and Alford 1998; Del Negro and Chandler 1998; Forsythe and Clements 1990; Glaum and Miller 1993; Schoepp and Conn 1993). HMs might also be influenced by mGluRs activation, because they express mGluRs (Hay et al. 1999) and receive glutamatergic inputs (Funk et al. 1993; O'Braien et al. 1997). However, there were no studies whether HMs possess functionally expressed mGluRs. Therefore, the

modulation of HM excitability and the regulation of excitatory synaptic transmission to them were examined. Multiple effects of mGluRs activation by their agonist *t*-ACPD were observed. *t*-ACPD depolarized HMs with a parallel increase in R_{in}. A similar depolarization due to reduction in the leakage current has been reported for several neurons (Del Negro and Chandler 1998; Guerineau et al. 1994; Mercuri et al. 1996; McCormick and von Krosigk 1992). While activation of mGluRs depresses slow AHP and decreases accommodation in hippocampal neurons (Baskys et al. 1990; Charpak et al. 1990; Stratton et al. 1989), the firing pattern of HMs was apparently unchanged by *t*-ACPD. No mAHP modulation by *t*-ACPD was observed in the present study. However, the delay of first AP in the train and first interspike interval were significantly prolonged. Even though this phenomenon was not further investigated, I_{Kfast} upregulation by mGluRs activation might be a suitable mechanism in analogy with the similar process described by Cochilla and Alford (1998). In addition to these direct actions on HMs, *t*-ACPD depressed evoked glutamatergic currents. Whether this phenomenon was due to a pre- or post-synaptic effect remains to be investigated, but the increased paired pulse facilitation suggest that a presynaptic site of action was likely.

It is possible that mGluRs on HMs might by activated under physiological conditions in vivo. HMs receive glutamatergic rhytmically active inputs from respiratory neurons during the inspiration phase (Funk et al. 1993, 1997). High frequency activity may cause glutamate accumulation and it would, thus, favor mGluRs activation.

8. Conclusions

The present study investigated the membrane conductances and mechanisms underlying excitability and firing of neonatal HMs in a brainstem slice preparation. For this purpose current and voltage clamp experiments were performed using the whole cell patch clamp technique. Finally, some hypotheses were tested by computer simulations.

Kinetics and voltage dependencies of three voltage activated membrane currents I_{Na}, I_{Kslow}, and I_{Kfast} were described. This description allowed the computer reconstruction of these currents and thus is useful for further simulation studies of HMs. Despite the incompleteness of the model, preliminary simulations led to important conclusions about the role of I_{Na}, I_{Kslow}, and I_{Kfast} in the control of firing. I_{Na} is responsible for the fast up-

stroke of AP. I_{Kslow} and I_{Kfast} were not capable to repolarize a single AP, but strongly influenced model HM firing by reducing frequency and producing adapting or accelerating firing, respectively. Slow inactivation of I_{Na} was observed in HMs and produced spike frequency adaptation in the model HM.

A Ca^{2+} dependent K^+ current sensitive to apamin was identified. This current underlies the mAHP, which had a fundamental role in maintaining low firing frequency in HMs. Block of mAHP always unmasked adapting firing pattern. mAHP was modulated by manipulating intracellular Ca^{2+} by BAPTA and agents emptying Ca^{2+} stores. This fact suggested that mAHP might be modulated during neuronal activity. In addition, mAHP was depressed via activation of muscarinic ACh receptors by carbachol, which also depolarized HMs. Activation of mGluRs by *t*-ACPD produced pre- and postsynaptic effects on HMs. *t*-ACPD depolarized HMs (with parallel increase in R_{in}) and depressed glutamatergic transmission. However *t*-ACPD apparently neither modulated mAHP nor changed the discharge pattern of HMs. The results of ACh and mGlu receptors activation provide new evidence that network activity or behavioral state can influence HM responsiveness to synaptic inputs by changing HM excitability.

REFERENCES

ADAMS, P.R., BROWN, D.A., AND CONSTANTI, A. Pharmacological inhibition of the M-current. *J. Physiol (Lond.).* 332: 223- 262, 1982.

ADAMS, P.R., CONSTANTI, A., BROWN, D.A., AND CLARK, R.B. Intracellular Ca^{2+} activates a fast voltage-sensitive K^+ current in vertebrate sympathetic neurones. *Nature* 296: 746- 749, 1982.

AGHAJANIAN, G.K. AND RASMUSSEN, K. Intracellular studies in the facial nucleus illustrating a simple new method for obtaining viable motoneurons in adult rat brain slices. *Synapse* 3: 331- 338, 1989.

ALDES, L.D. Topographically organized projections from the nucleus subceruleus to the hypoglossal nucleus in the rat: a light and electron microscopic study with complementary axonal transport techniques. *J. Comp. Neurol.* 302: 643- 656, 1990.

ALDES, L.D., CHAPMAN, M.E., CHRONISTER, R.B., AND HAYCOCK, J.W. Sources of noradrenergic afferents to the hypoglossal nucleus in the rat. *Brain Res. Bull.* 29: 931-942, 1992.

ALZHEIMER, C., SCHWINDT, P.C., AND CRILL, W.E. Modal gating of Na^+ channels as a mechanism of persistent Na^+ current in pyramidal neurons from rat and cat sensorimotor cortex. *J. Neurosci.* 13: 660- 673, 1993a.

ALZHEIMER, C., SCHWINDT, P.C. AND CRILL, W.E. Postnatal development of a persistent Na^+ current in pyramidal neurons from rat sensimotor cortex. *J. Neurophysiol.* 69: 290-292, 1993b.

AMRI, M., AND CAR, A. Projections from the medullary swallowing center to the hypoglossal motor nucleus: a neuroanatomical and electrophysiological study in sheep. *Brain Res.* 441: 119-126, 1988.

ARAKI, T., AND TERZUOLO, C. Membrane currents in spinal motoneurons associated with the action potential and synaptic activity. *J. Neurophysiol.* 25: 772-789, 1962.

ARMSTRONG, C.M. AND BEZANILLA, F. Charge movement associated with the opening and closing of the activation gates of the Na^+ channels. *J. Gen. Physiol.* 63: 533- 552, 1974.

BAKELS, R. AND KERNELL, D. Matching between motoneurone and muscle unit

properties in rat medial gastrocnemius. *J. Physiol. (Lond)* 463: 307- 324, 1993.

BALDISSERA, F. AND GUSTAFSSON, B. Firing behavior of a neuron model based on the afterhyperpolarization conductance time course and algebraical summation. Adaptation and steady state firing. *Acta Physiol. Scand.* 92: 27- 47, 1974a.

BALDISSERA, F. AND GUSTAFSSON, B. Firing behavior of a neuron model based on the afterhyperpolarization conductance time course. First interval firing. *Acta Physiol. Scand.* 91: 528-544, 1974b.

BALDISSERA, F.,. GUSTAFSSON, B., AND PARMIGGIANI, F. Saturating summation of the afterhyperpolarization conductance in spinal motoneurones: a mechanism for "secondary range" repetitive firing. *Brain Res.* 146: 69-82, 1978.

BALDISSERA, F. AND PARMIGGIANI, F. After hyperpolarization conductance time-course and repetitive firing in a motoneurone model with early inactivation of the slow potassium conductance system. *Biol. Cybernetics* 34: 233-240, 1979.

BARRETT, E.F., BARRETT, J.N., AND CRILL, W.E. Voltage-sensitive outward currents in cat motoneurones. *J. Physiol. (Lond.)* 304: 251-276, 1980.

BARRETT, J.N., AND CRILL, W.E. Voltage clamp of cat motoneurone somata: properties of the fast inward current. *J. Physiol. (Lond.)* 304: 231-249, 1980.

BARRETT, R.,. BAO, X., MISELIS, R., AND ALTSCHULER, S. Brain stem localization of rodent esophageal premotor neurons revealed by transneuronal passage of pseudorabies virus. *Gastroenterology* 107: 728-737, 1994.

BARRY, P.H. AND LYNCH, J.W. Liquid junction potentials and small cell effects in patch-clamp analysis. *J. Membrane Biol.* 121: 101- 117, 1991.

BASKYS, A. Metabotropic receptors and 'slow' excitatory actions of glutamate agonists in the hippocampus. *Trends Neurosci.* 15: 92- 6, 1992.

BASKYS, A. AND MALENKA, R.C. Agonists at metabotropic glutamate receptors presynaptically inhibit EPSCs in neonatal rat hippocampus. *J. Physiol. (Lond.)* 444: 687-701, 1991.

BASKYS, A., BERNSTEIN, N.K., BAROLET, A.W., AND CARLEN, P.L. NMDA and quisqualate reduce a Ca-dependent K^+ current by a protein kinase-mediated mechanism. *Neurosci. Lett.* 112: 76-81, 1990.

BAYLISS, D.A., UMEMIYA, M., AND BERGER, A.J. Inhibition of N- and P-type calcium currents and the afterhyperpolarization in rat motoneurons by serotonin. *J. Physiol.(Lond.)* 485: 635-647, 1995.

BAYLISS, D.A., VIANA, F., BELLINGHAM, M.C., AND BERGER, A.J. Characteristics and postnatal development of a hyperpolarization-activated inward current (I_h) in rat hypoglossal motoneurones *in vitro*. *J. Neurophysiol.* 71: 119-128, 1994a.

BAYLISS, D.A., VIANA, F., KANTER, R., SZYMECZEK-SEAY, C., BERGER, A., AND MILLHORN, D.E. Early postnatal development of thyrotropin-releasing hormone (TRH) expression, TRH receptor binding, and TRH responses in neurons of rat brainstem. *J. Neurosci.* 14: 821-833, 1994b.

BECKMAN, M. AND. WHITEHEAD, M. Intramedullary connections of the rostral nucleus of the solitary tract in the hamster. *Brain Res.* 557: 265-279, 1991.

BELLINGHAM, M.C. AND BERGER, A.J. Adenosine suppresses excitatory glutamatergic inputs to rat hypoglossal motoneurons *in vitro*. *Neurosci. Lett.* 177: 143-146, 1994.

BELLINGHAM, M.C. AND BERGER, A.J. Presynaptic depression of excitatory synaptic inputs to rat hypoglossal motoneurons by muscarinic M2 receptors. *J. Neurophysiol.* 76: 3758-3770, 1996.

BENARDO, L.S. AND PRINCE, D.A. Ionic mechanisms of cholinergic excitation in mammalian hippocampal pyramidal cells. *Brain Res.* 249: 333-344, 1982.

BENNETT, D., HULTBORN, H., FEDIRCHUK, B., AND GORASSINI, M. Synaptic activation of plateaus in hindlimb motoneurons of decerebrate cats. *J. Neurophysiol.* 80: 2023-2037, 1998a.

BENNETT, D., HULTBORN, H., FEDIRCHUK, B., AND GORASSINI, M. Short-term plasticity in hindlimb motoneurons of decerebrate cats. *J. Neurophysiol.* 80: 2038-2045, 1998b.

BERGER, A.J.,. BAYLISS, D.A., AND VIANA, F. Modulation of neonatal rat hypoglossal motoneuron excitability by serotonin. *Neurosci. Lett.* 143: 164-168, 1992.

BERGER, A.J., BAYLISS, D.A., AND VIANA, F. Development of hypoglossal motoneurons. *J. Appl. Physiol.* 81: 1039-1048, 1996.

BIGLAND-RITCHIE, B. AND WOODS, J.J. Changes in muscle contractile properties and neural control during human muscular fatigue. *Muscle Nerve* 7: 691-699, 1984.

BIGLAND-RITCHIE, B., JOHANSSON, R., LIPPOLD, O.C., SMITH, S., AND WOODS, J.J.

Changes in motoneurone firing rates during sustained maximal voluntary contractions. *J. Physiol. (Lond.)* 340: 335-346, 1983.

BONIFAZZI, C., BELUZZI, O., AND SACCHI, O. Kinetic analysis of incomplete current tracings according to the Hodgkin-Huxley model. *J. Theor. Biol.* 130: 183-190, 1988.

BORG-GRAHAM, L.J. Interpretation of data and mechanisms for hippocampal pyramidal cell models. In *Cerebral cortex, Volume 13: Cortical models* Edited by P.S. Ulinski, E.G. Jones, and A. Peters, New York: Plenum Press, 1998.

BORKE, R., NAU, M., AND RINGLER, R.J. Brain stem afferents of hypoglossal neurons in the rat. *Brain Res.* 269: 47-55, 1983.

BOUDIER, J.A., BERWALD-NETTER, Y., DELLMANN, H.D., BOUDIER, J.L., COURAUD, F., KOULAKOFF, A., AND CAU, P. Ultrastructural vizualization of Na^+-channel associated [^{125}I]α-scorpion toxin binding sites on fetal mouse nerve cells in culture. *Dev. Brain Res.* 20: 137- 142, 1985.

BROWN, D.A. AND SELYANKO, A.A. Two components of muscarine-sensitive membrane current in rat sympathetic neurones. *J. Physiol.(Lond.)* 358: 335-363, 1985.

BURKE, R.E. Motor units: anatomy, physiology, and the functional organization. In: *Handbook of Physiology. The Nervous System. Motor Systems.* Bethesda, MD: Am. Physiol. Soc., 1981, sect. I. vol. II, pt. 1, chapt. 10, p. 345-422.

BURKE, R.E. AND NELSON, P.G. Accommodation to current ramps in motoneurons of fast and slow twitch motor units. *Int. J. Neurosci.* 1: 347-356, 1971.

CASSELL, J.F. AND MCLACHLAN, E.M. Two calcium-activated potassium conductances in a subpopulation of coeliac neurones of guinea-pig and rabbit. *J. Physiol. (Lond.)* 394: 331-349, 1987.

CATTERALL, W.A. Localization of sodium channels in cultured neural cells. *J. Neurosci.* 1: 777- 783, 1981.

CATTERALL, W.A. Cellular and molecular biology of voltage-gated sodium channels. *Physiol. Rev.* 72: S15- 48, 1992.

CHANDLER, S.H., HSAIO, C.-F., INOUE, T., AND GOLDBERG, L.J. Electrophysiological properties of guinea pig trigeminal motoneurons recorded *in vitro*. *J. Neurophysiol.* 71: 129-145, 1994.

CHARPAK, S., GAHWILER, B.H., DO, K.Q., AND KNOPFEL, T. Potassium conductances in hippocampal neurons blocked by excitatory amino-acid transmitters. *Nature* 347: 765-767, 1990.

CLAY, J.R. Excitability of the squid giant axon revisited. *J. Neurophysiol.* 80: 903-913, 1998.

CLEMENTS, J.D. AND REDMAN, S.J. Cable properties of cat spinal motoneurones measured by combining voltage clamp, current clamp and intracellular staining. *J. Physiol. (Lond.)* 409: 63- 87, 1989.

COCHILLA, A.J. AND ALFORD, S. Metabotropic glutamate receptor-mediated control of neurotransmitter release. *Neuron* 20: 1007- 16, 1998.

COLE, A.E. AND NICOLL, R.A. Acetylcholine mediates a slow synaptic potential in hippocampal pyramidal cells. *Science* 221:1299- 1301, 1983.

COLE, A.E. AND NICOLL, R.A. Characterization of a slow cholinergic post-synaptic potential recorded in vitro from rat hippocampal pyramidal cells. *J. Physiol. (Lond.)* 352: 173- 188, 1984.

COLBERT, C.M. AND JOHNSTON, D. Axonal action-potential initiation and Na^+ channel densities in the soma and axon initial segment of subicular pyramidal neurons. *J. Neurosci.* 16: 6676- 86, 1996.

COLINO, A. AND HALLIWELL, J.V. Carbachol potentiates Q current and activates a calcium-dependent non-specific conductance in rat hippocampus *in vitro*. *Eur. J. Neurosci.* 5: 1198-1209, 1993.

CONNAUGHTON, M., PRIESTLEY, J.V., SOFRONIEW, M.V., ECKENSTEIN, F., AND CUELLO, A.C. Inputs to motoneurones in the hypoglossal nucleus of the rat: light and electron microscopic immunocytochemistry for choline acetyltransferase, substance P and enkephalins using monoclonal antibodies. *Neuroscience* 17: 205-24, 1986.

CONNOR, J.A. AND STEVENS C.F. Studies of a transient outward current in gastropod neural somata. *J. Physiol. (Lond.)* 213: 21-30, 1971a.

CONNOR, J.A. AND STEVENS, C.F. Prediction of repetitive firing behavior from voltage clamp data on an isolated neurone soma. *J. Physiol. (Lond.)* 213: 31-53, 1971b.

CONWAY, B., HULTBORN, H., KIEHN, O., AND MINTZ, I. Plateau potentials in alpha-motoneurones induced by intravenous injection of L-dopa and clonidine in the spinal cat. *J. Physiol. (Lond.)* 405: 369-384, 1988.

COOMBS, J.S., CURTIS, D.R., AND ECCLES, J.C. The generation of impulses in motoneurones. *J. Physiol. (Lond.)* 139: 232-249, 1957.

CRONE, C., HULTBORN, H., KIEHN, O., MAZIERES, L., AND WIGSTROM, H. Maintained changes in motoneuronal excitability by short-lasting synaptic inputs in the decerebrate cat. *J. Physiol. (Lond.)* 405: 321-343, 1988.

CRILL, W.E. Persistent sodium current in mammalian central neurons. *Annu. Rev. Physiol.* 58: 349-362, 1996.

CUMMINS, T.R., XIA, Y., AND HADDAD, G.G. Functional properties of rat and human neocortical voltage-sensitive sodium currents. *J. Neurophysiol.* 71: 1052- 64, 1994.

CURTIS, J.C. AND APPENTENG, K. The electrical geometry, electrical properties and synaptic connections onto rat V motoneurones *in vitro*. *J. Physiol. (Lond.)* 465: 85-119, 1993.

DAVIES, P.J., IRELAND, D.R., AND MCLACHLAN, E.M. Sources of Ca^{2+} for different Ca^{2+}-activated K^+ conductances in neurons of the rat superior cervical ganglion. *J. Physiol. (Lond.)* 495: 353- 366, 1996.

DELGADO-LEZAMA, R., PERRIER, J., NEDERGAARD, S., SVIRSKIS, G., AND HOUNSGAARD, J. Metabotropic synaptic regulation of intrinsic response properties of turtle spinal motoneurones. *J. Physiol. (Lond.)* 504: 97-102, 1997.

DEL NEGRO, C.A., AND CHANDLER, S.H. Regulation of intrinsic and synaptic properties of neonatal rat trigeminal motoneurons by metabotropic glutamate receptors. *J. Neurosci.* 18: 9216-9226, 1998.

DEL RIO, E., BEVILACQUA, J.A., MARSH, S.J., HALLEY, P., AND CAULFIELD, M.P. Muscarinic M1 receptors activate phosphoinositide turnover and Ca^{2+} mobilisation in rat sympathetic neurones, but this signalling pathway does not mediate M-current inhibition. *J. Physiol. (Lond.)* 520: 101- 11, 1999.

DEPAUL, R., ABBS, J.H., CALIGIURI, M., GRACCO, V.L., AND BROOKS, B.R. Hypoglossal, trigeminal, and facial motoneuron involvement in amyotrophic lateral sclerosis. *Neurology* 38: 281-283, 1988.

DESARMENIEN, M.G., CLENDENING, B., AND SPITZER, N.C. *In vivo* development of voltage-dependent ionic currents in embryonic *Xenopus* spinal neurons. *J. Neurosci.* 13: 2575-2581, 1993.

DOBBINS, E. G., AND FELDMAN, J. L. Differential innervation of protruder and retractor muscles of the tongue in rat. *J. Comp. Neurol.* 357: 376-394, 1995.

DOBLE, A. Excitatory amino acid receptors and neurodegeneration. *Therapie* 50: 319-337, 1995.

EKEN, T., HULTBORN, H., AND KIEHN, O. Possible functions of transmitter-controlled plateau potentials in alpha motoneurones. *Prog. Brain Res.* 80: 257-267, 1989.

ELSEN, F. P., AND RAMIREZ, J. M. Calcium currents of rhythmic neurons recorded in the isolated respiratory network of neonatal mice. *J. Neurosci.* 18: 10652-10662, 1998.

ENGISCH, K.L., WAGNER, J.J., AND ALGER, B.E. Whole-cell voltage-clamp investigation of the role of PKC in muscarinic inhibition of I_{AHP} in rat CA1 hippocampal neurons. *Hippocampus* 6: 183-191, 1996.

ENOKA RM, STUART DG. Neurobiology of muscle fatigue. *J. Appl. Physiol.* 72: 1631-1648, 1992.

FAN, S., STEWART, M., AND WONG, R.K.S. Differences in voltage-dependent sodium currents exhibited by superficial and deep layer neurons of guinea pig entorhinal cortex. *J. Neurophysiol.* 71: 1986- 91, 1994.

FELDER, C.C., POULTER, M.O., AND WESS, J. Muscarinic receptor-operated Ca^{2+} influx in transfected fibroblast cells is independent of inositol phosphates and release of intracellular Ca^{2+}. *Proc. Natl. Acad. Sci. USA* 89: 509- 13, 1992.

FIERRO, L. AND LLANO, I. High endogenous calcium buffering in Purkinje cells from rat cerebellar slices. *J. Physiol. (Lond.)* 496: 617- 625, 1996.

FIGENSCHOU, A., HU, G.-Y., AND STORM, J.F. Cholinergic modulation of the action potential in rat hippocampal neurons. *Eur. J. Neurosci.* 8: 211-219, 1996.

FISZMAN, M.L., BARKER, J.L., AND JONES, S.V.P. Electrophysiological responses to muscarinic receptor stimulation in cultured hippocampal neurons. *Brain Res.* 557: 1-4, 1991.

FLEIDERVISH, I.A., FRIEDMAN, A., AND GUTNICK, M.J. Slow inactivation of Na^+ current and slow cumulative spike adaptation in mouse and guinea-pig neocortical neurones in slices. *J. Physiol. (Lond.)* 493: 83-97, 1996.

FLESHMAN, J.W., MUNSON, J.B., AND SYPERT, G.W. Homonymous projection of individual group Ia-fibers to physiologically characterized medial gastrocnemius motoneurons in the cat. *J. Neurophysiol.* 46: 1339-1348, 1981.

FORSYTHE, I.D. AND CLEMENTS, J.D. Presynaptic glutamate receptors depress excitatory monosynaptic transmission between mouse hippocampal neurones. *J. Physiol. (Lond.)* 429: 1- 16, 1990.

FORSYTHE, I.D. AND REDMAN, S.J. The dependence of motoneurone potential on extracellular ion concentrations studied in isolated rat spinal cord. *J. Physiol. (Lond.)* 404: 83-99, 1988.

FRANKENHAEUSER, B. AND HUXLEY, A.F. The action potential in the myelinated nerve fibre of *Xenopus laevis* as computed on the basis of voltage clamp data. *J. Physiol. (Lond.)* 171: 302-315, 1964.

FRENCH, C.R., SAH, P., BUCKETT, K.J., AND GAGE, P.W. A voltage-dependent persistent sodium current in mammalian hippocampal neurons. *J. Gen. Physiol.* 95: 1139- 1157, 1990.

FRERMANN, D., KELLER, B. U., AND RICHTER, D. W. Calcium oscillations in rhythmically active respiratory neurones in the brainstem of mouse. *J. Physiol. (Lond.)* 515: 119-131, 1999.

FRIEL, D.D. AND TSIEN, R.W. A caffeine- and ryanodine-sensitive Ca^{2+} store in bullfrog sympathetic neurones modulates effects of Ca^{2+} entry on $[Ca^{2+}]_i$. *J. Physiol.* 450: 217-246, 1992.

FUNK, G.D., PARKIS, M.A., SELVARATNAM, S.R., AND WALSH, C. Developmental modulation of glutamatergic inspiratory drive to hypoglossal motoneurons. *Respir. Physiol.* 110: 125-37, 1997.

FUNK, G.D., SMITH, J.C., AND FELDMAN, J.L. Generation and transmission of respiratory oscillations in medullary slices: role of excitatory amino acids. *J. Neurophysiol.* 70:1497-515, 1993.

GARDINER, P.F. Physiological properties of motoneurons innervating different muscle

unit types in rat gastrocnemius. *J. Neurophysiol.* 69: 1160-1170, 1993.

GAUDA, E.B., MILLER, M.J., CARLO, W.A., DIFIORE, J.N., JOHNSEN, D.C., AND MARTIN, R.J. Genioglossus response to airway occlusion in apneic *versus* nonapneic infants. *Ped. Research* 22: 683-687, 1987.

GLAUM, S.R. AND MILLER, R.J. Metabotropic glutamate receptors depress afferent excitatory transmission in the rat nucleus tractus solitarii. *J. Neurophysiol.* 70: 2669- 72, 1993.

GOH, J.W., KELLY, M.E., AND PENNEFATHER, P.S. Electrophysiological function of the delayed rectifier (I_K) in bullfrog sympathetic ganglion neurones. *Pflugers Arch.* 413: 482-486, 1989.

GOH, J.W. AND PENNEFATHER, P.S. Pharmacological and physiological properties of the after-hyperpolarization current of bullfrog ganglion neurones. *J. Physiol. (Lond.)* 394: 315-330, 1987.

GORDON, D., MERRICK, D., AULD, V., DUNN, R., GOLDIN, A.L., DAVIDSON, N., AND CATTERALL, W.A. Tissue-specific expression of the RI and RII sodium channel subtypes. *Proc. Natl. Acad. Sci. USA* 84: 8682- 6, 1987.

GRANIT, R., KERNELL, D., AND SHORTESS, G. Quantitative aspect of repetitive firing of mammalian motoneurones, caused by injected currents. *J. Physiol. (Lond.)* 168: 911-931, 1963.

GUERINEAU, N.C., GAHWILER, B.H., AND GERBER, U. Reduction of resting K^+ current by metabotropic glutamate and muscarinic receptors in rat CA3 cells: mediation by G-proteins. *J. Physiol. (Lond.)* 474: 27-33, 1994.

GUERITAUD, J.P. Electrical activity of rat ocular motoneurons recorded *in vitro*. *Neuroscience* 24: 837-852, 1988.

GUSTAFSSON, B. AND PINTER, M.J. Relations among passive electrical properties of lumbar alpha-motoneurones of the cat. *J. Physiol. (Lond.)* 356: 401-31, 1984.

GUSTAFSSON, B. AND PINTER, M.J. On factors determining orderly recruitment of motor units: a role for intrinsic membrane properties. *Trends Neurosci.* 8: 431-433, 1985.

HADDAD, G.G., DONNELLY, D.F., AND GETTING, P.A. Biophysical properties of hypoglossal neurons *in vitro*: intracellular studies in adult and neonatal rats. *J. Appl. Physiol.* 69: 1509-1517, 1990.

HALLIWELL, J.V. AND ADAMS, P.R. Voltage-clamp analysis of muscarinic excitation in hippocampal neurons. *Brain Res.* 250: 71-92, 1982.

HAMILL, O.P., MARTY, A., NEHER, E., SAKMANN, B., AND SIGWORTH, F.J. Improved patch-clamp techniques for high-resolution current recording from cells and cell-free membrane patches. *Pflügers Arch.* 391: 85-100, 1981.

HAY, M., MCKENZIE, H., LINDSLEY, K., DIETZ, N., BRADLEY, S.R., CONN, P.J., AND HASSER, E.M. Heterogeneity of metabotropic glutamate receptors in autonomic cell groups of the medulla oblongata of the rat. *J. Comp. Neurol.* 403: 486-501, 1999.

HELMCHEN, F., IMOTO, K., AND SAKMANN, B. Ca^{2+} buffering and action potential-evoked Ca^{2+} signaling in dendrites of pyramidal neurons. *Biophys. J.* 70: 1069- 1081, 1996.

HENNEMAN, E. AND MENDELL, L. Functional organization of motoneuron pool and its inputs. In: *Handbook of Physiology. The Nervous System. Motor Systems*. Bethesda, MD: Am. Physiol. Soc., 1981, sect. I, vol. II, pt. 1, chapt. 11, p. 423-214.

HENNIG, R. AND LOMO, T. Gradation of force output in normal fast and slow muscles of the rat. *Acta Physiol. Scand.* 130: 133-142, 1987.

HENRY, J.N. AND MANAKER, S. Colocalization of substance P or enkephalin in serotonergic neuronal afferents to the hypglossal nucleus in the rat. *J. Comp. Neurol.* 391: 491-505, 1998.

HILLE, B. *Ionic Channels of Excitable Membranes*. Sunderland, MA: Sinauer Associates inc., 1992, p.607.

HIRONAKA, T. AND NARAHASHI, T. Cation permeability ratios of sodium channels in normal and grayanotoxin-treated squid axon membranes. *J. Membr. Biol.* 31: 359- 381, 1977.

HO, B. K., ALEXIANU, M. E., COLOM, L. V., MOHAMED, A. H., SERRANO, F., AND APPEL, S. H. Expression of calbindin-D28K in motoneuron hybrid cells after retroviral infection with calbindin-D28K cDNA prevents amyotrophic lateral sclerosis IgG-mediated cytotoxicity. *Proc. Natl. Acad. Sci. USA* 93: 6796-6801, 1996.

HOCHMAN, S., JORDAN, L.M., AND SCHMIDT, B.J. TTX-resistant NMDA-receptor-mediated voltage oscillations in mammalian lumbar motoneurons. *J. Neurophysiol.* 72: 2559-2562, 1994.

HODGKIN, A.L. AND HUXLEY, A.F. A quantitative description of membrane current and its application to conduction and excitation in nerve. *J. Physiol. (Lond.)* 117: 500-544, 1952.

HOFFER, J., SUGANO, N., LOEB, G., MARKS, W., O'DONOVAN, M., AND PRATT, C. Cat hindlimb motoneurons during locomotion. II. Normal activity patterns. *J. Neurophysiol.* 57: 530-553, 1987.

HOFFMAN, D.A., MAGEE, J.C., COLBERT, C.M., AND JOHNSTON, D. K^+ channel regulation of signal propagation in dendrites of hippocampal pyramidal neurons. *Nature* 387: 869-75, 1997.

HOUNSGAARD, J., HULTBORN, H., JESPERSEN, B., AND KIEHN, O. Bistability of alpha-motoneurones in the decerebrate cat and in the acute spinal cat after intravenous 5-hydroxytryptophan. *J. Physiol. (Lond.)* 405: 345-367, 1988a.

HOUNSGAARD, J., HULTBORN, H., AND KIEHN, O Transmitter-controlled properties of alpha-motoneurones causing long-lasting motor discharge to brief excitatory inputs. *Prog. Brain Res.* 64: 39-49, 1986.

HOUNSGAARD, J. AND KIEHN, O. Serotonin-induced bistability of turtle motoneurones caused by a nifedipine-sensitive calcium plateau potential. *J. Physiol. (Lond.)* 414: 265-282, 1989.

HOUNSGAARD, J. AND KIEHN, O. Calcium spikes and calcium plateaux evoked by differential polarization in dendrites of turtle motoneurones *in vitro*. *J. Physiol. (Lond.)* 468: 245-259, 1993.

HOUNSGAARD, J., KIEHN, O., AND MINTZ, I. Response properties of motoneurones in a slice preparation of the turtle spinal cord. *J. Physiol. (Lond.)* 398: 575-589, 1988b.

HOUNSGAARD, J. AND MINTZ, I. Calcium conductance and firing properties of spinal motoneurones in the turtle. *J. Physiol. (Lond.)* 398: 591-603, 1988.

HSIAO, C.F. AND CHANDLER, S.H. Characteristics of a fast transient outward current in guinea pig trigeminal motoneurons. *Brain Res.* 695: 217-226, 1995.

HSIAO, C.F., DEL NEGRO, C.A., TRUEBLOOD, P., AND CHANDLER, S.H. The ionic basis for serotonin-induced bistable membrane properties in guinea pig trigeminal motoneurons. *J. Neurophysiol.* 79: 2847-2856, 1998.

HUGUENARD, J.R., HAMILL, O.P., AND PRINCE, D.A. Developmental changes in Na^+

conductances in rat neocortical neurons: appearance of a slowly inactivating component. *J. Neurophysiol.* 59: 778- 795, 1988.

JACOBS, B.L. AND AZMITIA, E.C. Structure and function of the brain serotonin system. *Physiol. Rev.* 72: 165-229, 1992.

JAHROMI, B.S., ZHANG, L., CARLEN, P.L., AND PENNEFATHER, P. Differential time-course of slow afterhyperpolarizations and associated Ca^{2+} transients in rat CA1 pyramidal neurons: further dissociation by Ca^{2+} buffer. *Neuroscience* 88: 719- 26, 1999.

JODKOWSKI, J.S., VIANA, F., DICK, T.E., AND BERGER, A.J. Repetitive firing properties of phrenic motoneurons in the cat. *J. Neurophysiol.* 60: 687-702, 1988.

JOHNSON, S. M., SMITH, J. C., FUNK, G. D., AND FELDMAN, J. L. Pacemaker behavior of respiratory neurons in medullary slices from neonatal rat. *J. Neurophysiol.* 72: 2598-2608, 1994.

KAWAI, T. AND WATANABE, M. Effects of ryanodine on the spike after-hyperpolarization in sympathetic neurones of the rat superior cervical ganglion. *Pflugers Arch.* 413: 470- 5, 1989.

KERNELL, D. The adaptation and the relation between discharge frequency and current strenght of cat lumbosacral motoneurones stimulated by long-lasting injected currents. *Acta Physiol. Scand.* 65: 65-73, 1965a.

KERNELL, D. High-frequency repetitive firing of cat lumbosacral motoneurones stimulated by long-lasting injected currents. *Acta Physiol. Scand.* 65: 74-86, 1965b.

KERNELL, D. AND MONSTER, A.W. Time course and properties of late adaptation in spinal motoneurones of the cat. *Exp. Brain. Res.* 46:191-196, 1982.

KERNELL, D. AND SJOHOLM, H. Motoneurone models based on 'voltage clamp equations' for peripheral nerve. *Acta Physiol. Scand.* 86: 546-562, 1972.

KERNELL, D. AND SJOHOLM, H. Repetitive impulse firing: comparisons between neurone models based on 'voltage clamp equations' and spinal motoneurones. 87: 40-56, 1973.

KERNELL, D. AND ZWAAGSTRA, B. Input conductance axonal conduction velocity and cell size among hindlimb motoneurones of the cat. *Brain Res.* 204: 311-26, 1980.

KIEHN, O. AND EKEN, T. Prolonged firing in motor units: evidence of plateau potentials in human motoneurons? *J. Neurophysiol.* 78: 3061-3068, 1997.

KIEHN, O. AND EKEN, T. Functional role of plateau potentials in vertebrate motor neurons. *Curr. Opin. Neurobiol.* 8: 746-752, 1998.

KIERNAN, J. A., AND HUDSON, A. J. Changes in sizes of cortical and lower motor neurons in amyotrophic lateral sclerosis. *Brain* 114: 843-853, 1991.

KIRKWOOD, P. AND MUNSON, J. The incidence of initial doublets in the discharges of motoneurones of two different inspiratory muscles in the cat. *J. Physiol. (Lond.)* 493: 577-587, 1996.

KLEMIC, K.G., DURAND, D.M., AND JONES, S.W. Activation kinetics of the delayed rectifier potassium current of bulfrog sympathetic neurons. *J. Neurophysiol.* 79: 2345-2357, 1998.

KOBAYASHI, M., INOUE, T., MATSUO, R., MASUDA, Y., HIDAKA, O., KANG, Y., AND MORIMOTO, T. Role of calcium conductances on spike afterpotentials in rat trigeminal motoneurons. *J. Neurophysiol.* 77: 3273-3283, 1997.

KOSTYUK, P. AND VERKHRATSKY, A. Calcium stores in neurons and glia. *Neuroscience* 63: 381- 404, 1994.

KRIEGER, C., JONES, K., KIM, S. U., AND EISEN, A. A. The role of intracellular free calcium in motor neuron disease. *J. Neurol. Sci.* 124: 27-32, 1994.

KRIEGER, C., LANIUS, R. A., PELECH, S. L., AND SHAW, C. A. Amyotrophic lateral sclerosis: the involvement of intracellular Ca^{2+} and protein kinase C. *Trends Pharmacol. Sci.* 17: 114-120, 1996.

KRNJEVIC, K., LAMOUR, Y., MACDONALD, J.F., AND NISTRI, A. Effects of some divalent cations on motoneurones in cats. *Can. J. Physiol. Pharmac.* 57: 944-956, 1979.

KRNJEVIC, K., PUIL, E., AND WERMAN, R. Evidence for Ca^{2+}-activated K^+ conductance in cat spinal motoneurons from intracellular EGTA injections. *Can. J. Physiol. Pharmacol.* 53: 1214-1218, 1975.

KUBIN, L., TOJIMA, H., REIGNIER, C., PACK, A. I., AND DAVIES, R. O. Interaction of serotonergic excitatory drive to hypoglossal motoneurons with carbachol-induced, REM sleep-like atonia. *Sleep* 19: 187-195, 1996.

KUDINA, L. AND ALEXEEVA, N. Repetitive doublets of human motoneurones: analysis of interspike intervals and recruitment pattern. *Electroencephalogr. Clin. Neurophysiol.* 85: 243-247, 1992.

KUDO, Y., OGURA, A., AND IJIMA, T. Stimulation of muscarinic receptors in hippocampal neuron induces characteristic increase in cytosolic free Ca^{2+}. *Neurosci. Lett.* 85: 345- 350, 1988.

LANCASTER, B. AND ADAMS, P.R. Calcium-dependent current generating the afterhyperpolarization of hippocampal neurons. *J. Neurophysiol.* 55: 1268- 1282, 1986.

LANCASTER, B. AND NICOLL, R.A. Properties of two calcium activated hyperpolarizations in rat hippocampal neurones. *J. Physiol. (Lond.)* 389: 187- 203, 1987.

LANCASTER, B. AND PENNEFATHER, P. Potassium currents evoked by brief depolarizations in bull-frog symphatetic ganglion cells. *J. Physiol. (Lond.)* 387: 519-548, 1987.

LEE, R.H., AND HECKMAN, C.J. Influence of voltage-sensitive dendritic conductances on bistable firing and effective synaptic current in cat spinal motoneurons *in vivo*. *J. Neurophysiol.* 76: 2107-2110, 1996.

LEE, R.H., AND HECKMAN, C.J Bistability in spinal motoneurons *in vivo*: systematic variations in rhythmic firing patterns. *J. Neurophysiol.* 80: 572-582, 1998a.

LEE, R.H., AND HECKMAN, C.J Bistability in spinal motoneurons *in vivo*: systematic variations in persistent inward currents. *J. Neurophysiol.* 80: 583-593, 1998b.

LI, Y., TAKADA, M., AND MIZUNO, N. The sites of origin of serotoninergic afferent fibers in the trigeminal motor, facial, and hypoglossal nuclei in the rat. *Neurosci. Res.* 17: 307-313, 1993.

LI, Y., TAKADA, M., KANEKO, T., AND MIZUNO, N. Distribution of GABAergic and glycinergic premotor neurons projecting to the facial and hypoglossal nuclei in the rat. *J. Comp. Neurol.* 378: 283-294, 1997.

LINDSAY, A.D. AND FELDMAN, J.L. Modulation of respiratory activity of neonatal rat phrenic motoneurones by serotonin. *J. Physiol. (Lond.)* 461: 213-233, 1993.

LIPS, M.B. AND KELLER, B.U. Endogenous calcium buffering in motoneurones of the nucleus hypoglossus from mouse. *J. Physiol. (Lond.)* 511: 105-117, 1998.

LIPS, M.B. AND KELLER, B.U. Activity-related calcium dynamics in motoneurons of the nucleus hypoglossus from mouse. *J. Neurophysiol.* 82: 2936-2946, 1999.

LLINAS, R.R. The intrinsic electrophysiological properties of mammalian neurons: insights into central nervous system function. *Science* 242: 1654-1664, 1988.

LOWE, A.A. The neural regulation of tongue movements. *Prog. Neurobiol.* 15: 295-344, 1981.

LÜSCHER, H.R. AND LARKUM, M.E. Modeling action potential initiation and back-propagation in dendrites of cultured rat motoneurons. *J. Neurophysiol.* 80: 715-729, 1998.

MADISON, D.V. AND NICOLL, R.A. Control of the repetitive discharge of rat CA 1 pyramidal neurones *in vitro*. *J. Physiol. (Lond.)* 354: 319- 331, 1984.

MAGISTRETTI, J., MANTEGAZZA, M., GUATTEO, E., AND WANKE, E. Action potentials recorded with patch-clamp amplifiers: are they genuine? *Trends Neurosci.* 19: 530- 534, 1996.

MAGEE, J.C. Dendritic hyperpolarization-activated currents modify the integrative properties of hippocampal CA1 pyramidal neurons. *J. Neurosci.* 18: 7613-7624, 1998.

MAGEE, J.C. Dendritic I_h normalizes temporal summation in hippocampal CA1 neurons. *Nat. Neurosci.* 2: 508-14, 1999.

MAINEN, Z.F. AND SEJNOWSKI, T.J. Influence of dendritic structure on firing pattern in model neocortical neurons. *Nature* 382: 363- 366, 1996.

MANAKER, S. AND TISCHLER, L.J. Origin of serotoninergic afferents to the hypoglossal nucleus in the rat. *J. Comp. Neurol.* 334: 466-476, 1993.

MANAKER, S., TISCHLER, L.J., AND MORRISON, A.R. Raphespinal and reticulospinal axon collaterals to the hypoglossal nucleus in the rat. *J. Comp. Neurol.* 322: 68-78, 1992.

MARTIN, L.J., BLACKSTONE, C.D., LEVEY, A.I., HUGANIR, R.L., AND PRICE, D.L. AMPA glutamate receptor subunits are differentially distributed in rat brain. *Neuroscience* 53: 327-358, 1993.

MEDINA, L., FIGUEREDO-CARDENAS, G., ROTHSTEIN, J.D., AND REINER, A. Differential abundance of glutamate transporter subtypes in amyotrophic lateral sclerosis (ALS)-vulnerable *versus* ALS-resistant brain stem motor cell groups. *Exp. Neurol.* 142: 287-295, 1996.

MCCORMICK, D.A. AND PRINCE, D.A. Two types of muscarinic response to acetylcholine in mammalian cortical neurons. *Proc. Natl. Acad. Sci. USA* 82: 6344- 8, 1985.

MCCORMICK, D.A. AND VON KROSIGK, M. Corticothalamic activation modulates thalamic firing through glutamate "metabotropic" receptors. *Proc. Natl. Acad. Sci. USA*

89: 2774- 8, 1992.

MCLARNON, J.G. Potassium currents in motoneurones. *Prog. Neurobiol.* 47: 513-531, 1995.

MCLARNON, J.G., KIM, S., MICHIKAWA, M., AND XU, R. Properties of inward and outward potassium currents in cultured mouse motoneurons. *Neuroscience* 64: 139-151, 1995.

MCPHERSON, P.S., KIM, Y.K., VALDIVIA, H., KNUDSON, C.M., TAKEKURA, H., FRANZINI-ARMSTRONG, C., CORONADO, R., AND CAMPBELL, K.P. The brain ryanodine receptor: a caffeine-sensitive calcium release channel. *Neuron* 7: 17- 25, 1991,

MERCURI, N.B., BONCI, A., CALABRESI, P., AND BERNARDI, G. Characterization of a barium-sensitive outward current following glutamate application on rat midbrain dopaminergic cells. *Eur. J. Neurosci.* 8: 1780- 6, 1996.

MOORE, J.A. AND APPENTENG, K. The membrane properties and firing characteristics of rat jaw-elevator motoneurones. *J. Physiol. (Lond.)* 423: 137-153, 1990.

MOORE, J.A., STOCKBRIDGE, N., AND WESTERFIELD, M. On the site of impulse initiation in a neurone. *J. Physiol. (Lond.)* 336: 301-311, 1983.

MONAGHAN, D.T. AND COTMAN, C.W. Distribution of *N*-methyl-D-aspartate-sensitive L-[^{3}H]glutamate-binding sites in rat brain. *J. Neurosci.* 5: 2909-2919, 1985.

MOSFELDT LAURSEN, A. AND REKLING, J.C. Electrophysiological properties of hypoglossal motoneurons of guinea-pigs studied *in vitro*. *Neuroscience* 30: 619-637, 1989.

MYNLIEFF, M. AND BEAM, K.G. Characterization of voltage-dependent calcium currents in mouse motoneurons. *J. Neurophysiol.* 68: 85-92, 1992.

NEHER, E. Correction for liquid junction potentials in patch clamp experiments. *Meth. Enzymol.* 207: 123-131, 1992.

NEHER, E. AND SAKMANN, B. Single-channel currents recorded from membrane of denervated frog muscle fibres. *Nature* 260: 799- 802, 1976.

NICOLL, R.A. The coupling of neurotransmitter receptors to ion channels in the brain. *Science* 421: 545-551, 1988.

NISHIMURA, Y., SCHWINDT, P.C., AND CRILL, W.E. Electrical properties of facial motoneurons in brainstem slices from guinea pig. *Brain Res.* 502: 127-142, 1989.

NODA, M., IKEDA, T., KAYANO, T., SUZUKI, H., TAKESHIMA, H., KURASAKI, M., TAKAHASHI, H., AND NUMA, S. Existence of distinct sodium channel messenger RNAs in rat brain. *Nature* 320: 188- 192, 1986a.

NODA, M., IKEDA, T., SUZUKI, H., TAKESHIMA, H., TAKAHASHI, T., KUNO, M., AND NUMA, S. Expression of functional sodium channels from cloned cDNA. *Nature* 322: 826- 828, 1986b.

NUMANN, R.E., WADMAN, W.J., AND WONG, R.K.S. Outward currents of single hippocampal cells obtained from the adult guinea-pig. *J. Physiol.* 393: 331-353, 1987.

NUNEZ-ABADES, P.A., SPIELMANN, J.M., BARRIONUEVO, G., AND CAMERON, W.E. *In vitro* electrophysiology of developing genioglossal motoneurons in the rat. *J. Neurophysiol.* 70: 1401-1411, 1993.

O'BRIEN, J.A. AND BERGER, A.J. Cotransmission of GABA and glycine to brain stem motoneurons. *J. Neurophysiol.* 82: 1638-41, 1999.

O'BRIEN, J.A., ISAACSON, J.S., AND BERGER, A.J. NMDA and non-NMDA receptors are co-localized at excitatory synapses of rat hypoglossal motoneurons. *Neurosci. Lett.* 227: 5-8, 1997.

OHTA, T., ITO, S., AND OHGA, A. Inhibitory action of dantrolene on Ca-induced Ca^{2+} release from sarcoplasmic reticulum in guinea pig skeletal muscle. *Eur. J. Pharmacol.* 178: 11-19, 1990.

OKABE, S., HIDA, W., KIKUCHI, Y., TAGUCHI, O., TAKISHIMA, T., AND SHIRATO, K. Upper airway muscle activity during REM and non-REM sleep of patients with obstructive apnea. *Chest* 106: 767-773, 1994.

ONO, T., ISHIWATA, Y., INABA, N., KURODA, T., AND NAKAMURA, Y. Hypoglossal premotor neurons with rhythmical inspiratory-related activity in the cat: localization and projection to the phrenic nucleus. *Exp. Brain Res.* 98: 1- 12, 1994

O'REILLY, P.M.R., AND FITZGERALD, M.J.T. Fibre composition of the hypoglossal nerve in the rat. *J. Anat.* 172: 227-243, 1990.

PAPE, H.C. Queer current and pacemaker: the hyperpolarization-activated cation current in neurons. *Annu. Rev. Physiol.* 58: 299-327, 1996.

PARKIS, M.A., BAYLISS, D.A., AND BERGER, A.J. Actions of norepinephrine on rat hypoglossal motoneurons. *J. Neurophysiol.* 74: 1911-1919, 1995.

PARTRIDGE, L.D., MÜLLER, T.H., AND SWANDULLA, D. Calcium-activated non-selective channels in the nervous system. *Brain Res. Rev.* 19: 319-325, 1994.

PERKINS, K.L. AND WONG, R.K.S. Intracellular QX-314 blocks the hyperpolarization-activated inward current I_q in hippocampal CA1 pyramidal cells. *J. Neurophysiol.* 73:911-915, 1995.

PETHIG, R., KUHN, M., PAYNE, R., ADLER, E., CHEN, T.H., AND JAFFE, L.F. On the dissociation constants of BAPTA-type calcium buffers. *Cell Calcium* 10: 491- 498, 1989.

PIERCE, R.J. AND WORSNOP, C.J. Upper airway function and dysfunction in respiration. *Clin. Exp. Pharmacol. Physiol.* 26: 1-10, 1999.

PIERREFICHE, O., BISCHOFF, A. M., RICHTER, D. W., AND SPYER, K. M. Hypoxic response of hypoglossal motoneurones in the *in vivo* cat. *J. Physiol. (Lond.)* 505: 785-795, 1997.

PINTER, M.J., CURTIS, R.L., AND HOSKO, M.J. Voltage threshold and excitability among variously sized cat hindlimb motoneurons. *J. Neurophysiol.* 50:644-57, 1983.

PLANT, T., SCHIRRA, C., KATZ, E., UCHITEL, O., AND KONNERTH, A. Single-cell RT-PCR and functional characterization of Ca^{2+} channels in motoneurons of the rat facial nucleus. *J. Neurosci.* 18: 9573-9584, 1998.

POLIAKOV, A.V., POWERS, R.K., SAWCZUK, A., AND BINDER, M.D. Effects of background noise on the response of rat and cat motoneurones to excitatory current transients. *J. Physiol. (Lond.)* 495: 143-57, 1996.

POLIAKOV, A.V., POWERS, R.K., AND BINDER, M.D. Functional identification of the input-output transforms of motoneurones in the rat and cat. *J. Physiol. (Lond.)* 504: 401-24, 1997.

POWERS, R.K. A variable-threshold motoneuron model that incorporates time- and voltage-dependent potassium and calcium conductances. *J. Neurophysiol.* 70: 246-262, 1993.

POWERS, R.K., SAWCZUK, A., MUSICK, J.R., AND BINDER, M.D. Multiple mechanisms of spike-frequency adaptation in motoneurones. *J. Physiol. (Paris)* 93: 101-114, 1999.

RAAPPANA, P. AND ARVIDSSON, J. Location, morphology, and central projections of mesencephalic trigeminal neurons innervating rat masticatory muscles studied by axonal transport of choleragenoid-horseradish peroxidase. *J. Comp. Neurol.* 328: 103-114, 1993.

RANDALL, A.D. AND TSIEN, R.W. Contrasting biophysical and pharmacological properties of T-type and R-type calcium channels. *Neuropharmacology* 36: 879-893, 1997.

REINER, A., MEDINA, L., FIGUEREDO-CARDENAS, G., AND ANFINSON, S. Brainstem motoneuron pools that are selectively resistant in amyotrophic lateral sclerosis are preferentially enriched in parvalbumin: evidence from monkey brainstem for a calcium-mediated mechanism in sporadic ALS. *Exp. Neurol.* 131:239- 250, 1995.

REKLING, J.C. AND MOSFELDT LAURSEN, A. Evidence for a persistent sodium conductance in neurons from the nucleus prepositus hypoglossi. *Brain Res.* 500: 276-286, 1989.

RICHMONDS, C. R., AND HUDGEL, D. W. Hypoglossal and phrenic motoneuron responses to serotonergic active agents in rats. *Resp. Physiol.* 106: 153-160, 1996.

ROBINSON, D.W. AND CAMERON, W.E. Time-dependent changes in input resistance of rat hypoglossal motoneurons associated with whole-cell recording. *J. Neurophysiol.* 83: 3160- 3164, 2000.

ROGAWSKI M.A. The A-current: how ubiquitous a feature of excitable cells is it? *Trends Neurosci.* 8: 214-219, 1985.

ROTTER, A., BIRDSALL, N.J., FIELD, P.M., AND RAISMAN, G. Muscarinic receptors in the central nervous system of the rat. II. Distribution of binding of [3H]propylbenzilylcholine mustard in the midbrain and hindbrain. *Brain Res.* 180: 167-183, 1979.

RUDY, B. Inactivation in *Myxicola* giant axons responsible for slow and accumulative adaptation phenomena. *J. Physiol. (Lond.)* 312: 531- 549, 1981.

RUDY, B. Diversity and ubiquity of K channels. *Neuroscience* 25: 729-749, 1988.

RYBAK, I.A., PATON, J.F.R., AND SCHWABER, J.S. Modeling neural mechanisms for genesis of respiratory rhytm and pattern. I. Models of respiratory neurons. *J. Neurophysiol.* 77: 1994- 2006, 1997.

SAFRONOV, B. AND VOGEL, W. Single voltage-activated Na^+ and K^+ channels in the somata of rat motoneurones. *J. Physiol. (Lond.)* 487: 91-106, 1995.

SAFRONOV, B. AND VOGEL, W. Large conductance Ca^{2+}-activated K^+ channels in the soma of rat motoneurones. *J. Membr. Biol.* 162: 9-15, 1998.

SAFRONOV, B.V., WOLFF, M., AND VOGEL, W. Axonal expression of sodium channels in rat spinal neurones during postnatal development. *J. Physiol. (Lond.)* 514: 729- 734, 1999.

SAFRONOV, B.V., WOLFF, M., AND VOGEL, W. Excitability of the soma in central nervous system neurons. *Biophys. J.* 78: 2998-3010, 2000.

SAH, P. Ca^{2+}- activated K^+ currents in neurones: types, physiological roles and modulation. *Trends Neurosci.* 19: 150-154, 1996.

SAH, P., GIBB, A.J., AND GAGE, P.W. The sodium current underlying action potentials in guinea pig hippocampal CA1 neurons. *J. Gen. Physiol.* 91: 373- 98, 1988.

SAH, P. AND MCLACHLAN, E. Ca^{2+}-activated K^+ currents underlying the afterhyperpolarization in guinea pig vagal neurons: a role for Ca^{2+}-activated Ca^{2+} release. *Neuron* 7: 257- 264, 1991.

SAH, P. AND MCLACHLAN, E. Potassium currents contributing to action potential repolarization and the afterhyperpolarization in rat vagal motoneurons. *J. Neurophysiol.* 68: 1834-1841, 1992.

SAWCZUK, A., POWERS, R.K., AND BINDER, M.D. Spike frequency adaptation studied in hypoglossal motoneurons of the rat. *J. Neurophysiol.* 73: 1799-1810, 1995.

SAWCZUK, A., POWERS, R.K., AND BINDER, M.D. Contribution of outward currents to spike frequency adaptation in hypoglossal motoneurons of the rat. *J. Neurophysiol.* 73: 1799- 1810, 1997.

SCHOEPP, D.D. AND CONN, P.J. Metabotropic glutamate receptors in brain function and pathology. *Trends Pharmacol. Sci.* 14: 13- 20, 1993.

SCHOMBURG, E. AND STEFFENS, H. Bistable characteristics of motoneurone activity during DOPA induced fictive locomotion in spinal cats. *Neurosci. Res.* 26: 47-56, 1996.

SCHOPPA, N.E. AND SIGWORTH, F.J. Activation of Shaker potassium channels. III. An activation gating model for wild-type and V2 mutant channels. *J. Gen. Physiol.* 111: 313-342, 1998.

SCHWINDT, P.C. Membrane-potential trajectories underlying motoneuron rhythmic firing at high rates. *J. Neurophysiol.* 36: 434-439, 1973.

SCHWINDT, P.C. AND CRILL, W.E. Role of a persistent inward current in motoneuron bursting during spinal seizures. *J. Neurophysiol.* 43: 1296-1318, 1980a.

SCHWINDT, P.C. AND CRILL, W.E. Properties of a persistent inward current in normal and TEA-injected motoneurons. *J. Neurophysiol.* 43: 1700-1724, 1980b.

SCHWINDT, P.C. AND CRILL, W.E. Effects of barium on cat spinal motoneurons studied by voltage clamp. *J. Neurophysiol.* 44: 827-846, 1980c.

SCHWINDT, P.C. AND CRILL, W.E. Differential effects of TEA and cations on outward ionic currents of cat motoneurons. *J. Neurophysiol.* 46: 1-16, 1981.

SCHWINDT, P.C. AND CRILL, W.E. Factors influencing motoneuron rhythmic firing: results from a voltage-clamp study. *J. Neurophysiol.* 48: 875-890, 1982.

SCHWINDT, P.C., SPAIN, W.J., FOEHRING, R.C., CHUBB, M.C., AND CRILL, W.E. Slow conductances in neurons from cat sensimotor cortex *in vitro* and their role in slow excitability changes. *J. Neurophysiol.* 59: 450- 467, 1988.

SCHWINDT, P.C., SPAIN, W.J., AND CRILL, W.E. Effects of intracellular calcium chelation on voltage-dependent and calcium-dependent currents in cat neocortical neurons. *Neuroscience* 47: 571- 578, 1992a.

SCHWINDT, P.C., SPAIN, W.J., AND CRILL, W.E. Calcium-dependent potassium currents in neurons from cat sensimotor cortex. *J. Neurophysiol.* 67: 216-226, 1992b.

SEGAL, M. Multiple action of acetylcholine at a muscarinic receptor studied in the rat hippocampal slice. *Brain Res.* 246: 77- 87, 1982.

SERODIO, P. AND RUDY, B. Differential expression of Kv4 K^+ channel subunits mediating subthreshold transient K^+ (A-type) currents in rat brain. *J. Neurophysiol.* 79: 1081-1091, 1998.

SHAW, P.J., INCE, P.G., JOHNSON, M., PERRY, E.K., AND CANDY, J.M. The quantitative autoradiographic distribution of [^{3}H]MK-801 binding sites in the normal human brainstem in relation to motor neuron disease. *Brain Res.* 572: 276-280, 1992.

SHMIGOL, A., KIRISCHUK, S., KOSTYUK, P., AND VERKHRATSKY, A. Different properties of caffeine-sensitive Ca^{2+} stores in peripheral and central mammalian neurones. *Pflugers Arch.* 426: 174- 176, 1994.

SINGER, J.H., BELLINGHAM, M.C., AND BERGER, A.J. Presynaptic inhibition of glutamatergic synaptic transmission to rat motoneurons by serotonin. *J. Neurophysiol.* 76: 799-807, 1996.

SINGER, J.H., TALLEY, E.M., BAYLISS, D.A., AND BERGER, A.J. Development of

glycinergic synaptic transmission to rat brain stem motoneurons. *J. Neurophysiol.* 80: 2608-20, 1998.

SMITH, J. C., BALLANYI, K., AND RICHTER, D. W. Whole-cell patch-clamp recordings from respiratory neurons in neonatal rat brainstem *in vitro*. *Neurosci. Lett.* 134: 153-156, 1992.

SMITH, J. C., ELLENBERGER, H. H., BALLANYI, K., RICHTER, D. W., AND FELDMAN, J. L. Pre-Botzinger complex: a brainstem region that may generate respiratory rhythm in mammals. *Science* 254: 726-729, 1991.

SOKOLOFF, A. J., AND DEACON, T. W. Musculotopic organization of the hypoglossal nucleus in the cynomolgus monkey, *Macaca fascicularis*. *J. Comp. Neurol.* 324: 81-93, 1992.

SPIELMANN JM, LAOURIS Y, NORDSTROM MA, ROBINSON GA, REINKING RM, STUART DG. Adaptation of cat motoneurons to sustained and intermittent extracellular activation. *J. Physiol. (Lond.)* 464: 75-120, 1993.

SPITZER, N.C. A developmental handshake: neuronal control of ionic currents and their control of neuronal differentiation. *J. Neurobiol.* 22: 659-673, 1991.

SPRUSTON, N. AND JOHNSTON, D. Perforated patch-clamp analysis of the passive membrane properties of three classes of hippocampal neurons. *J. Neurosci.* 67: 508- 529, 1992.

STALEY, K.J., OTIS, T.S., AND MODY, I. Membrane properties of dentate gyrus granule cells: comparison of sharp microelectrode and whole-cell recordings. *J. Neurophysiol.* 67: 1346-1358, 1992.

STORM, J.F. Action potential repolarization and a fast after-hyperpolarization in rat hippocampal pyramidal cells. *J. Physiol. (Lond.)* 385: 733-759, 1987.

STORM, J.F. An after-hyperpolarization of medium duration in rat hippocampal pyramidal cells. *J. Physiol. (Lond.)* 409: 171-190, 1989.

STORM, J.F. Potassium currents in hippocampal pyramidal cells. *Prog. Brain Res.* 83: 161-187, 1990.

STRATTON, K.R., WORLEY, P.F., AND BARABAN, J.M. Excitation of hippocampal neurons by stimulation of glutamate Qp receptors. *Eur. J. Pharmacol.* 173: 235- 237, 1989.

STÜHMER, W., METHFESSEL, C., SAKMANN, B., NODA, M., AND NUMA, S. Patch clamp

characterization of sodium channels expressed from rat brain cDNA. *Eur. Biophys. J.* 14: 131- 138, 1987.

SUZUE, T. Respiratory rhythm generation in the *in vitro* brain stem-spinal cord preparation of the neonatal rat. *J. Physiol. (Lond.)* 354: 173-183, 1984.

SVIRSKIS, G. AND HOUNSGAARD, J. Transmitter regulation of plateau properties in turtle motoneurons. *J. Neurophysiol.* 79: 45-50, 1998.

TAKADA, M., ITOH, K., YASUI, K., MITANI, A., NOMURA, S., AND MIZUNO, N. Distribution of premotor neurons for the hypoglossal nucleus in the cat. *Neurosci. Lett.* 52: 141-146, 1984.

TAKAHASHI T. Membrane currents in visually identified motoneurones of neonatal rat spinal cord. *J. Physiol. (Lond.)* 423: 27-46, 1990.

TALLEY, E.M., LEI, Q., SIROIS, J.E., AND BAYLISS, D.A. TASK-1, a two-pore domain K^+ channel, is modulated by multiple neurotransmitters in motoneurons. *Neuron* 25: 399-410, 2000.

TALLEY, E.M., SADR, N.N., AND BAYLISS, D.A. Postnatal development of serotonergic innervation, 5-HT_{1A} receptor expression, and 5-HT responses in rat motoneurons. *J. Neurosci.* 17: 4473- 4485, 1997.

THAYER, S.A., HIRNING, L.D., AND MILLER, R.J. The role of caffeine-sensitive calcium stores in the regulation of the intracellular free calcium concentration in rat sympathetic neurons *in vitro*. *Mol. Pharmacol.* 34: 664- 673, 1988.

THURBON, D., LUSCHER, H.R., HOFSTETTER, T., AND REDMAN, S.J. Passive electrical properties of ventral horn neurons in rat spinal cord slices. *J. Neurophysiol.* 79: 2485-2502, 1998.

TRAUB, R.D., WONG, R.K.S., MILES, R., AND MICHELSON, H. A model of a CA3 hippocampal pyramidal neuron incorporating voltage-clamp data on intrinsic conductances. *J. Neurophysiol.* 66: 635- 650, 1991.

TRAVERS, J. AND NORGREN, R. Afferent projections to the oral motor nuclei in the rat. *J. Comp. Neurol.* 220: 280-298, 1983.

TOPERT, C., DORING, F., WISCHMEYER, E., KARSCHIN, C., BROCKHAUS, J., BALLANYI, K., DERST, C., AND KARSCHIN, A. Kir2.4: a novel K^+ inward rectifier channel associated with motoneurons of cranial nerve nuclei. *J. Neurosci.* 18: 4096- 4105, 1998.

TSIEN, R.W., ELLINOR, P.T., AND HORNE, W.A. Molecular diversity of voltage-dependent Ca^{2+} channels. *Trends Pharmacol. Sci.* 12: 349-354, 1991.

ULFHAKE, B. AND KELLERTH, J.O. A quantitative morphological study of HRP-labelled cat alpha-motoneurones supplying different hindlimb muscles. *Brain Res.* 264: 1-19, 1983.

UMEMIYA, M. AND BERGER, A.J. Properties and function of low- and high-voltage-activated Ca^{2+} channels in hypoglossal motoneurons. *J. Neurosci.* 14: 5652-5660, 1994a.

UMEMIYA, M. AND BERGER, A.J. Activation of adenosine A1 and A2 receptors differentially modulates calcium channels and glycinergic synaptic transmission in rat brainstem. *Neuron* 13: 1439-1446, 1994b.

UMEMIYA, M. AND BERGER, A.J. Single-channel properties of four calcium channel types in rat motoneurons. *J. Neurosci.* 15: 2218-2224, 1995a.

UMEMIYA, M. AND BERGER, A.J. Presynaptic inhibition by serotonin of glycinergic inhibitory synaptic currents in the rat brain stem. *J. Neurophysiol.* 73: 1192-1201, 1995b.

USACHEV, Y., SHMIGOL, A., PRONCHUK, N., KOSTYUK, P., AND VERKHRATSKY, A. Caffeine-induced calcium release from internal stores in cultured rat sensory neurons. *Neuroscience* 57: 845- 859, 1993.

VELUMIAN, A.A. AND CARLEN, P.L. Differential control of three after-hyperpolarizations in rat hippocampal neurones by intracellular calcium buffering. *J. Physiol. (Lond.)* 517: 201- 216, 1999.

VIANA, F., BAYLISS, D.A., AND BERGER A.J. Calcium conductances and their role in the firing behavior of neonatal rat hypoglossal motoneurones. *J. Neurophysiol.* 69: 2137-2149, 1993a.

VIANA, F., BAYLISS, D.A., AND BERGER, A.J. Multiple potassium conductances and their role in the action potential repolarisation and repetitive firing behavior of neonatal rat hypoglossal motoneurons. *J. Neurophysiol.* 69: 2150-2163, 1993b.

VIANA, F., BAYLISS, D.A., AND BERGER, A.J. Postnatal changes in rat hypoglossal motoneuron membrane properties. *Neuroscience* 59: 131-148, 1994.

VIANA, F., BAYLISS, D.A., AND BERGER, A.J. Repetitive firing properties of developing rat brainstem motoneurones. *J. Physiol. (Lond.)* 486: 745-761, 1995.

WALMSLEY, J.K., LEWIS, M.S., YOUNG, W.S., AND KUHAR, M.J. Autoradiographic localization of muscarinic cholinergic receptors in rat brainstem. *J. Neurosci.* 1: 176-191, 1981.

WALTON, K. AND FULTON, B.P. Ionic mechanisms underlying the firing properties of rat neonatal motoneurons studied *in vitro*. *Neuroscience* 19: 669-683, 1986.

WARMAN, E.N., DURAND, D.M., AND YUEN, L.F. Reconstruction of hippocampal pyramidal cell electrophysiology by computer simulation. *J. Neurophysiol.* 71: 2033-2045, 1994.

WEISER, M., VEGA-SAENZ DE MIERA, E., KENTROS, C., MORENO, H., FRANZEN, L., HILLMAN, D., BAKER, H., AND RUDY, B. Differential expression of *Shaw*-related K^+ channels in the rat central nervous system. *J. Neurosci.* 14: 949-972, 1994.

WIEGAND, L. AND ZWILLICH, C.W. Obstructive sleep apnea. *Dis. Mon.* 40: 197-252, 1994.

WIEGAND, L., ZWILLICH, C.W., WIEGAND, D., AND WHITE, P. Changes in upper airway muscle activation and ventilation during phasic REM sleep in normal men. *J. Appl. Physiol.* 71: 488-491, 1991.

WILLIAMSON, A. AND ALGER, B.E. Characterization of an early afterpolarization after a brief train of action potentials in rat hippocampal neurons *in vitro*. *J. Neurophysiol.* 63: 72-81, 1990.

WILLINGER, M. SIDS- a challenge. *J. NIH Res.* 1: 73-80, 1989.

WOLFF, M., VOGEL, M., AND SAFRONOV, B.V. Uneven distribution of K^+ channels in soma, axon and dendrites of rat spinal neurones: functional role of the soma in generation of action potentials. *J. Physiol. (Lond.)* 509: 767-776, 1998.

WOLLNER, D.A. AND CATTERALL, W.A. Localization of sodium channels in axon hillocks and initial segments of retinal ganglion cells. *Proc. Natl. Acad. Sci. USA* 83: 8424- 8428, 1986.

WOMBLE, M.D. AND MOISES, C.H. Muscarinic inhibition of M-current and a potassium leak conductance in neurones of the rat basolateral amygdala. *J. Physiol. (Lond.)* 457: 93-114, 1992.

YANG, C.C., CHAN, J.Y., AND CHAN, S.H. Excitatory innervation of caudal hypoglossal nucleus from nucleus reticularis gigantocellularis in the rat. *Neuroscience* 65: 365-374,

1995.

YAO, J.A. AND TSENG, G.N. Modulation of 4-AP block of a mammalian A-type K channel clone by channel gating and membrane voltage. *Biophys. J.* 67: 130- 142, 1994.

YAROM, Y., SUGIMORI, M., AND LLINAS, R. Ionic currents and firing patterns of mammalian vagal motoneurons *in vitro*. *Neuroscience* 16: 719-737, 1985.

ZAJAC, F. AND YOUNG, J. Discharge properties of hindlimb motoneurons in decerebrate cats during locomotion induced by mesencephalic stimulation. *J. Neurophysiol.* 43: 1221-1235, 1980.

ZHANG, L. AND KRNJEVIC, K. Apamin depresses selectively the after-hyperpolarization of cat spinal motoneurons. *Neurosci. Lett.* 74: 58-62, 1987.

ZHANG, L. AND MCBAIN, C.J. Potassium conductances underlying repolarization and after-hyperpolarization in rat CA1 hippocampal interneurones. *J. Physiol. (Lond.)* 488: 661-672, 1995.

ZHANG, L., PENNEFATHER, P., VELUMIAN, A., TYMIANSKI, M., CHARLTON, M., AND CARLEN, P.L. Potentiation of a slow Ca^{2+}-dependent K^{+} current by intracellular Ca^{2+} chelators in hippocampal CA1 neurons of rat brain slices. *J. Neurophysiol.* 74: 2225- 41, 1995.

ZWAAGSTRA, B. AND KERNELL, D. The duration of after-hyperpolarization in hindlimb alpha motoneurones of different sizes in the cat. *Neurosci. Lett.* 19: 303-307, 1980.